Control and investigation of effector export by the bacterial type III secretion system using optogenetics

Dissertation

zur Erlangung des Grades eines
Doktor der Naturwissenschaften
(Dr. rer. nat.)

des Fachbereichs Biologie
der Philipps-Universität Marburg

vorgelegt
von

Florian Lindner
aus Schmalkalden

Marburg (Lahn), Oktober 2021

Die Studien zur vorliegenden Arbeit wurden von November 2018 bis Oktober 2021 am Max-Planck-Institut für Terrestrische Mikrobiologie, Department für Ökophysiologie, unter der Supervision von Dr. Andreas Diepold durchgeführt.

Vom Fachbereich Biologie der Philipps-Universität Marburg (Hochschulkennziffer 1180) als Dissertation angenommen am 03.11.2021

Erstgutachter: Dr. Andreas Diepold

Zweitgutachter: Prof. Dr. Martin Thanbichler

Weitere Mitglieder der Prüfungskommission:

Prof. Dr. Lars-Oliver Essen

Prof. Dr. Lennart Randau

Tag der mündlichen Prüfung am: 22.11.2021

Für meine Familie und Freunde, die immer an mich geglaubt und mich auf meinem Weg begleitet haben.

Table of contents

Table of Figures

Teile der während der Promotion erzielten Ergebnisse wurden in folgender Originalpublikation veröffentlicht:

Lindner F, Milne-Davies B, Langenfeld K, Stiewe T, Diepold A. LITESEC-T3SS - Light-controlled protein delivery into eukaryotic cells with high spatial and temporal resolution. Nat Commun. 2020 May 13;11(1):2381. doi: 10.1038/s41467-020-16169-w.

Abstract

The type III secretion system (T3SS) is a needle-like structure that is used by many pathogenic Gram-negative bacteria to translocate effector proteins from the bacterial cytosol into host cells. It has been successfully applied to deliver non-native cargo into various host cells for different purposes such as vaccination or immunotherapy. However, bacterial T3SS are not restricted to specific target cells and inject effector proteins into any eukaryotic host cell upon contact. Lack of target specificity is therefore a main obstacle in the further development and application of the T3SS as a specific protein delivery tool. Previous studies have shown that the cytosolic complex of the T3SS acts as a highly dynamic interface, in which parts permanently exchange and shuttle between the cytosol and the T3SS, and that this exchange is directly linked to protein secretion function. These findings raise a new possibility to control the T3SS activity via specific sequestration and release of cytosolic T3SS components.

Optogenetic applications, up to now mainly established in eukaryotic cell research, provide a new toolbox to achieve precise control over protein interactions with light. In my PhD work, I incorporated optogenetic interaction switches to bacteria, with the aim to specifically control cellular events. The combination of optogenetic interaction switches with a dynamic essential cytosolic component of the T3SS enables reversible spatial and temporal control of the T3SS function and resulting in the application LITESEC-T3SS (**L**ight-**i**nduced **t**ranslocation of **e**ffectors through **s**equestration of **e**ndogenous **c**omponents of the **T3SS**). This enhances the use of the T3SS as a specific tool for protein delivery into eukaryotic cells and enables broad applications. We present in this work that the secretion of native effector proteins and non-native cargo proteins, as well as the translocation of cargos into eukaryotic host cells can be efficiently controlled by light in the engineered strains. As a direct biological application, we present the delivery of pro-apoptotic cargos into cancer cells.

I further utilized the optogenetic protein association and dissociation principle to investigate dynamic cellular events of the T3SS with focus on the dynamics of the cytosolic complex and its proposed link to effector shuttling and sorting events.

Zusammenfassung

Das Typ-III-Sekretionssystem (T3SS) ist eine nadelförmige Struktur, die von vielen pathogenen gramnegativen Bakterien genutzt wird, um Effektorproteine vom bakteriellen Zytosol aus in Wirtszellen zu transportieren. Es wurde bereits erfolgreich eingesetzt, um nicht-native Proteine in verschiedene Wirtszellen für unterschiedliche Zwecke, zum Beispiel als Impfung oder zur Immuntherapie, einzuschleusen. Das bakterielle T3SS ist jedoch nicht auf bestimmte Zielzellen beschränkt und injiziert bei Kontakt Effektorproteine in jegliche Art eukaryontischer Zelle. Die fehlende Zielspezifität ist daher ein Haupt-Hindernis für die weitere Entwicklung und Anwendung des T3SS als spezifisches Proteintranslokationstool. Frühere Studien haben gezeigt, dass der zytosolische Komplex des T3SS als hochdynamische Schnittstelle fungiert, in dem Proteine permanent zwischen dem Zytosol und dem T3SS ausgetauscht werden und dass dieser Austausch direkt mit der Funktion der Proteinsekretion zusammenhängt. Diese Erkenntnisse eröffnen eine neue Möglichkeit, die T3SS-Aktivität durch gezielte Sequestrierung und Freisetzung von zytosolischen T3SS-Komponenten zu steuern.

Optogenetische Anwendungen, die bisher vor allem in der eukaryontischen Zellforschung etabliert sind, bieten ein neues Instrument zur präzisen Steuerung von Proteininteraktionen mit Licht. In meiner Doktorarbeit habe ich optogenetische Interaktionsschalter in Bakterien eingebaut, um zelluläre Ereignisse gezielt zu steuern. Die Kombination von optogenetischen Interaktionsschaltern mit einer dynamischen und essentiellen zytosolischen Komponente des T3SS ermöglicht eine reversible räumliche und zeitliche Kontrolle der T3SS-Funktion. Dies bildet die Grundlage für unsere Anwendung LITESEC-T3SS (**L**icht-**i**nduzierte **T**ranslokation von **E**ffektoren durch **S**equestrierung **e**ndogener **K**omponenten des **T3SS**). Dadurch verbessert sich die Nutzung des T3SS als spezifisches Werkzeug für die Proteineinschleusung in eukaryontische Zellen und ermöglicht eine großflächige Anwendung. In dieser Arbeit zeigen wir, dass die Sekretion, sowohl von nativen Effektorproteinen als auch nicht-nativen „Wunschproteinen“, sowie die Translokation von Proteinen in eukaryontische Wirtszellen in den manipulierten Stämmen effizient durch Licht gesteuert werden kann. Als direkte biologische Anwendung stellen wir den Transport pro-apoptotischer Proteine in Krebszellen vor, die zum gezielten Zelltod führen.

Darüber hinaus habe ich das Prinzip der optogenetischen Proteinassoziation und -dissoziation genutzt, um dynamische zelluläre Ereignisse des T3SS, mit Fokus auf der Dynamik des zytosolischen Komplexes und einer möglichen direkten Verbindung zur Funktion, näher zu untersuchen.

1 Introduction

1.1 The genus *Yersinia* – model systems for invasive pathogenic bacteria

The genus *Yersinia* comprises a collection of diverse Gram-negative, rod-shaped and sometimes pathogenic bacteria, with the three well-known human pathogen representatives *Y. pseudotuberculosis*, *Y. pestis* and *Y. enterocolitica* (McNally *et al.*, 2016). From an evolutionary point of view, *Y. enterocolitica* and *Y. pseudotuberculosis* have evolved independently from a joint predecessor of pathogenic *Yersinia*, while *Y. pestis,* the plague causing species*,* evolved from *Y. pseudotuberculosis* in a very short time span of 5,000 - 20,000 years (Wren, 2003). Like other pathogenic *Enterobacteria* such as *Salmonella, Shigella* or *Escherichia coli, Yersinia* receives survival benefits from being in contact with host cells (Bottone, 1999). Interestingly, even when *Y. enterocolitica* and *Y. pseudotuberculosis* evolved independently, they are causing highly similar diseases of gastroenteritis. After ingestion via contaminated food or water, the bacteria developed mechanisms to cross and resist the acidic environment of the digestion tract (De Koning-Ward and Robins-Browne, 1995). Inside human hosts, they enter the lymphatic system through the M cells in the small intestines (Heroven and Dersch, 2014) and cause local infections by multiplying and persisting inside the tissues and can further disseminate to the liver and spleen or the lymph nodes (Wren, 2003) (Figure 1). *Y. pestis* has a different infection way, mainly transmitted through the bite of a flea vector into rodents but also humans, where the bacteria cause local infections in lymphatic vessels under the skin (*bubonic plaque*), but can also further disseminate into the lung and cause the fatal and highly infectious *pneumonic plague* (Wren, 2003) (Figure 1).

The species of *Y. enterocolitica* can be divided into several biogroups according to their biochemical characteristics, including a highly pathogenic biogroup 1B and a non-pathogenic biogroup 1A, due to loss of the plasmid of *Yersinia* virulence (pYV) (Cornelis *et al.*, 1987; Wren, 2003). This pYV plasmid is the basis of the pathogenicity of *Yersinia* (Bottone and Mollaret, 1977). Beside genes for adhesion (*YadA*) that are needed for host cell contact (Uliczka *et al.*, 2011), the pYV plasmid encodes for a type III protein secretion system (T3SS), which translocates native effector proteins (so called *Yersinia* outer proteins (Yops)) in a one-step transport mechanism from the bacterial cytosol to the cytoplasm of recipient eukaryotic host cells (Rosqvist, Magnusson and Wolf-Watz, 1994). *Y. enterocolitica* is able to grow at temperatures from 4° C to 42° C, while the optimal metabolic activity and growth is at ~ 28° C (Cornelis *et al.*, 1987). At 37° C, the host body temperature, *Y. enterocolitica* stops its growth and motility and starts with expression of virulence genes located on the pYV plasmid.

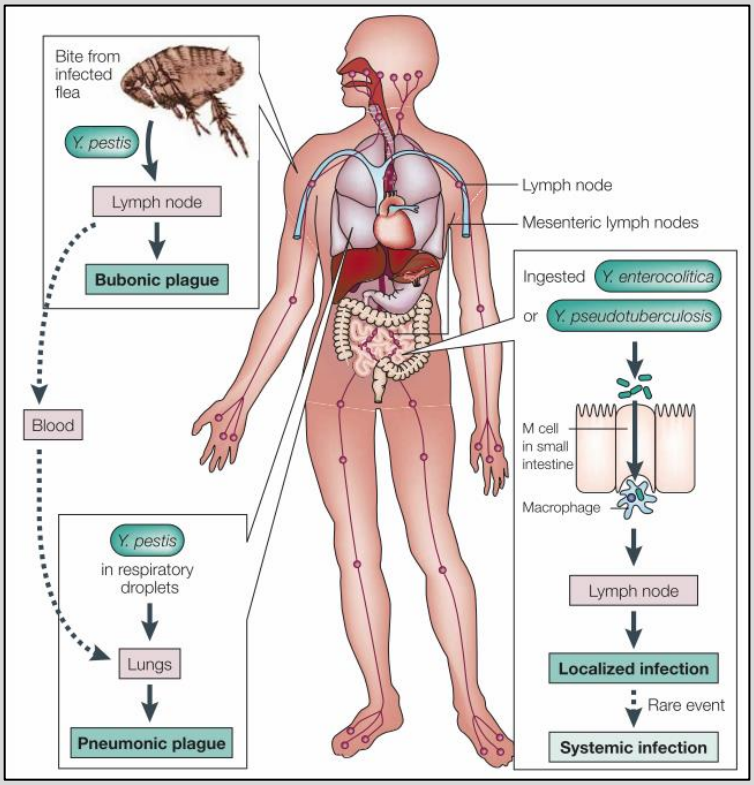

Figure 1: Infection pathways of *Yersinia* (Wren, 2003) – *Y. pestis* is mainly transmitted via a flea vector and can cause local infections in the lymph nodes (bubonic plague) or further disseminate to the lungs and cause the highly infectios pneumonic plague, which can be transmitted via aerosol droplets across humans. *Y. enterocolitica* and *Y. pseudotuberculosis* are ingested via contaminated food or water and enter the lymphatic system through the M cells in the small intestines, where they cause local infections and in rare cases disseminate to tissues such as the liver or spleen to cause systemic infections.

1.2 Secretion systems in Gram-negative bacteria

Bacteria have evolved different ways to secrete proteins into and beyond their cytoplasmic membrane. The two most common secretory ways are the general secretion pathway (Sec), where unfolded proteins are transported across the bacterial membrane and the twin-arginine pathway (Tat) that mediates the secretion of folded substrates (Natale, Brüser and Driessen, 2008). Substrates that are secreted by those pathways either remain in the inner membrane, such as membrane proteins, or are released into the periplasm and can be further secreted outside the bacterial cell in a Sec- or Tat-dependent way. In Gram-negative bacteria, this Sec- or Tat-dependent secretion occurs via a two-step mechanism and is coupled with a bacterial secretion system (T2SS, T5SS) that transports proteins from the periplasm across the outer membrane (Green and Mecsas, 2016). Additionally, Gram-negative bacteria have evolved further secretion machineries that span the two bacterial membranes (T1SS) and an additional host membrane (T3SS, T4SS, T6SS) (Figure 2). T8SS and T9SS are specific for some Gram-negative bacterial species and not further mentioned here.

Those secretion systems allow a one-step, Sec- or Tat-independent transport of substrates from the bacterial cytosol either to the outside environment or into host cells (Green and Mecsas, 2016). Therefore, substrates either need an N- or C-terminal signal that is recognized by the secretion system and mediates secretion. Gram-positive bacteria use a T7SS, which was first discovered in *Mycobacterium tuberculosis,* for extracellular protein secretion and virulence (Stanley *et al.*, 2003). The purpose of protein secretion, mediated by secretion systems, range from the interaction with eukaryotic (T3SS) or bacterial/eukaryotic (T6SS) host cells, mainly to translocate toxic effector proteins into hosts, to non-pathogenic interbacterial interactions like DNA-conjugation or -uptake (T4SS) (Green and Mecsas, 2016).

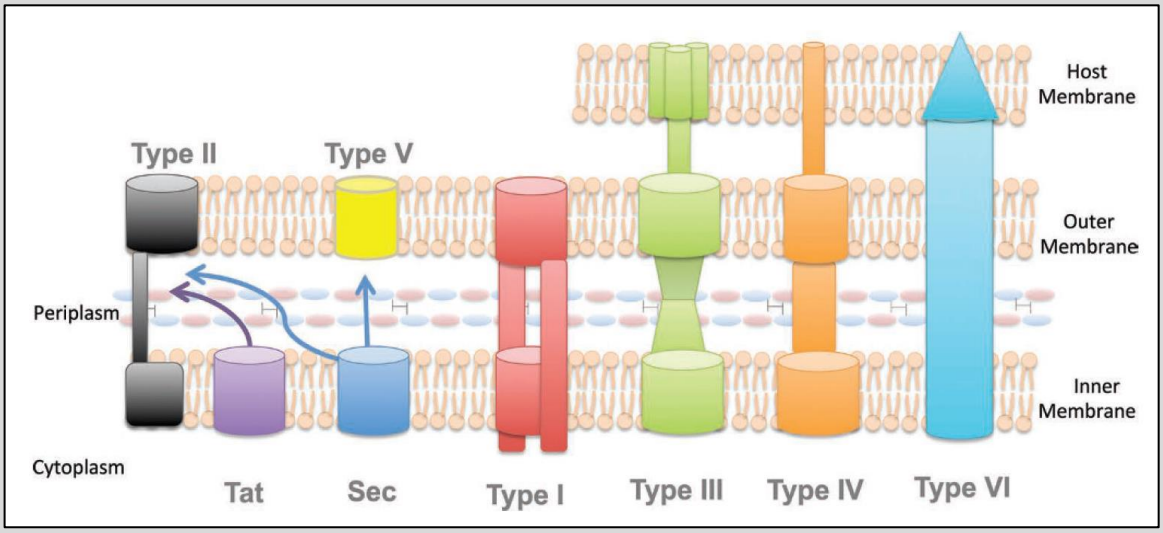

Figure 2: Secretion systems in Gram-negative bacteria (Green and Mecsas, 2016) – Protein secretion across the bacterial inner membrane is either mediated by the Tat-pathway (folded proteins) or Sec-pathway (unfolded proteins). Proteins in the perisplasm can be further secreted outside the bacterial cell by the T2SS (folded substrates) or the T5SS (unfolded substrates). Gram-negative bacteria have also evolved secretion systems that transport substrates in a one-step, Sec- or Tat-independent way from the bacterial cytosol either outside the cell (T1SS) or into host cells (T3SS, T4SS, T6SS). The underlying mechanism of substrate secretion is very diverse among the different secretion systems.

1.3 The type III secretion system (T3SS) of *Y. enterocolitica*

Bacterial type III secretion systems (T3SS), also termed “injectisomes”, are found in many Gram-negative pathogens or symbionts of plants or animals (Buttner, 2012). These systems span the two bacterial membranes and an additional host membrane and mediate the translocation of unfolded effector proteins into corresponding eukaryotic host cells. T3SS are essential for interaction with the host organism and are mainly used to manipulate host immune responses (e.g. pathogenic *Salmonella* or symbiotic *Rhizobia*) or signal transduction pathways (Buttner, 2012; Deng *et al.*, 2017) (Figure 3B).

Some bacterial species like *S. enterica* or *Y. enterocolitica* biotype 1B even comprise two distinct T3SS, mostly associated with more efficient virulence. Hereby, the *Yersinia* Ysa-T3SS, which is closely related and shares sequence homology to the *Salmonella* SPI-1 T3SS (Foultier *et al.*, 2001), plays an important role in early infection, ranging from early colonization of the intestinal tissue to host cell entry (Fàbrega and Vila, 2012). On the other hand, the *Salmonella* SPI-2 T3SS that is mainly used for the maintenance of a *Salmonella*-containing vacuole (SCV) and following replication inside host cells (Figueira and Holden, 2012; Deng *et al.*, 2017) differs to the *Yersinia* Ysc-T3SS, which is used for resistance against macrophages and to suppress immune responses (Fàbrega and Vila, 2012; Deng *et al.*, 2017). In other *Y. enterocolitica* biotypes that are lacking the Ysa-T3SS, host cell attachment and entry is mainly mediated by the outer-membrane proteins YadA and Invasin, while the T3SS is mainly used to prevent phagocytosis by macrophages (Uliczka *et al.*, 2011; Bliska *et al.*, 2013).

1.3.1 Structure of the *Y. enterocolitica* T3SS

The structure of the T3SS injectisome is highly conserved and evolutionary related to the flagellum (Diepold and Armitage, 2015). The injectisome spans the inner and the outer membrane of the bacterium and the cell membrane of the host organism and consists of several substructures including a needle with translocon tip, an inner and outer membrane anchored base plate, an inner membrane export apparatus and a cytosolic part with a six-pod wheel-like structure that differs in structure and function from the flagellar C-ring homologue ((Buttner, 2012; Deng *et al.*, 2017; Hu *et al.*, 2017) (Figure 3A).

The needle of the injectisome in *Y. enterocolitica* is composed of a single protein, SctF[1], which polymerizes and forms a hollow conduit with a length of 30-70 nm (Galán *et al.*, 2014) (Figure 3A). To prevent that SctF polymerizes already in the cytosol prior to the outside assembly of the needle, YscG[1] and YscE act as chaperones and bind to SctF until contact with the export apparatus (Sun *et al.*, 2008). The translocator protein SctA locates at the tip of the needle complex and facilitates injection of a pore forming complex (SctE/SctB) into the host membrane (Broz *et al.*, 2007; Ekestubbe *et al.*, 2016) (Figure 3A).

The base plate consists of two membrane ring-structures, the outer membrane ring, which is formed by SctC and the inner membrane ring, which is composed of SctD and SctJ. SctC (secretin), mediated by the pilotin SctG, forms highly stable ring structures in the bacterial outer membrane (Worrall *et al.*, 2016).

[1] The Sct nomenclature correspond to the unified nomenclature, proposed by (Hueck, 1998) and later evolved by (Wagner and Diepold, 2020), whereas the Ysc nomenclature is *Yersinia*-specific. An overview table is provided in the supplementary.

These membrane rings act as a membrane anchor for the injectisome (Izoré, Job and Dessen, 2011).

The inner membrane export apparatus is composed of five hydrophobic structural proteins (SctR, -S, -T, -U, -V) that are highly conserved between the injectisome and the flagellum (Wagner *et al.*, 2010). SctR, -S, and -T mainly consist of transmembrane helices, whereas the structure of SctU and SctV also include large cytosolic domains (Galán *et al.*, 2014; Wagner *et al.*, 2018). It was shown that substrates interact with the cytosolic domain of the export apparatus protein SctV and that it is therefore directly involved in the secretion process (Portaliou *et al.*, 2017).

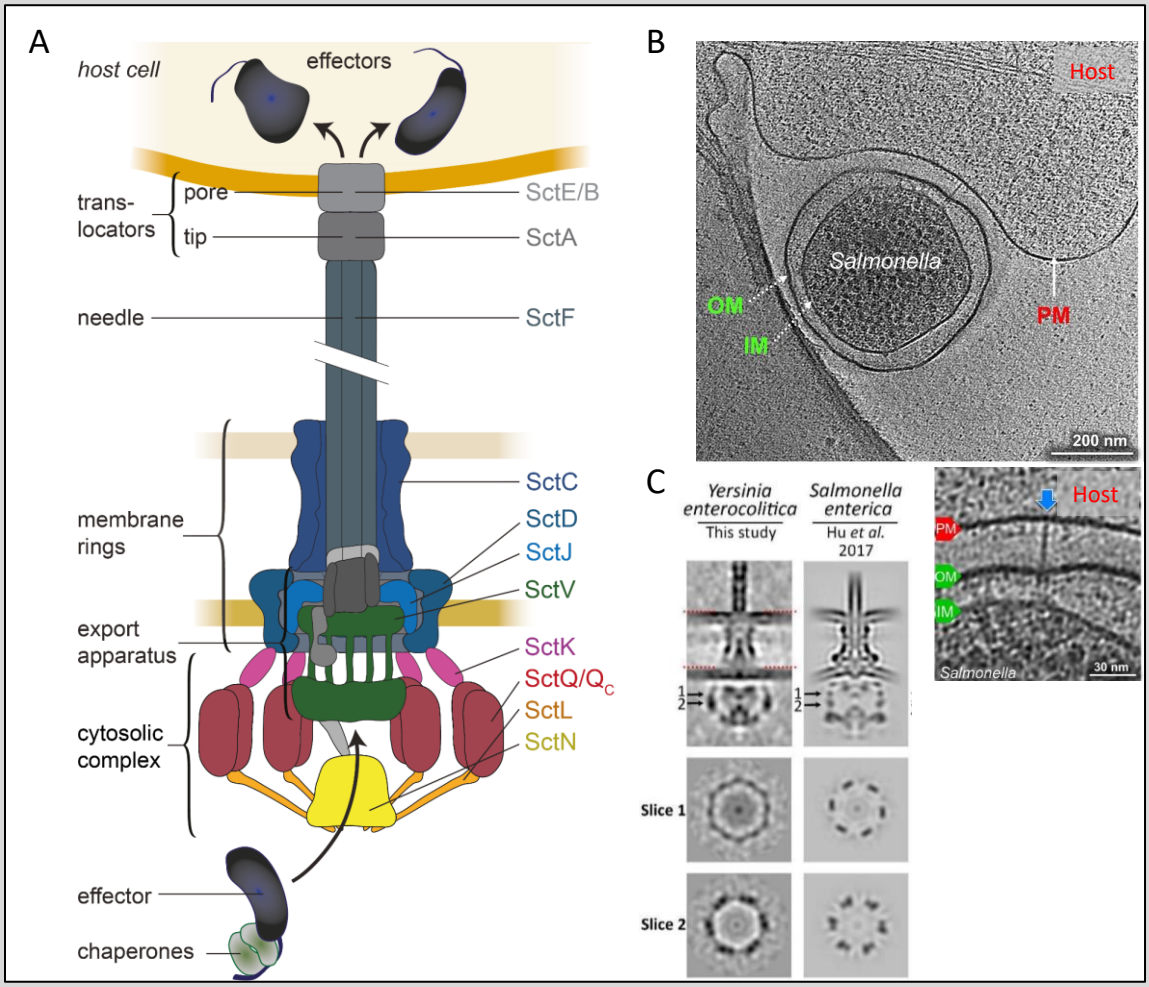

Figure 3: Structure and Function of the T3SS – (**A**) Structural segmentation of the T3SS injectisome of *Y. enterocolitica* with its predestined function, effector translocation into a eukaryotic host cell, indicated – derived and modified from (Diepold et al., 2017). (**B**) A *Salmonella* minicell with an assembled T3SS in close contact to a host cell – in larger scale and in focus. Outer membrane (OM), inner membrane (IM), plasma membrane (PM), blue arrow indicate T3SS attached to the host PM. Images were obtained with cryo-ET (Park et al., 2018). (**C**) Subtomogram average structures of a *Y. enterocolitica* T3SS and a S. enterica T3SS obtained by cryo-FBI-ET data. Arrows and numbers indicate positions of different orthogonal slices with view on the cytosolic complex. (Berger et al., 2021)

Five interacting proteins at the cytosolic interface are essential for the function of the T3SS (Diepold et al., 2015). The ATPase SctN, which shares structural similarity with the flagellar homologue FliI (Buttner, 2012), is activated by oligomerization (Pozidis et al., 2003) and is involved in substrate recognition, chaperone release and unfolding of substrates prior to secretion (Akeda and Galán, 2005). SctL negatively regulates the activity of the ATPase and links it to the rest of the cytosolic complex (Blaylock et al., 2006). SctQ, $SctQ_C$ (a C-terminal fragment of SctQ that is homologous to the small flagellar C-ring component FliN (Bzymek, Hamaoka and Ghosh, 2012)) and SctK, which connects the cytosolic complex to the inner membrane ring protein SctD, compose the six-pod wheel-like structure at the cytosolic interface to the export apparatus (Hu et al., 2017) (Figure 3A, C). In *Salmonella sp*. these proteins have been shown to act as a sorting platform, which binds chaperones and determines the order of protein secretion (Lara-Tejero et al., 2011). Currently, there is no evidence for a similar function in *Y. enterocolitica*, however, it was suggested that a defined secretion hierarchy seem to be crucial for the T3SS function (Lara-Tejero *et al.*, 2011). Further information about the cytosolic complex is described in the section 1.4.

1.3.2 Regulation of the T3SS in *Y. enterocolitica*

Formation of the injectisome is often induced by temperature. In *Yersinia*, incubation at 37°C, which mimics the host body temperature, leads to expression of the main T3SS transcription activator VirF/LcrF by the dissociation of the DNA repressor YmoA, which blocks its transcription at lower temperatures (de Rouvroit, Sluiters and Cornelis, 1992). This initiates the expression of the T3SS genes on the pYV virulence plasmid and assembly of the injectisome. At the same time, the bacteria downregulate the expression of flagellar proteins and therefore their motility, when a temperature shift to 37° C occurs (Fàbrega and Vila, 2012). Secretion of effector proteins is suppressed and initially triggered upon host cell contact or low Ca^{2+} in the environment (Cornelis, 2006), which can be easily mimicked in vitro by the depletion of Ca^{2+} with EGTA. It was shown that the synthesis of new substrates is directly linked to the secretion (Cornelis *et al.*, 1998) and an addition of Ca^{2+} can reversibly block secretion and therefore also decreases the expression of new substrates again (Bölin and Wolf-Watz, 1988). This Ca^{2+}-sensing ability of the T3SS is mediated through a plug-complex, consisting of SctW-TyeA-YscB-SycN that can sterically block secretion upon Ca^{2+} sensing (Yother and Goguen, 1985; Dewoody, Merritt and Marketon, 2013). How this mechanism works in detail remains unclear. *Y. enterocolitica* is also able to return to growth after the secretion process (Milne-Davies *et al.*, 2019).

1.3.3 Assembly of the T3SS in *Y. enterocolitica*

The assembly of the injectisome can be divided into a Sec-dependent and a T3SS-dependent way (Figure 4). The assembly of the membrane associated components of the injectisome are mediated by the Sec-pathway (Green and Mecsas, 2016; Tsirigotaki *et al.*, 2017) and starts with the outer membrane ring protein SctC that assembles with the help of the pilotin SctG (Burghout *et al.*, 2004). Then the inner membrane ring (SctD and SctJ) of the basal body follows (Figure 4 - 2, 3) (Diepold *et al.*, 2010). These proteins show a conserved wedge-shaped fold, which is a common ring-building motif for the inner and outer membrane rings and is thought to facilitate ring assembly (Spreter *et al.*, 2009). In parallel, the export apparatus assembles at the inner membrane and docks to the inner membrane ring of the basal body (Figure 4 - 4, 5) (Wagner *et al.*, 2010). The proteins of the cytosolic complex are highly dependent on each other and only assemble to the export apparatus as an entire complex (Figure 4 - 6). Single deletions of one cytosolic component lead to a secretion deficiency and no complex assembly of the other cytosolic components (Diepold *et al.*, 2010, 2017).

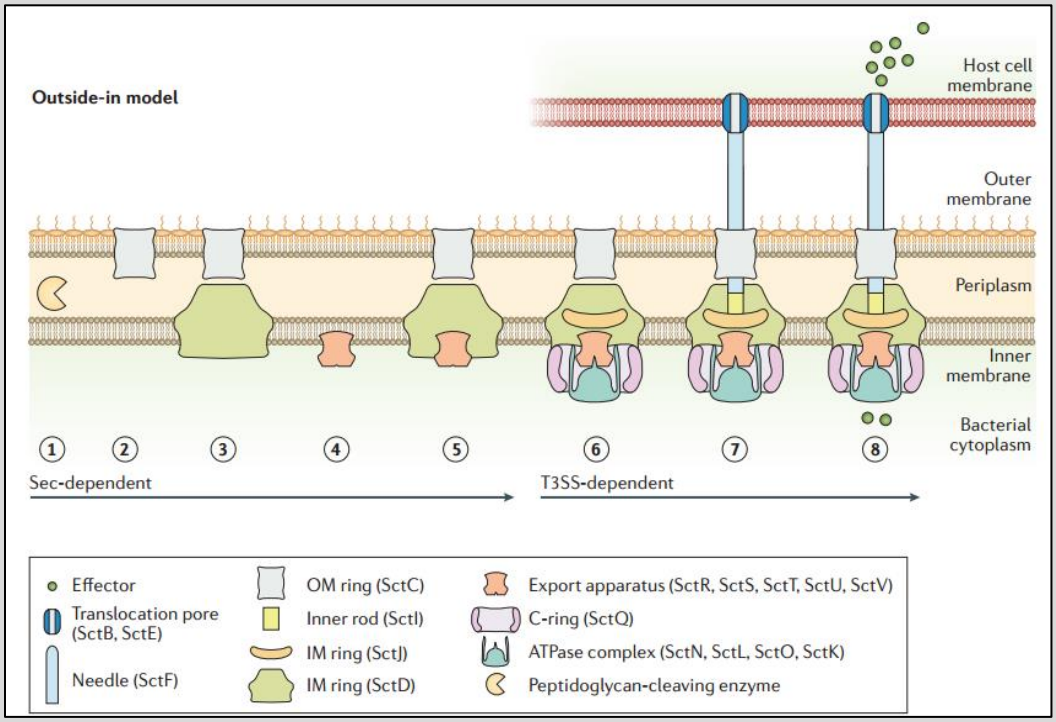

Figure 4: Outside-in model of the T3SS assembly in *Y. enterocolitica* (Deng et al., 2017) – The secretin (SctC) localizes to the outer membrane and forms the outer membrane ring through oligomerization (step 2). After that the inner membrane ring (SctD, SctJ) assembles and bridge with the outer membrane ring (step 3). Then the export apparatus assembles to the inner membrane and link to the cytosolic domain of the inner membrane ring (step 4, 5). The assembly of the membrane associated proteins requires the Sec-pathway. At later stages, the cytosolic components that consists of ATPase (SctN), negative regulator (SctL) and C-ring (SctQ, -Q_C, -K) assemble as a full complex to the export apparatus (step 6). The secretion starts with early substrates (needle and inner rod proteins (SctF)), then followed by middle substrates (translocators (SctA, -E, -B)) (stage 7) and at the end late substrates (effectors – green) (stage 8) (Deng et al., 2017).

After the assembly of the cytosolic complex, the T3SS-dependent export starts and assembly continues with the early substrates SctI (inner rod), SctF (needle) and SctP (needle length regulator). The inner rod is a small connector between the export apparatus and the needle, with an inner diameter of around 20 Å that assembles at the inside of the basal body, on which the needle forming proteins SctF assembles and extends (Loquet *et al.*, 2012). After the assembly of the needle, middle substrates are secreted that form the needle tip (SctA). Upon contact to a host cell, the translocon pore based on SctB/E assemble in the host membrane and builds a closed channel from the bacterial cytosol via the injectisome into the host cell (Figure 3B). Following, late substrates (effectors) are exported in a one-step mechanism through the injectisome into host cells. Those effectors fulfill different purposes, ranging from host cell invasion (SipA/B/C in *Salmonella*) to the prevention of inflammatory responses (YopH/M/T) and defending against macrophages (YopO/E) in *Yersinia* (Navarro, Alto and Dixon, 2005; Hajra, Nair and Chakravortty, 2021).

1.4 Function and Dynamics of the cytosolic complex and its link to effector secretion

The cytosolic components of the T3SS (SctQ, $SctQ_C$, SctK, SctL, SctN) form a complex at the cytosolic interface of the injectisome (Figure 5A) and are essential for its function (Akeda and Galán, 2005; Diepold *et al.*, 2015). The C-terminal fragment of SctQ, $SctQ_C$, which is not included in the structural model in Figure 5A, was shown to be an essential cytosolic component for the injectisome in *Yersinia enterocolitica* (Bzymek, Hamaoka and Ghosh, 2012). In *Salmonella* it has been shown that $SctQ_C$ is not essential (Bernal *et al.*, 2019), but enhances the function of the injectisome and that parts of the cytosolic components can already interact with a proposed stoichiometry (SctQ-2$SctQ_C$) or (SctQ-2$SctQ_C$-SctL, SctQ-2$SctQ_C$-2SctL-SctN) prior to assembly at the injectisome as a full complex (Bernal *et al.*, 2019). The fact that cytosolic sub-complexes exist are already shown before within a flagellum model in *E. coli* (Gauthier and Finlay, 2003) or for the injectisome (Johnson and Blocker, 2008). Diepold and colleagues have further shown that the binding properties between the cytosolic components differ between secreting and non-secreting conditions, and that binding properties are heavily influenced by deletions within the cytosolic complex (Diepold *et al.*, 2017) (Figure 5C). It is important to mention that the studies of cytosolic interactions were mainly done by immunoblot or native mass spectrometry and a way to investigate those binding properties in the living cell is still missing. One component of the cytosolic complex (SctQ) was also shown to be a highly dynamic interface, in which molecules permanently exchange and shuttle between the cytosol and the T3SS (Figure 5) and it was shown that this exchange is linked to protein secretion (Diepold *et al.*, 2015, 2017).

While the binding properties of the cytosolic components are stronger under non-secreting conditions, their dynamic behavior is increased under secreting conditions (Diepold *et al.*, 2015, 2017). For the flagellum it has been shown that several parts of the T3SS display dynamic behaviors such as FliM (SctQ) (Fukuoka *et al.*, 2010), FlhA (SctV) (Li and Sourjik, 2011) or FliI (SctN) (Bai *et al.*, 2014) (reviewed in (Tusk, Delalez and Berry, 2018)), whereas for the injectisome, SctQ is the only published component that displays a dynamic nature. A similar dynamic behavior for the other cytosolic components still needs to be investigated. In *S. typhimurium*., the cytosolic complex has been proposed to contribute to substrate selection and transport during needle assembly and translocation of effectors and is therefore termed as a "sorting platform" (Lara-Tejero *et al.*, 2011). Also in the flagella T3SS, a model was proposed where a $FliH_2I$ ($SctL_2N$) complex binds chaperones and acts as a dynamic carrier (Bai *et al.*, 2014; Wagner *et al.*, 2018). But there are doubts that the cargo shuttle is directly linked to effector secretion, since the measured export rate of up to ~ 60-200 molecules per second (Enninga *et al.*, 2005; Schlumberger *et al.*, 2005; Ittig *et al.*, 2015) is way higher than the calculated speed of the cytosolic turnover (half-time t½ of exchange: 68.2 ± 7.9 s for SctQ) (Diepold *et al.*, 2015) – reviewed in (Diepold, 2020).

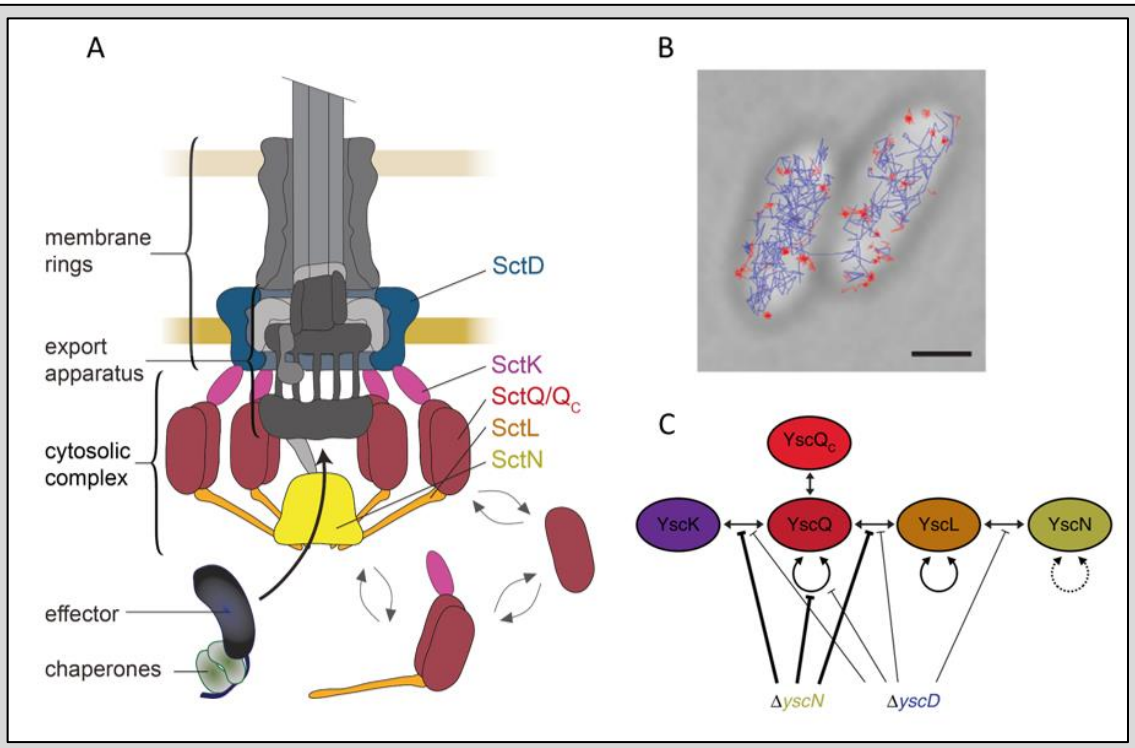

Figure 5: Schematic structure and dynamic properties of the cytosolic T3SS components – (A) Overview of structural T3SS segmentation with focus on its cytosolic components and the dynamic exchange indicated - derived and modified from (Diepold et al., 2017). (B) Cellular distribution of motile (blue) and stationary (red) photoactivatable (PAmCherry)-SctQ molecules in photoactivated localization microscopy. Scale bar, 1 µm (Diepold et al., 2015). (C) Schematic representation of interactions of the cytosolic T3SS components investigated by immunoblot and the influence of YscN (SctN) / YscD (SctD) -knockouts (Diepold et al., 2017).

A similar model that the cytosolic complex acts as a sorting platform in other organism, carrying a T3SS injectisome, still has to be proven (Diepold *et al.*, 2015; Wagner *et al.*, 2018). The dynamic nature of the cytosolic complex of the T3SS (Diepold *et al.*, 2017) and its important role for the assembly and function of the injectisome provided a new way to govern this dynamic function and therefore control the activity of the T3SS injectisome, for example by introducing an optogenetic dimerization switch (Lindner *et al.*, 2020) (Figure 6, 9).

1.5 The T3SS as a protein delivery tool[2]

As a machinery evolved to efficiently translocate proteins into eukaryotic cells, the T3SS has been successfully used to deliver cargo proteins into various host cells for different purposes such as vaccination or immunotherapy (antigen delivery), gene editing (nuclease delivery e.g. Cre) or reporter protein delivery (e.g. ß-lactamase, eGFP) (reviewed in Bai et al, 2018). Different short N-terminal secretion signals can be used to mark cargo proteins for delivery by the T3SS (Wilharm *et al.*, 2004). Since substrates have to be unfolded prior to secretion, the folding stability of the protein cargo is important for T3SS delivery and large or stably folded proteins like GFP are exported to a lower degree (Jacobi *et al.*, 1998; Ittig *et al.*, 2015). This can lead to a jamming effect where cargos block or slow down secretion of the injectisome. However, the T3SS injectisome is not restricted to specific target cells and inject effector proteins into host cells as soon as the bacteria are in contact to the host cell (J Pettersson *et al.*, 1996). Lack of target specificity is therefore a main obstacle in the further development and application of this method (Felgner *et al.*, 2017; Walker, Stan and Polizzi, 2017), especially for potentially powerful applications such as the delivery of pro-apoptotic proteins into living cancer tissue (Bai *et al.*, 2018; Lindner *et al.*, 2020). By establishing an optogenetic interaction switch to govern the dynamic function of the T3SS cytosolic components, such a desired control was achieved by our lab (Lindner *et al.*, 2020) and is presented in this thesis.

1.6 Optogenetic control of protein interactions[3]

Optogenetic systems offer a toolbox for combining optical and genetic methods to temporally achieve precise gain or loss of function in living cells or tissues. They allow for easy and often reversible manipulation of protein functionality and localization (Guglielmi, Falk and De Renzis, 2016), metabolism (Berry and Wojtovich, 2020), intracellular interaction of enzymes and

[2] Passages from this paragraph were stated in (Lindner *et al.*, 2020)

[3] Passages from this section are also included in a Review (Lindner & Diepold 2021 – which is currently under review)

substrates (Huang *et al.*, 2020), or processes like gene expression (de Mena, Rizk and Rincon-Limas, 2018) with light.

Its fast and easy tunability gives light an advantage over chemical inducers and other environmental triggers like pH or temperature and enables more precise spatiotemporal control (Deisseroth, 2011; Liu *et al.*, 2018), even up to a single-cell level (Chait *et al.*, 2017). These abilities can give optogenetic approaches further advantage over knockdown, overexpression, or mutant strain analysis, which often display slower activation and a broader effect (Toettcher, Voigt, *et al.*, 2011). Most optogenetic tools are based on modified opsins, rhodopsins or phototropins, which are light-inducible proteins that undergo a conformational change upon irradiation. In most cases, the direct reaction to illumination occurs in a bound chromophore cofactor (e.g. flavin-adenine-di/mono-nucleotide (FAD/FMN) for LOV-based systems or phycocyanobilin (PCB) for phytochrome-based systems (Liu *et al.*, 2018)), which features the conjugated electron system that can absorb photons. This light-triggered change in conformation is then transmitted to the apoprotein and can change the properties of the proteins and can lead to association/dissociation with an interaction partner or partial folding/unfolding of the protein structure (Endo and Ozawa, 2017).

Optogenetic systems can be mainly grouped and characterized by their purpose of either intermolecular or intramolecular control, consisting of one or more interacting proteins (Figure 6). Optical dimerization systems for intermolecular control often consists of derived light-oxygen-voltage (LOV) domains, chryptochromes or phytochromes and a modified interaction partner whose affinity is strongly altered upon irradiation with light of a certain wavelength (Pathak et al., 2014; Kawano et al., 2015; Wang et al., 2016; Zimmerman et al., 2016). Mutations of specific amino acids in the optogenetic proteins can modulate the binding affinity and corresponding dissociation or association rate from a few seconds up to several minutes (Kawano et al., 2015; Wang et al., 2016; Zimmerman et al., 2016). These systems mostly exploit light-induced homo- and hetero-dimerization or -dissociation, although examples of light-induced oligomerization exist. This basic principle can be used to directly activate (or, in special cases, inactivate) protein function via dimerization, to recruit a fused POI to its site of action, or, conversely, to sequester it from its site of action, such as the cytosol.

Optogenetic applications have been predominantly characterized in eukaryotic cells. Nevertheless, the utilization of optogenetics to investigate biological processes also in bacteria has markedly increased. The purpose of optogenetic control in bacteria can be mainly sub grouped into transcriptional control (I), second messenger conversion (II) and post-translational control (III) (Figure 6).

To date, the most established application of optogenetic systems in prokaryotes is the light-mediated control of gene expression (Liu *et al.*, 2018; Baumschlager and Khammash, 2021). Beyond that, optogenetic control was applied for bacteria to mediate the conversion of second messenger molecules like cAMP/cGMP (Ryu *et al.*, 2010) or c-di-GMP (O'Neal *et al.*, 2017), with applications ranging from the control of biofilm formation (Mukherjee *et al.*, 2018) to the control of host cell infection by *P. aeruginosa* in mouse models (Xia *et al.*, 2021). The establishment of optogenetic dimerization switches in bacteria, with the purpose of post-translational protein control (Figure 6) to control cellular events like the function of the T3SS remains, up to date, exclusive for the study presented in this thesis (Lindner *et al.*, 2020). Other optogenetic applications in bacteria that aim at post-translational control, either were applied for outer surface attachment in bacteria (Chen and Wegner, 2017; Sentürk *et al.*, 2020), the assembly of cytotoxic or bacteriostatic multimers (Giraldo, 2019; He *et al.*, 2021), as a method for protein purification (Tang *et al.*, 2021) or for intramolecular control (Lee *et al.*, 2008).

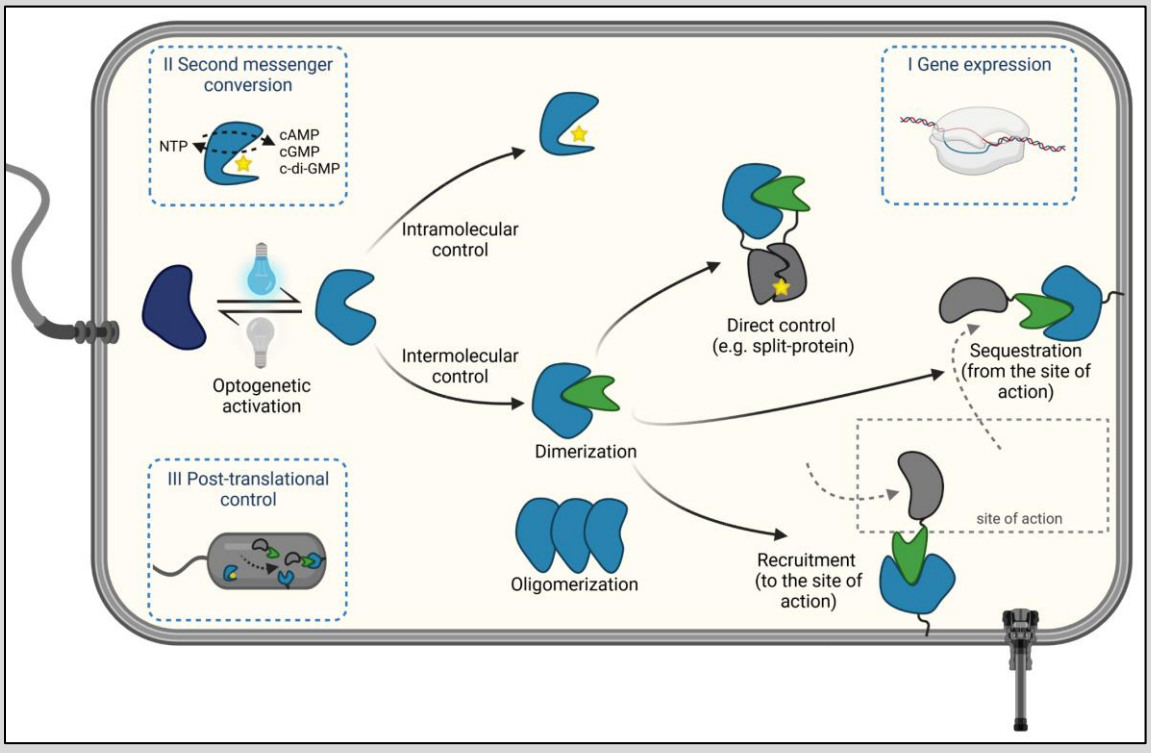

Figure 6: Optogenetics in bacteria – Main pathways (center) and application classes (corners, blue dashed boxes) of main optogenetic control purposes in bacteria. Light induces a conformational change of an optogenetic protein that can then either lead to an intramolecular control, e.g. by the activation of an enzymatic place or is used in intermolecular control for either dimerization of an optogenetic interaction switch or oligomerization of several optogenetic proteins. Light-dependent dimerization can be applied for direct protein control (e.g. a split-protein), to seqester a protein of interest from a specific site of action to disable its function or vice versa via recruitment to a site of action. Figure was created with biorender.com (Lindner & Diepold 2021 review – submitted under review)

1.7 Optogenetics in combination with the *Y. enterocolitica* T3SS – preliminary results based on my Master work

The following results and parts of the introduction were derived from and presented in my Master thesis (Lindner – 2018). For a better understanding of the topic, some findings that are relevant for the thesis are presented in this section.

1.7.1 The establishment of optogenetic interaction switches in *Y. enterocolitica*

During the Master studies, I screened for suitable optogenetic systems that can be established in *Y. enterocolitica* with the final aim to control the dynamics and therefore the function of the T3SS. After preliminary experiments, we decided for two different optogenetic interaction switches, whose action upon illumination is opposed, allowing to specifically release a bait protein (and, subsequently, to activate processes that require its presence) in the dark or upon illumination, respectively (Table 1).

(i) The LOVTRAP system (LOV), which consists of the two interacting proteins LOV2 (a photo sensor domain from *Avena sativa* phototropin 1) and Zdk1 (Z subunit of the protein A of *B. subtilis*). These proteins are bound to each other in the dark. After irradiation with blue light (~ 480 nm wavelength) LOV2 undergoes a conformational change and Zdk1 is released with a following re-association half time rate of ~100 s (Wang *et al.*, 2016) in the dark. Wang and colleagues have further investigated several point mutations of the LOV2 binding domain, which modulate the binding affinity and dissociation rate ranging from 2 to 500 seconds (Wang *et al.*, 2016).

(ii) The iLID system consists of two interacting proteins: iLID (AsLOV2-SsrA), which is derived from an LOV2 domain from *Avena sativa* phototropin 1 and a binding partner, in our case SspB_Nano. This combination was chosen because of its fast recovery half-time of 90-180 s. The iLID system has a low binding affinity in the dark and a high affinity upon irradiation with blue light (Guntas *et al.*, 2015; Zimmerman *et al.*, 2016). In both optogenetic systems, release and binding of the interaction switches is reversible for several times (Kawano *et al.*, 2015; Wang *et al.*, 2016; Zimmerman *et al.*, 2016).

Table 1: Overview of optogenetic systems
Optogenetic systems that were investigated in previous work and later applied for the LITESEC-T3SS

System	System class and properties	Used *anchor* and bait proteins	Dissociation rate after activation	Reference	Application in LITESEC-T3SS
LOV	Light-released Dark = bound state Light = unbound state	*LOV2* Zdk1	~ 100 s	(Wang *et al.*, 2016)	Release of bait protein by blue light → activation of secretion
iLID	Dark-released Dark = unbound state Light = bound state	*iLID* SspB_Nano	~ 90-180 s	(Guntas *et al.*, 2015)	Tethering of bait protein by blue light → suppression of secretion

1.7.2 Protein stability and functionality of optogenetic systems in *Y. enterocolitica*

Since optogenetic dimerization switches were never applied for direct post-translational protein control by sequestration and release (Figure 6) in bacteria, and one comparable study was just published recently (Tang *et al.*, 2021), we started with preliminary experiments. As a "proof of principle" and to characterize the chosen optogenetic dimerization switches iLID and LOVTRAP in *Y. enterocolitica,* we first tested the dynamics of the interaction (Figure 7) and protein expression and stability of the resulting fusion proteins (Figure 8). Because bacteria are less compartmentalized than eukaryotic cells, we designed a system where the larger interaction partner of the dimerization switch was anchored to the inner membrane (IM) and further named *anchor* (Table 1, Figure 7). This was achieved by fusing the optogenetic protein to an extended transmembrane helix domain (TMH) of the TatA protein (Gohlke *et al.*, 2005). The additional amino acids Valine and Leucine were chosen to extend and stabilize the membrane anchor (F. Alcock, Oxford, personal communication) (Figure 7). The smaller cytosolic interaction partner of the interaction switch (further named *bait*) was fused to either fluorescence proteins for initial proof of principle experiments (Figure 7, 8) or essential cytosolic T3SS components (Figure 9) (Lindner *et al.*, 2020) and the wild type (wt) T3SS protein was replaced by the fusion protein via allelic exchange on the genome. Depending on the system, the two optogenetic interacting proteins (anchor + bait) are unbound/bound to each other prior to illumination (Table 1). Upon illumination with blue light (~ 480 nm), the optogenetic anchor domain undergoes a conformational change and the binding or release of the optogenetic bait protein is induced (Guntas *et al.*, 2015; Wang *et al.*, 2016) (Figure 7). To assess the function and efficiency of the established optogenetic interaction switches as sequestration systems in prokaryotes, and to monitor their dynamics, we visualized the components of iLID- and LOV-based sequestration systems (Guntas *et al.*, 2015; Wang *et al.*, 2016) in live *Y. enterocolitica* by time-lapse fluorescence microscopy (Figure 7).

To this aim, the localization of mCherry-bait fusions was determined by fluorescence microscopy in live *Y. enterocolitica* expressing the corresponding unlabeled anchor proteins. Beforehand, we confirmed by fluorescence microscopy that mCherry fused to the membrane anchor (LOV2) showed a strict membrane localization (Figure 8A), indicating a stable fusion and a functional TMH motif. Bacteria were grown in the dark and the distribution of the bait proteins was monitored before and after a short pulse of blue light (Figure 7). To quantify the change of the normalized fluorescence signal across the bacterial cells, line scans were performed (Figure 7C, D). For the iLID system, the fluorescence signal of the bait-mCherry was cytosolic in the pre-activated state, partly shifted to the membrane after illumination and returned to the cytosol within the next 3 minutes (Figure 7A, C), indicating the dynamics of this system in *Y. enterocolitica*. In contrast, for the LOVTRAP-based sequestration system, the fluorescence signal of the bait-mCherry was mainly membrane localized in the pre-activated

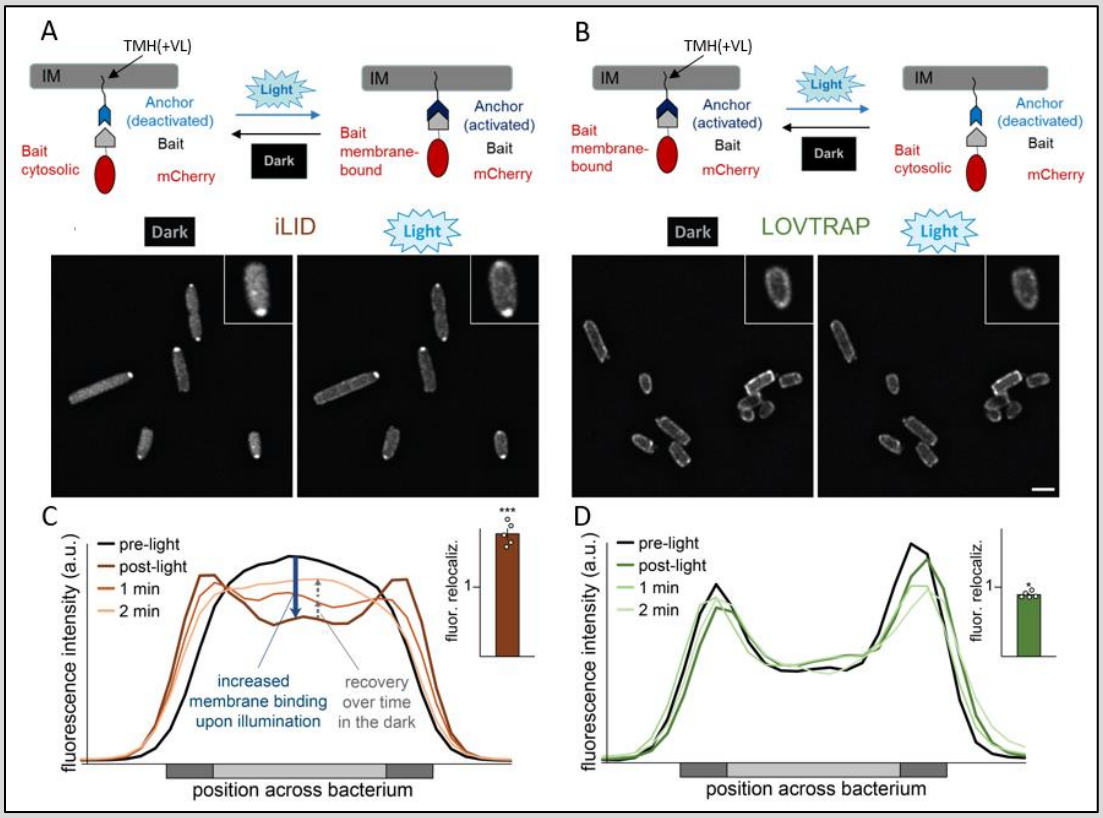

Figure 7: Activation and recovery kinetics of the optogenetic systems – (**A**/**B**) Optogenetic principle scheme and fluorescence micrographs of mCherry-labeled bait proteins in the iLID-based (A) and LOVTRAP-based (B) sequestration systems, before (left) and directly after (right) illumination with blue light. Size bar, 2 µm. (**C**/**D**) Representative fluorescence signal quantification across bacteria over time in the iLID-based (C) and LOVTRAP-based (D) sequestration systems; dark grey: membrane, light grey: cytosol. Insets: Fluorescence relocalization factor (fluor. reloc. = $R_{post\text{-}light}/R_{pre\text{-}light}$, where R represents the ratio of fluorescence intensities at the membrane and in the cytosol, before and after illumination, respectively), based on 121-131 line scans across five cells per strain and time point. Single data relocalization factor values (n=5) indicated by circles. Bars show mean values; error bars represent the standard deviation, *, p=0.0002; ***, $p=6.2*10^{-6}$ against no relocalization in a two-tailed homoscedastic t-test (Lindner et al., 2020).

state und could not be efficiently released into the cytosol after illumination (Figure 7B, D), suggesting that the majority of bait protein remained bound to the anchor even after illumination (Lindner *et al.*, 2020). Because Wang et al., 2016 mentioned that the concentration of the membrane anchor has to be 5-10 times higher than the bait (for eukaryotic applications), we also tested the protein expression and stability of both, membrane anchor (MA) and bait fused to mCherry in a Western blot (Figure 8B). LOVTRAP based anchor and bait displayed nearly similar expression level, whereas for the iLID system the anchor was expressed ~ five times higher than the bait protein (Figure 8B). All fusion proteins showed a specific cleavage pattern, probably due to internal translational start sites of the mCherry (Carroll *et al.*, 2014). We further tested the protein stability of the cytosolic bait fused to the essential cytosolic T3SS component SctQ (results show stable fusions without mCherry) (Diepold *et al.*, 2017) (Figure 8C, D), which is also the basis of the LITESEC-system, presented in this thesis (Lindner *et al.*, 2020).

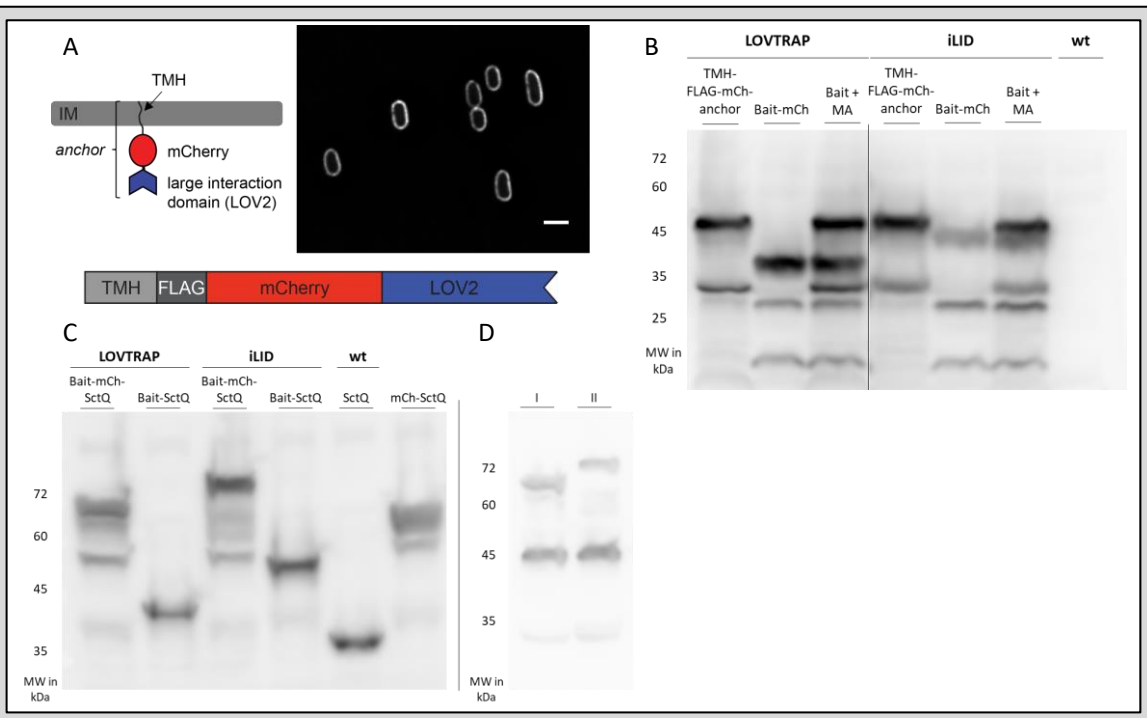

Figure 8: Protein expression and stability of the optogenetic systems – (**A**) Schematic representation of the membrane anchor (MA) protein and distribution in the bacterial cell visualized by fluorescence microscopy. Scale bar 2 µm. (Lindner et al., 2020) (**B**) Western blot using an anti-mCherry antibody for total cell samples of 3 × 10^8 bacteria to test stability and expression of the MA (TMH-FLAG-mCh-anchor) and the bait-mCh of both optogenetic systems LOVTRAP: i) TMH-FLAG-mCh-LOV2 (exp. molecular weight (MW): 47.6 kDa) ii) Zdk1-mCh (exp. MW: 33.8 kDa) and iLID: i) TMH-FLAG-mCh-iLID (exp. MW: 48.7 kDa) ii) SspB_Nano-mCh (exp. MW: 39.7 kDa). dHOPEMTasd (wt) was used as a control. Left side, MW marker in kDa. (**C**) Western blot using an anti-SctQ antibody for total cell samples of 2 × 10^8 bacteria to test stability and expression of the bait in combination with mCh and/or SctQ. LOVTRAP: i) Zdk1-mCh-SctQ (exp. MW: 67.8 kDa) ii) Zdk1-SctQ (exp. MW: 40.8 kDa) and iLID: : i) SspB_Nano-mCh-SctQ (exp. MW: 73.7 kDa) ii) SspB_Nano-SctQ (exp. MW: 46.7 kDa). dHOPEMTasd (wt-SctQ (exp. MW: 34 kDa)) and mCh-SctQ (exp. MW: 61 kDa) were used as a control. Left side, molecular weight marker in kDa. (**D**) Western blot anti-mCh of MA-mCh and bait-mCh-SctQ of LOVTRAP (I) and iLID (II) in combination.

2 Aim of the study

Current research actively aims to establish the T3SS as a specific tool for protein delivery into eukaryotic host cells. The big disadvantage up to now was the lack in target specifity and controllability of the function, since the T3SS injects substrates as soon as it attaches to a host cell. Previous findings that revealed a dynamic behavior of cytosolic parts of the injectisome and showed a direct link between dynamics and the secretion function disclose a potential new way to govern this function, for example with optogenetic interaction switches. Those optogenetic interaction switches with the aim of post-translational protein control were up to now mainly established in eukaryotic cells. The main aim of my PhD was the incorporation of optogenetic interaction switches to the cytosolic part of the T3SS of *Y. enterocolitica* with the purpose to control the dynamic behavior of an essential cytosolic T3SS component and therefore the T3SS function (effector secretion) with light. In addition to the functional control, which advances the T3SS as a specific tool for protein delivery and introduces spatiotemporal controllability, optogenetics also allows to control and investigate dynamic processes *in vivo*. The principle of optogenetic mediated protein interactions was used to investigate open questions in the field of the T3SS, with focus on the dynamic function and a potential link to substrate shuttling.

3.1 Results – Part I – LITESEC-T3SS – Light-controlled protein delivery into eukaryotic cells with high spatial and temporal resolution

With the establishment of optogenetic interaction switches inside *Y. enterocolitica* and the combination of those with essential cytosolic components of the T3SS, we created a tool, with which we can control cellular events like the secretion of proteins and translocation into eukaryotic host cells in a resolved spatiotemporal manner with light.

The following Result – Part I and the corresponding Discussion – Part I were mainly adapted from the LITESEC publication, at some points modified and extended.

The following study has been peer-reviewed and published in Nature Communications (2020).

Lindner F, Milne-Davies B, Langenfeld K, Stiewe T, Diepold A. LITESEC-T3SS - Light-controlled protein delivery into eukaryotic cells with high spatial and temporal resolution. Nat Commun. 2020 May 13;11(1):2381. doi: 10.1038/s41467-020-16169-w.

Author contributions:

I have created and characterized the LITESEC strains and performed the majority of the experiments and data analysis.

Bailey Milne-Davies established the infections assays and participated in experiments and data analysis. Data especially presented in Figure 15 were obtained with a great help of Bailey.

Katja Langenfeld provided the eukaryotic cell culture and participated in infection assays.

Thorsten Stiewe provided methodological input and reagents for analysis of apoptosis.

Andreas Diepold conceived the study and experimental setup, participated in data analysis and wrote the manuscript.

3.1.1 Abstract

Many bacteria employ a type III secretion system (T3SS) injectisome to translocate proteins into eukaryotic host cells. Although the T3SS can efficiently export heterologous cargo proteins, a lack of target cell specificity currently limits its application in biotechnology and healthcare. In this study, we exploit the dynamic nature of the T3SS to govern its activity. Using optogenetic interaction switches to control the availability of the dynamic cytosolic T3SS component SctQ, T3SS-dependent effector secretion can be regulated by light. The resulting system, LITESEC-T3SS (**L**ight-**i**nduced **t**ranslocation of **e**ffectors through **s**equestration of **e**ndogenous **c**omponents of the **T3SS**), allows rapid, specific, and reversible activation or deactivation of the T3SS upon illumination. We demonstrate the light-regulated translocation of heterologous reporter proteins and induction of apoptosis in cultured eukaryotic cells. LITESEC-T3SS constitutes a new method to control protein secretion and translocation into eukaryotic host cells with unparalleled spatial and temporal resolution.

3.1.2 Controlling the activity of the T3SS with light

To establish a method to control protein translocation by the T3SS, we took advantage of recent findings that some essential cytosolic T3SS components constantly exchange between the cytosol and the injectisome (Diepold *et al.*, 2015, 2017). We combined one of these components, SctQ, with one partner domain of an optogenetic interaction switch (bait), and targeted the other partner domain to the bacterial inner membrane (anchor). We reasoned that this might allow to control SctQ availability in the cytosol, and therefore T3SS-based protein export and translocation into host cells, by light. To be able to control T3SS activity in both directions, we developed two complementary systems (Figure 9B):

A) LITESEC-supp, a system that confers suppression of T3SS-dependent protein translocation by blue light illumination

B) LITESEC-act, a system that confers activation of T3SS-dependent protein translocation by blue light illumination

Both systems rely on two interaction partners, which we have engineered:

(i) A membrane-bound **anchor protein**, which is a fusion between the N-terminal transmembrane helix (TMH) of a well-characterized transmembrane protein, *Escherichia coli* TatA, extended by two amino acids (Val-Leu) for more stable insertion in the IM, a Flag peptide for detection and spacing, and the larger domain of the respective optogenetic interaction switches, iLID (for LITESEC-supp) or LOV2 (for LITESEC-act). The resulting fusion proteins, **TMH-FLAG-iLID / TMH-FLAG-LOV2**, are expressed from a plasmid.

(ii) A **bait protein**, which consists of a fusion between the essential cytosolic T3SS component SctQ and the smaller domain of the interaction switches, SspB_Nano (LITESEC-supp) / Zdk1 (LITESEC-act). Based on the estimated cellular SctQ concentration of 1-2 µM (approximately 1000 molecules per bacterium) (Diepold *et al.*, 2017), we chose SspB_Nano, which has a dissociation constant of 132 nM in the light and 4.7 µM in the dark, over SspB_Micro and SspB_Milli, which have roughly 10 and 1000 times higher dissociation constants (Zimmerman *et al.*, 2016). The resulting fusion proteins, **SspB_Nano-SctQ / Zdk1-SctQ**, replace the wild-type SctQ protein on the *Y. enterocolitica* virulence plasmid by allelic exchange of the genes (K Kaniga, Delor and Cornelis, 1991).

Co-expression of both interaction partners provides the basis for light-controlled protein translocation by the T3SS (Figure 9). For the iLID-based LITESEC-supp system, the bait protein is tethered to the membrane anchor in the light, and SctQ is therefore not available to interact with the T3SS (Figure 9B). As SctQ is essential for the function of the T3SS, protein secretion by the T3SS is prevented (Figure 9C). In the dark, the bait protein is not bound to the membrane, and can therefore functionally interact with the T3SS, allowing protein secretion by the T3SS (Figure 9A). Conversely, in the LOV-based LITESEC-act system, the bait protein is released from the membrane upon irradiation with blue light, licensing protein secretion by the T3SS.

3.1.3 Inhibition of protein secretion by light in LITESEC-supp

Can we use LITESEC to control T3SS secretion by light? We first tested the LITESEC-supp1 system, designed to suppress T3SS protein secretion upon illumination, in an *in vitro* protein secretion assay under conditions that usually lead to effector secretion (presence of 5 mM EGTA in the medium) (Cornelis, 2006). The control strain lacking the membrane anchor secreted effectors irrespective of the illumination (Figure 10A - lanes 4-5), confirming the functionality of the used SctQ fusion protein. Strikingly, the LITESEC-supp1 system showed a high level of secretion when grown in the dark, but strongly reduced secretion when grown under blue light (Figure 10A - lanes 6-7). To quantify the difference of secretion under light and dark conditions, we define the light/dark secretion ratio (L/D ratio) as the ratio of secretion efficiency under light and dark conditions. For the LITESEC-supp1 system, the L/D ratio was 0.28, with normalized secretion efficiencies of 23.5 ± 8.1% and 85.1 ± 5.1% in light and dark conditions, respectively. Protein secretion in wild-type *Y. enterocolitica* was not influenced by the used illumination (Figure 10B), and the blue light had no influence on growth of *Y. enterocolitica* (Figure 10C).

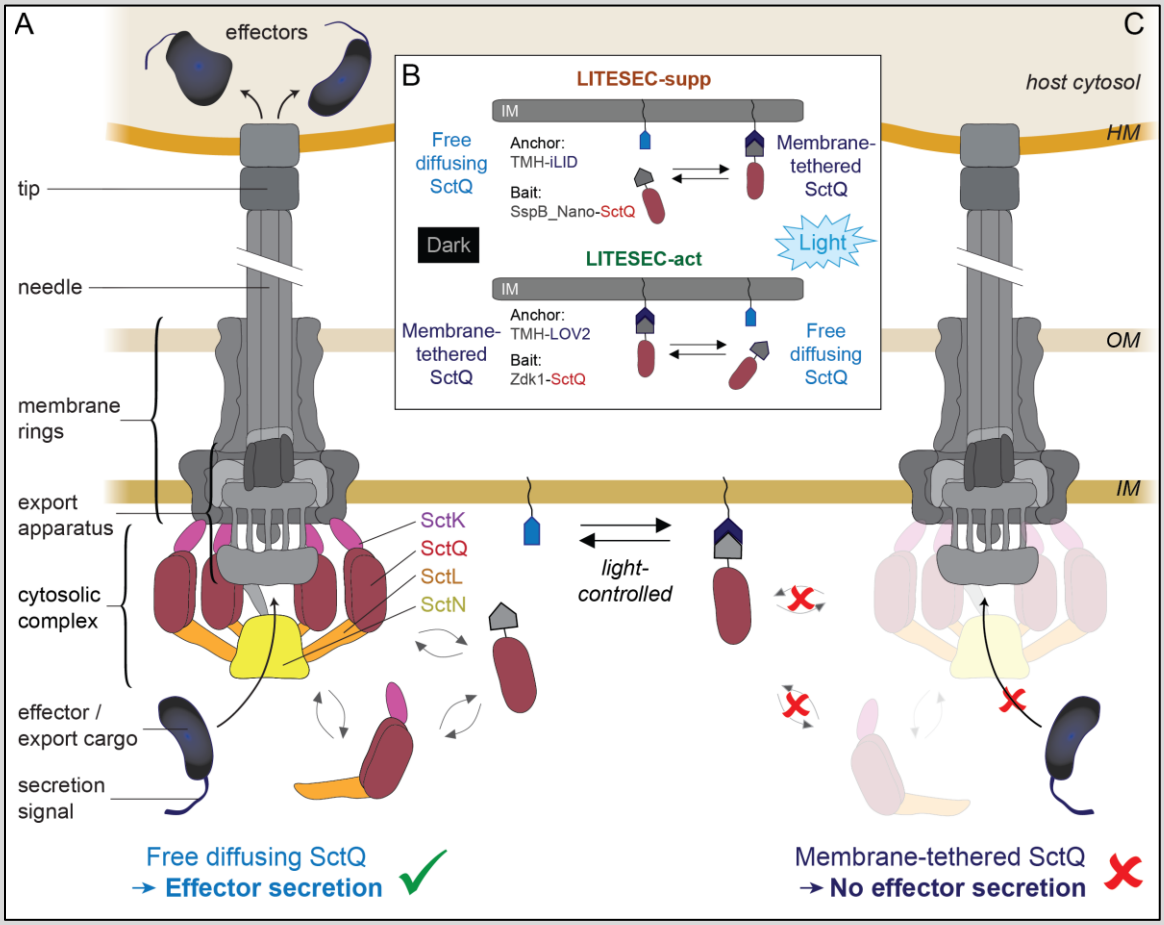

Figure 9: Working principle of the LITESEC systems – light-controlled activation and deactivation of protein translocation by the type III secretion system – (**A**) Schematic representation of the active T3SS injectisome - modified from (Diepold et al., 2017). Left side, main substructures; right side, dynamic cytosolic T3SS components. Effector translocation by the T3SS is licensed by the functional interaction of the unbound bait-SctQ fusion with the T3SS. (**B**) Different states of the bait and anchor proteins in dark and light conditions. In the LITESEC-supp system (top), the bait protein, a fusion of the smaller interaction switch domain SspB_Nano and the essential T3SS component SctQ, is tethered to the inner membrane (IM) by a membrane anchor, a fusion of a transmembrane helix (TMH) and the larger interaction switch domain, iLID, in the light, and gets released in the dark. Conversely, in the LITESEC-act system (bottom), the bait protein, a fusion of the smaller interaction switch domain, Zdk1, and the essential T3SS component SctQ, is tethered to the membrane anchor, a TMH fusion of the larger interaction switch domain, LOV2, in the dark, and gets released by illumination. (**C**) Sequestration of the bait-SctQ fusion protein to the membrane prevents effector secretion. HM, host membrane; OM, bacterial outer membrane; IM, bacterial inner membrane.

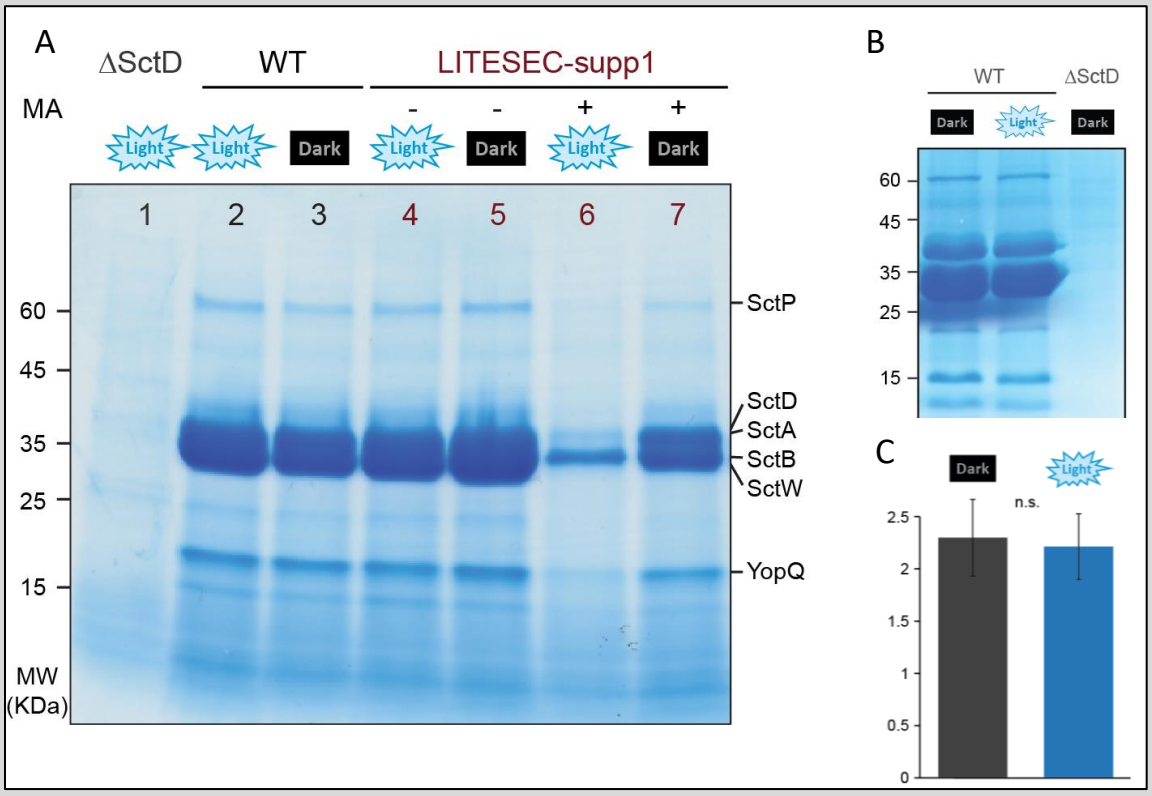

Figure 10: Secretion of effector proteins by the type III secretion system can be controlled by light – (**A**) In vitro secretion assay showing light-dependent export of native T3SS substrates (indicated on the right) in the LITESEC-supp1 strain. Proteins secreted by $3*10^8$ bacteria during a 180 min incubation period were precipitated and analyzed by SDS-PAGE. A strain lacking the membrane anchor (MA), the wild-type strain ΔHOPEMTasd and the T3SS-negative strain ΔsctD were used as controls. MW, molecular weight in kDa. (**B**) In vitro secretion assay showing export of T3SS substrates in the indicated strains (WT, wild-type; ΔsctD, T3SS-negative control) in dark or light (constant low-level illumination of ~ 1 mW cm-2 at λ=488 nm) conditions, as indicated. Proteins secreted by $3*10^8$ bacteria during a 180 min incubation period were precipitated and analyzed by SDS-PAGE. Left side, molecular weight in kDa. (**C**) Average optical density at 600 nm of wild-type cultures in secreting conditions after 180 min in dark conditions (grey, left) or light conditions (blue, right) as used in the optogenetics experiments. N=3 optical density values from independent experiments; single data points indicated by circles. Error bars display standard deviation; n.s., no statistically significant difference (p=0.77 in a two-tailed homoscedastic t-test).

3.1.4 Improvement of LITESEC-act functionality

We next tested the LITESEC-act1 system, designed for induction of secretion by blue light illumination, and detected only a very weak activation of protein export under light conditions (Figure 11 - lanes 1-2). Based on the fact that secretion was wild-type-like in the absence of the membrane anchor (Figure 11 - lane 7), and the results of the earlier sequestration experiment (Figure 7), we concluded that bait and anchor interact too strongly in the LITESEC-act1 system.

Therefore, we constructed and tested additional versions of the system, using the mutated anchor version V416L, which displays a weaker affinity to the bait (Wang *et al.*, 2016). We hypothesized that a lower anchor/bait expression ratio could additionally lead to more efficient release of the bait and activation of T3SS secretion upon illumination, and expressed the V416L version of the anchor both from the medium-high expression pBAD vector used previously (LITESEC-act2), and a constitutive low-expression vector, pACYC184 (LITESEC-act3). We confirmed that the anchor proteins expressed from the pBAD plasmids show a higher expression level than the anchor proteins expressed from the pACYC184 plasmid (Suppl. Figure 1). The response of the resulting LITESEC systems to light was tested in an *in vitro* secretion assay (Figure 11). LITESEC-act2 showed significant induction of protein secretion in the light, compared to dark conditions (L/D ratio 2.16, Figure 11 - lanes 3-4). Even more markedly, LITESEC-act3 allowed an almost complete activation of secretion upon illumination (L/D ratio 4.18, Figure 11 - lanes 5-6). Both new strains retained the low level of export in the dark. We also expressed the anchor for the LITESEC-supp system from pACYC184. The resulting LITESEC-supp2 system showed efficient secretion in the dark and strong suppression of secretion upon illumination (L/D ratio 0.26), comparable with the LITESEC-supp1 system (Figure 11 - lanes 8-11). To additionally characterize the influence of the light intensity, we tested the secretion activity under ambient light conditions, where LITESEC-act3 showed intermediate secretion efficiency, whereas LITESEC-supp2 displayed almost full secretion levels (Suppl. Figure 2).

3.1.5 Light-dependent T3SS activation depends on anchor/bait ratio

To more thoroughly explore the connection between the anchor/bait expression ratio and the responsiveness of the T3SS to illumination, we compared the secretion levels under light and dark conditions for different expression levels of the anchor in the LITESEC-act2 system. The results show that indeed, the light responsiveness of the system (the difference between secretion levels under light and dark conditions) was optimal for intermediate anchor expression levels ~1 (Figure 12). Low expression levels of the anchor showed nearly no controllability of the secretion (Figure 12 - 0.01-0.02% L-ara) , whereas a higher expression level allowed no further secretion activation under dark (on) conditions (Figure 12 – 0.5% L-ara). Those findings are new compared to the observations by other researchers that have established the LOVTRAP system in eukaryotic cells and stated a best working anchor/bait ratio of 5-10 (Wang *et al.*, 2016).

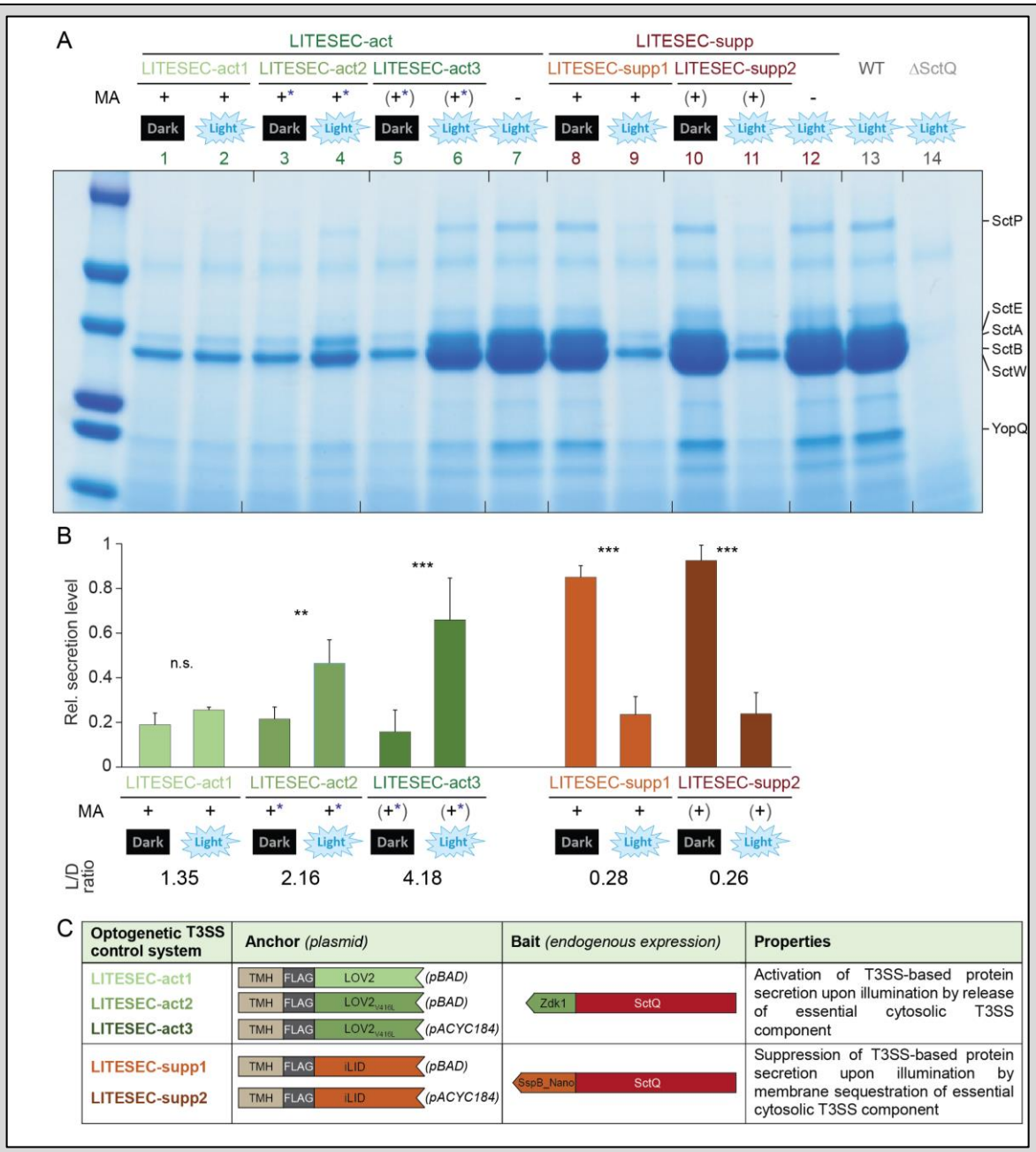

Figure 11: Secretion efficiency and light responsiveness in different versions of the LITESEC strains – (**A**) In vitro secretion assay showing light-dependent export of native T3SS substrates (indicated on the right) in various variants of the LITESEC-act strains (lanes 1-7) and LITESEC-supp strains (lanes 8-12), as indicated below. Proteins secreted by $3*10^8$ bacteria during a 180 min incubation period were precipitated and analyzed by SDS-PAGE. MA, expression level of membrane anchor; +, high expression level; (+), low expression level; -, no expression. *, V416L anchor mutant. (**B**) Quantification of secretion efficiency and light/dark secretion ratio (L/D ratio) for the different LITESEC strains and illuminations indicated above (as in (A)). Secretion efficiency was determined by gel densitometry for the SctE/SctA/SctB/SctW bands and normalized for the secretion efficiency in wild-type strains (lane 13 in (A)). N=3/6/3/4/7 gel densitometry values from independent experiments for both conditions for LITESEC-act1/2/3/-supp1/2, respectively. Bars show mean values; error bars display standard deviation. Single data points indicated by circles. **, $p<0.01$; ***, $p<0.001$ in a two-tailed homoscedastic t-test; n.s., difference not statistically significant (exact values from left to right, $0.08/0.005/4*10^{-5}/4*10^{-4}/5*10^{-8}$). (**C**) Schematic overview of the LITESEC systems and their optogenetic components. All bait proteins are expressed from their native genetic locus. TMH, extended transmembrane helix.

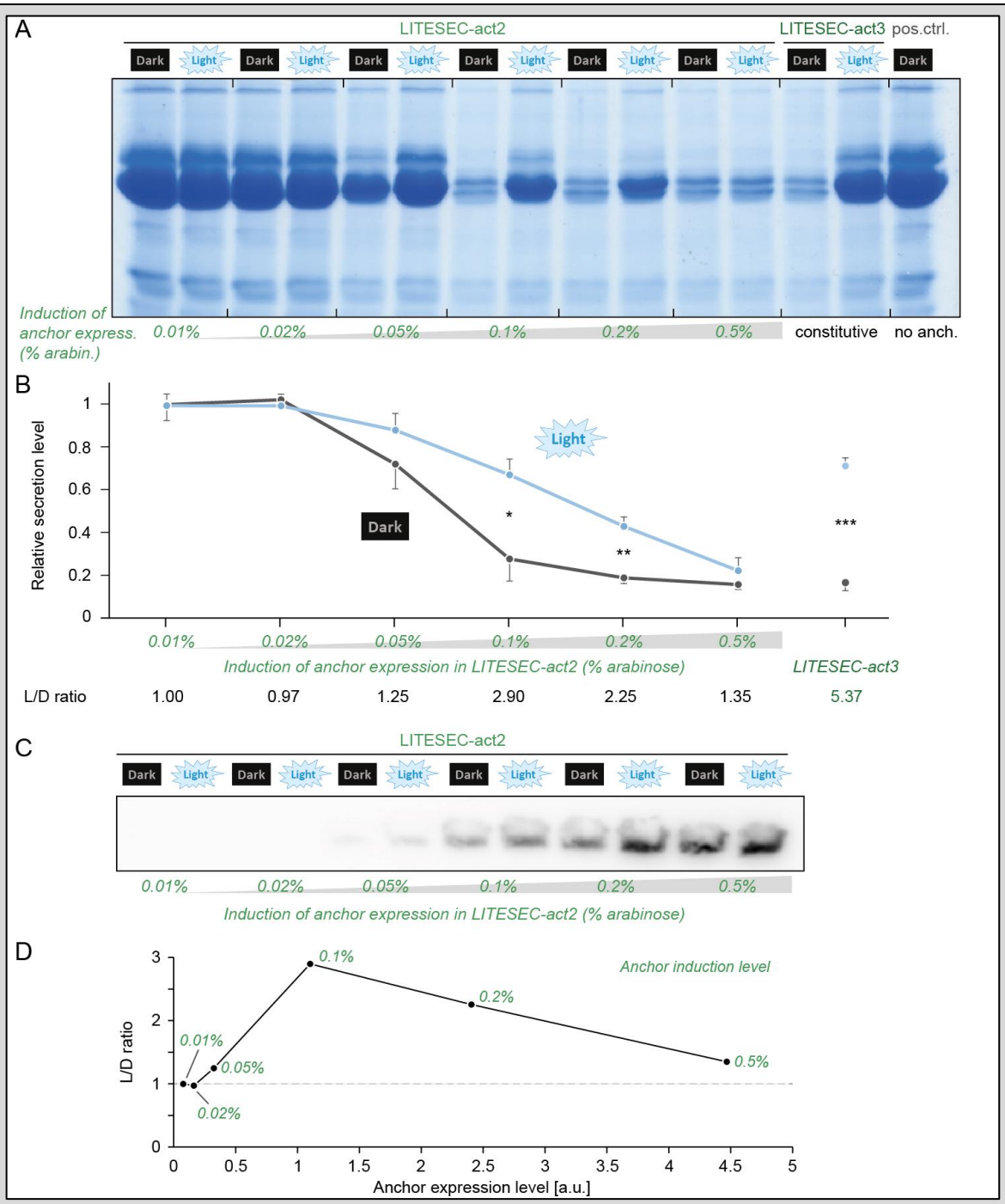

Figure 12: The expression ratio of anchor and bait protein dictates the function and light responsiveness of protein secretion in LITESEC-act2 – (**A**) In vitro secretion assay showing light-dependent export of native T3SS substrates in the LITESEC-act2 strain at different induction levels of anchor expression. (**B**) Quantification of secretion efficiency and light/dark secretion ratio (L/D ratio) for the different expression levels indicated above (as in (A)). N=3 gel densitometry values from independent experiments for LITESEC-act2 induced with 0.02 or 0.2% arabinose and LITESEC-act3; N=4 for all other conditions; error bars display standard error of the mean. */**/***, p<0.05/0.01/0.001 in a two-tailed homoscedastic t-test (exact values from left to right, 0.95/0.67/0.24/0.012/0.009/0.29/3*10-5). (**C**) Western blot anti-FLAG of total cellular protein of $2*10^8$ bacteria in the LITESEC-2 strain at the indicated induction levels and conditions. (**D**) Correlation between light/dark secretion ratio (L/D ratio) as determined in (B) and anchor expression level. Labels indicate anchor induction levels (arabinose concentrations for LITESEC-act2); the grey dashed line denotes an L/D ratio of 1, indicating light-independent secretion.

3.1.6 Light-controlled export of heterologous T3SS substrates

The T3SS-dependent export of heterologous cargo has been shown and applied for many purposes in earlier studies (Ittig *et al.*, 2015; Walker, Stan and Polizzi, 2017; Bai *et al.*, 2018). To confirm that we can control the export of heterologous proteins in the LITESEC strains, we combined the LITESEC-act3 and -supp2 systems with a plasmid expressing a heterologous cargo protein, the luciferase NanoLuc, fused to a short N-terminal secretion signal, $YopE_{1-53}$ (Sory *et al.*, 1995; Köberle *et al.*, 2009; Autenrieth *et al.*, 2010), and a C-terminal FLAG tag for detection. The cargo protein was exclusively exported in light conditions by the LITESEC-act3 strain, and exclusively in the dark by the LITESEC-supp2 strain, whereas export was light-independent in a wild-type strain (Figure 13).

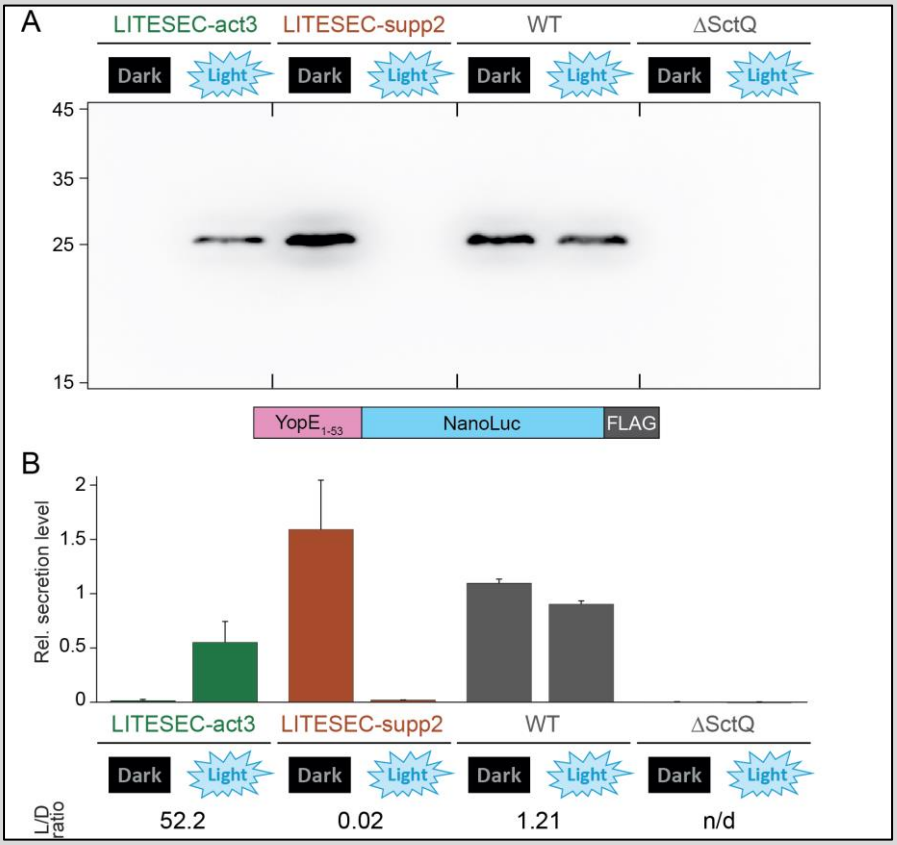

Figure 13: Heterologous cargo can be exported in a light-dependent manner – (**A**) In vitro secretion assay showing light-dependent export of $YopE_{1-53}$-NanoLuc-FLAG (see scheme below; exp. MW, 28.7 kDa), in the indicated strains. Western blot using anti-FLAG antibodies for the culture supernatant of $3*10^8$ bacteria per strain. Left side, molecular weight in kDa. (**B**) Quantification of light-dependent $YopE_{1-53}$-NanoLuc-FLAG export by densitometric analysis of Western blots, normalized by average secretion of the wild-type control (WT), n=3 densitometry values from independent experiments. Single data points indicated by circles, error bars display the standard error of the mean. L/D ratio, ratio of secretion under light and dark conditions.

3.1.7 Kinetics of light-induced T3SS activation and inactivation

How efficiently can the LITESEC system be inactivated, and what are the kinetics of light-induced T3SS activation and deactivation? Protein secretion for the LITESEC-act3 and -supp2 strains was analyzed for bacteria incubated consecutively for 60 min under inactivating conditions (dark for LITESEC-act3, light for LITESEC-supp2), 60 min under activating conditions, and another 60 min under inactivating conditions. After each incubation period, the culture medium was replaced, and a sample was tested for secretion. Secretion of the heterologous export substrate $YopE_{1-53}$-NanoLuc-FLAG in LITESEC-act3 was specifically induced in light conditions, and efficiently suppressed in the dark, whereas LITESEC-supp2 displayed the opposite behavior (Figure 14A). Similar results were obtained for native secretion substrates (Suppl. Figure 3). The WT strains continuously secreted proteins irrespective of the illumination. These results show that the activity of the LITESEC systems can be efficiently toggled. Besides the Western blot, we used a sensitive bioluminescence-based luciferase assay (Westerhausen, Nowak, Torres-Vargas, *et al.*, 2020) to quantify the export efficiency of the reporter protein $YopE_{1-53}$-NanoLuc-FLAG (Figure 14B). We also used this assay to more precisely determine the activation and deactivation kinetics of the LITESEC system under changing illumination. Therefore, we performed a secretion assay, took samples every 4 min and added $CaCl_2$ to the samples to step secretion immediately. In the LITESEC-supp2 strain, secretion of the heterologous substrate dropped to background levels within four to eight minutes after the start of blue light illumination, and recovered within the first four minutes after shifting the bacteria to dark conditions again. The LITESEC-act3 strain showed an increase of secretion activity over 20 minutes in light conditions, and required 12-16 minutes to shut down secretion in the dark (Figure 14C).

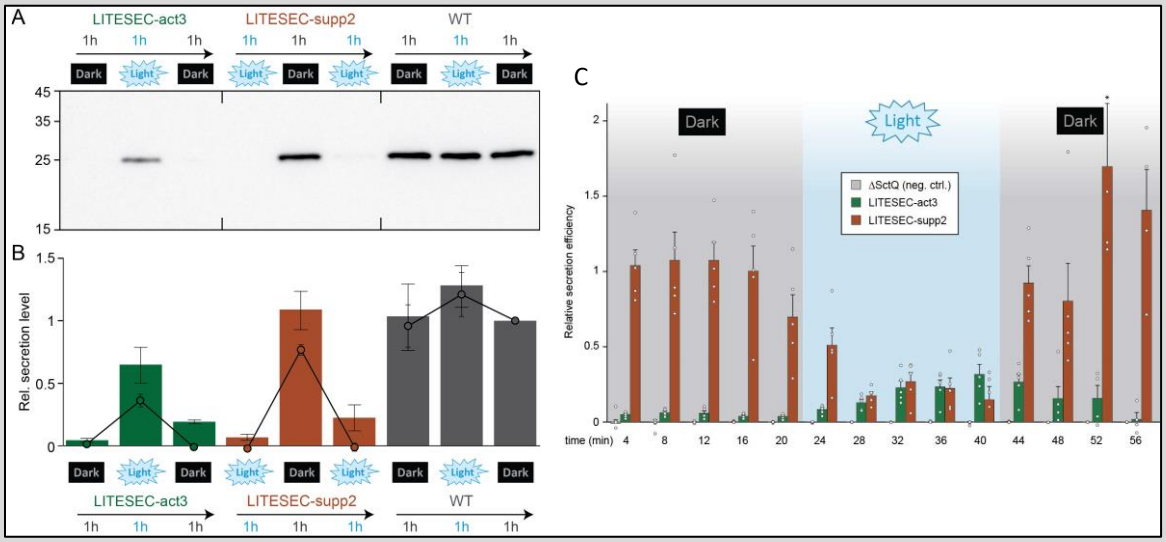

Figure 14: Secretion of effector proteins can be controlled by light over time – (**A**) Export of the heterologous substrate YopE$_{1-53}$-NanoLuc-FLAG in the indicated strains. Secretion-competent bacteria were subsequently incubated under inactivating, activating and inactivating light conditions for 60 min each, as indicated, and the supernatant of 3*10^8 bacteria was analyzed. (**B**) Quantification of the relative export efficiency (normalized to the wild-type level in the third incubation period) of the strains and conditions shown (A) for export of YopE$_{1-53}$-NanoLuc-FLAG as determined by chemiluminescence (bars; n=3 densitometry values from independent experiments, single data points shown as black dots) and immunoblot (circles, continuous line; n=2, single data points shown as grey points); bars show mean values; error bars denote standard deviation. Values for a negative control (ΔsctQ expressing YopE$_{1-53}$-NanoLuc-FLAG) were too small to display in the NanoLuc chemiluminescence assay (<0.001 for all time points). (**C**) Secretion-competent bacteria were incubated under the indicated conditions. Every four minutes, samples were removed, in which secretion was immediately stopped by addition of 10 mM $CaCl_2$, and bacteria were harvested by centrifugation. Secretion of YopE$_{1-53}$-NanoLuc-FLAG was quantified by a luciferase-based luminescence assay in a plate reader. The increase in secretion in comparison to the previous time point was determined and normalized for the secretion of a wild-type strain. Values for the negative control are too small to see in some cases. N=5; single data points displayed as circles (*, one data point off chart at y=2.93), error bars denote the standard error of the mean.

3.1.8 Light-induced protein translocation into eukaryotic host cells

Having found that secretion of heterologous T3SS substrates can be tightly controlled by the LITESEC system, we wanted to employ the LITESEC-act system to control the injection of a cargo protein, YopE$_{1-53}$-ß-lactamase, into eukaryotic host cells upon illumination. Translocation of ß-lactamase can be visualized by the cleavage of a Förster resonance energy transfer (FRET) reporter substrate, CCF2, within host cells (Charpentier and Oswald, 2004; Marketon *et al.*, 2005), which results in a green to blue shift in the emission wavelength. To quantify the light-dependent translocation of the T3SS substrate, we analyzed 671-2694 host cells per bacterial strain and condition. As expected, a wild-type strain translocated the YopE$_{1-53}$-ß-lactamase reporter substrate into a high fraction of host cells irrespective of the illumination. The negative control, the same strain expressing the ß-lactamase reporter without a secretion

signal, displayed a significantly lower rate of blue fluorescence (Figure 15A), showing that translocation was T3SS-dependent. The LITESEC-act3 strain translocated the transporter in a light-dependent manner, leading to a significantly higher fraction of translocation-positive host cells in light than in dark conditions (close to the positive and negative controls, respectively (Figure 15B).

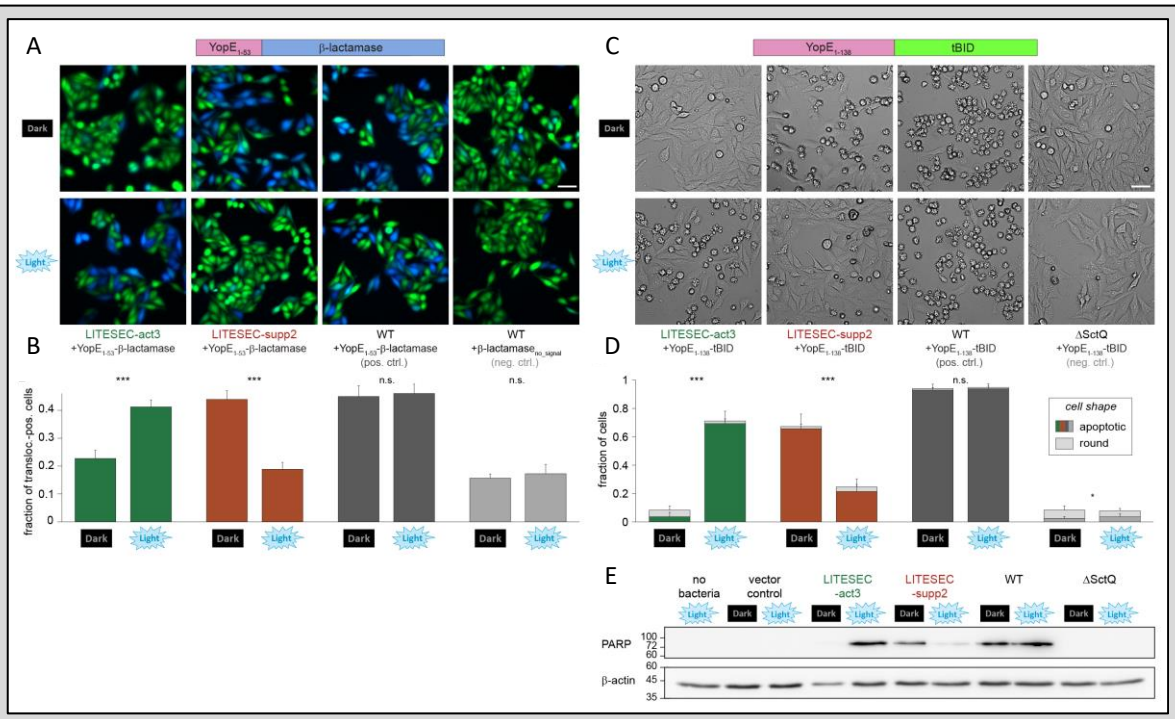

Figure 15: Light-dependent translocation of heterologous cargo into eukaryotic host cells – (**A**) Fluorescence micrographs depicting cultured HEp-2 cells that were incubated with the indicated strains expressing either a heterologous T3SS substrate, YopE1-53-ß-lactamase, or ß-lactamase without a secretion signal as a negative control, for 60 min. Translocation of β-lactamase is detected by cleavage of the intracellular ß-lactamase substrate CCF2 (leading to loss of FRET, and a transition from green to blue fluorescence emission). Scale bar, 50 µm. (**B**) Fraction of ß-lactamase-positive HEp-2 cells used in (A) (blue fluorescence). 2343/2423/2226/2694 cells from 26/28/25/27 fields of view from 3 independent experiments were analyzed for the LITESEC strains under the given conditions from left to right (809/671/995/823 cells from 8/8/10/9 fields of view from 3 independent experiments for the controls). Single data points (percentage of positive cells per field of view) indicated by circles; error bars display the standard error of the mean. ***, p<0.001 in a two-tailed homoscedastic t-test; n.s., difference not statistically significant (exact values from left to right, 6*10-6/2*10-8/0.80/0.65). (**C**) Micrographs depicting cultured HEp-2 cells that have been incubated with the indicated strains expressing a heterologous T3SS substrate, YopE1-138-tBID (Ittig et al., 2015) for 60 min. Translocation of tBID induces apoptosis, which leads to a condensed star-shaped host cell morphology. Scale bar, 50 µm. (**D**) Visual classification of HEp-2 cells used in (C) after infection. 1522/1914/1510/1600/2299/1218/1468/1194 cells from 17/18/17/19/14/13/14/12 fields of view from five independent experiments were analyzed per strain and condition (from left to right). Single data points (percentage of apoptotic cells per field of view) indicated by circles; error bars display the standard error of the mean amongst fields of view. */***, p<0.05/0.001 in a two-tailed homoscedastic t-test; n.s., difference not statistically significant (exact values from left to right, 2*10-25/1*10-15/0.40/0.038). (**E**) Translocation of tBID induces cleavage of poly (ADP-ribose) polymerase (PARP), which was monitored by Western blot analysis of HEp-2 cells used in (C). ß-actin was used as a loading control. Left, molecular weight in kDa.

In contrast, the LITESEC-supp2 strain showed the opposite behavior (Figure 15B). There was no visible reaction of host cells to incubation with T3SS-inactive bacteria, even after extended incubation times (Suppl. Figure 4), indicating little T3SS-independent effects of bacteria on the used eukaryotic cells. Taken together, these results confirm that translocation of heterologous proteins into eukaryotic host cells by the T3SS can be controlled by external light.

3.1.9 Light-induced induction of apoptosis in eukaryotic cells

To directly apply these findings, we established a protocol for the light-controlled induction of apoptosis in host cells, using the pro-apoptotic protein truncated human BH3 interacting-domain death agonist (tBID) as a T3SS substrate ($YopE_{1-138}$-tBID) (Ittig *et al.*, 2015) in the LITESEC strain background. As controls, we used wild-type bacteria and the T3SS-deficient *ΔsctQ* strain expressing the same plasmid. Strikingly, strong apoptosis was induced within one hour after infection, specifically in the HEp-2 cells incubated with bacteria of the LITESEC-act3 strain under light conditions, the LITESEC-supp2 strain under dark conditions, and the positive control (irrespective of the illumination) (Figure 15C, D). To specifically test for the induction of apoptosis, we detected the apoptosis marker Poly (ADP-ribose) polymerase (PARP) by Western blot in the host cells (Figure 15E).

In addition, we tested the spatial resolution of the activation of the LITESEC-act3 by partially blocking light access to an infection plate, and imaging the host cells afterwards. In line with previous results (Figure 15C), apoptosis was strongly induced in infected cells in the illuminated area and a small (0.25 mm) intermediary region likely to have received some diffracted light (Figure 16). Apoptosis induction in dark areas were strongly reduced. In summary, these results provide a clear example for the application potential of the LITESEC system in cell biology and biotechnology and highlights its spatial controllability.

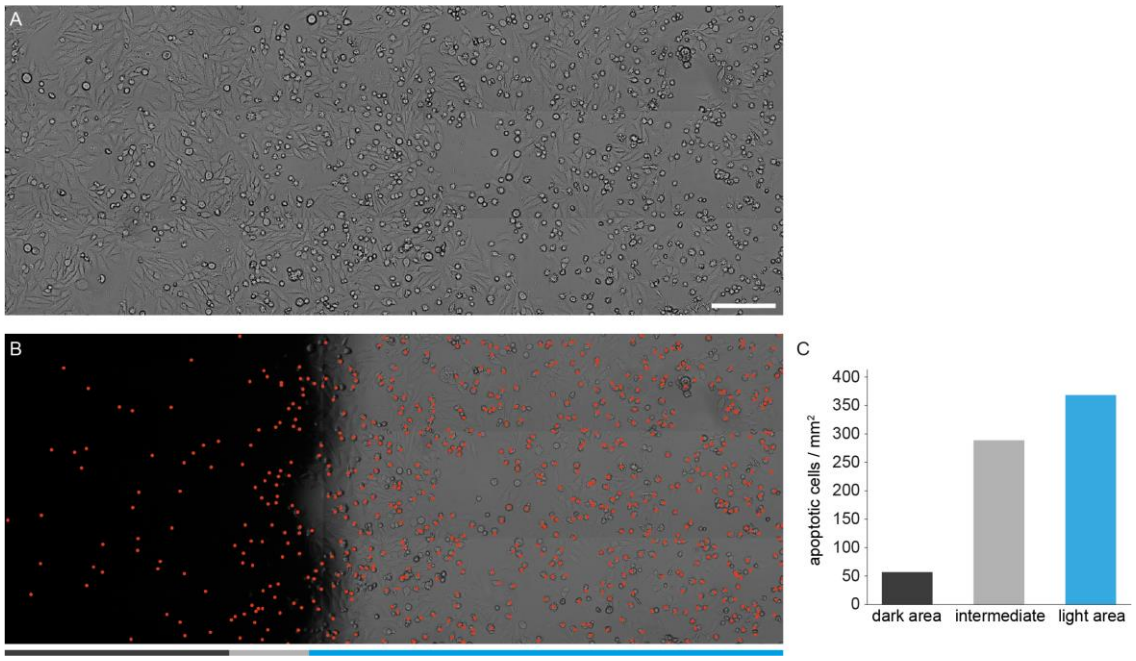

Figure 16: Spatial resolution of LITESEC-act3 – HEp-2 cells were infected with LITESEC-act3 bacteria expressing $YopE_{1-138}$-tBID, as in Figure 15C-E, under light conditions. In a part of the well, light was blocked by an intransparent plastic inset. After infection, the region around the edge of the plastic sheet was imaged with and without the inset and apoptotic cells were determined by shape. (**A**) Light micrograph in the absence of the inset. Images from three adjacent rows of eight neighboring fields of view were taken with a 20x objective and combined using softWoRx 7.0.0. Scale bar, 0.2 mm. (**B**) Light micrograph of the same area in presence of the inset, showing the approximate area of illumination during infection, as well as the localization of apototic cells determined in (A) (red points). Bottom, areas assigned as dark (dark grey bar), intermediate (0.25 mm wide adjacent area, light grey bar) and light (blue bar). (**C**) Density of apoptotic cells per mm^2 in each of the areas determined in (B).

3.2 Results – Part II – Adaptation and applications of LITESEC-T3SS

With the development of the LITESEC-T3SS (Results – Part I), we followed the novel path of establishing an application based on optogenetic dimerization switches in prokaryotes, with the final aim to control a cellular function by tethering an essential protein to the bacterial inner membrane (Liu *et al.*, 2018; Lindner *et al.*, 2020). Contrary to the establishment of those switches in eukaryotic studies (Wang et al., 2016, Kawano et al., 2015, reviewed in Bai et al., 2018), we found that a tight "sweet spot" of anchor to bait expression ratio is crucial for the functionality of those switches in prokaryotes (Figure 12). This could help other researchers with the establishment of further optogenetic applications to control cellular processes in prokaryotes. I further wanted to enhance this application by incorporating a red-/far-red light optogenetic switch into the LITESEC-system for applications inside living tissue and animal models. Even when this establishment was not successful, we have learned that the cofactor (phycocyanobilin) is toxic to *Yersinia* and therefore other optogenetic switches that use different cofactors (e.g. biliverdin) would be advantageous (discussed later). In collaborations with other research labs from Marburg, we tested and optimized the translocation of different cargo proteins into host cells. During those studies, we investigated the importance of protein stability and chaperone co-expression for the efficiency of cargo delivery into eukaryotic host cells. In these studies, we could show basic requirements for successful translocation of cargos into host cells, which is an essential prerequisite for the application of the LITESEC system.

3.2.1 Establishment of a red-light optogenetic switch into the LITESEC application

For application in living tissues and animal models, we wanted to combine the application of LITESEC with a red/far-red light optogenetic switch (redLITESEC), as blue light does not penetrate deeper tissue layers (Ash *et al.*, 2017). Several red-light optogenetic systems have been characterized (Shimizu-Sato *et al.*, 2002; Toettcher, Gong, *et al.*, 2011; Kaberniuk, Shemetov and Verkhusha, 2016; Reichhart *et al.*, 2016); however, all of these systems require a cofactor, which is naturally not present in bacteria and has to be synthesized from the bacterial vector as well. Based on advice from Prof. Dr. Lars-Oliver Essen, we decided to establish the far-red light optogenetic system PhyB-PIF6 (Pathak *et al.*, 2014)), as this switch seems to fulfill the best requirements for our tethering principle (strong on/off ratio, available on site). Exposure to 650 nm induces binding of PIF and Phy, while exposure to 750 nm light induces dissociation of PIF from Phy. This would give us the advantage to use light of different wavelength to induce both the start and stop of protein secretion within several minutes (Toettcher, Gong, *et al.*, 2011).

The PhyB/PIF6 system is based on a light-controllable binding interaction between two genetically encoded components: (i) a modified fragment of *Arabidopsis thaliana* phytochrome B (AtPhyB) (used as anchor) consisting of residues 1–651 of the PhyB protein and (ii) a modified fragment of the phytochrome interaction factor 6 (PIF6A) (used as bait) consisting of residues 1–100 of *A. thaliana* PIF6 protein. Both interacting proteins were provided by the research group of Prof. Lars-Oliver Essen (Golonka *et al.*, 2019). These proteins were shown to retain their function when they are fused to further subdomains (Toettcher, Gong, *et al.*, 2011), which is an essential ability to use this system in the LITESEC application to control the function of the T3SS. Similar to the previously used blue-light systems, we created a fusion protein PIF6A-SctQ (bait) and integrated it onto the genome via allelic exchange. Since the literature mentioned that the interaction partner AtPhyB works best as an N-terminal fusion to the membrane anchor motive (AtPhyB-TMH) (Toettcher, Gong, *et al.*, 2011), we decided to try both combinations: i) the modified TMH domain, like it was used in the blue light LITESEC applications, just works as N-terminal fusion (TMH-PhyB). ii) for the C-terminal membrane anchor motive we chose a hypothetical membrane domain (HMD) SCO7096 (Craney *et al.*, 2011) as a fusion to AtPhyB (AtPhyB-HMD). This HMD was selected by testing several hypothetical C-terminal membrane domains (Craney *et al.*, 2011) as a fusion to a soluble protein like GFP and predicted the membrane properties of the hypothetical proteins with Phobius (phobius.sbc.su.se) (Figure 18A). We expressed the anchor proteins (TMH-FLAG-AtPhyB / AtPhyB-FLAG-HMD), where we also added a FLAG-tag for detection, from an inducible expression plasmid to adjust for possible expression ratio “sweet spots”, like it was shown for the LITESEC application (Lindner *et al.*, 2020). For light-induced dimerization, a membrane-permeable small molecule chromophore, phycocyanobilin (PCB) is needed, which can be expressed by the bacteria from an expression plasmid, encoding for the two synthesis genes *Ho1* and *PcyA* (Gambetta and Lagarias, 2001). For this purpose, we obtained an expression plasmid from Addgene (pSR33.4r #63198 (Schmidl *et al.*, 2014)) which was used for PCB synthesis in *E. coli* and serves as a template for the PCB expression plasmid in *Yersinia*. Since PhyB-PIF interaction was shown to work best under high PhyB expression and the PCB to PhyB ratio also is important (Toettcher, Gong, *et al.*, 2011), we integrated the PCB synthesis onto another IPTG-inducible expression plasmid pMMB67EH (Christen *et al.*, 2010), so that we can test several expression ratio combinations. This would allow a co-expression of a cargo protein from another constitutive plasmid (pACYC) for later application.

To test whether the PCB synthesis works in *Y. enterocolitica* as well, we performed a metabolomics mass spectrometry (MS) analysis (with the help of the MPI Metabolomics facility – Nicole Paczia) (Figure 17A). The results indicate that we indeed have a synthesis of the cofactor chromophore PCB in the redLITESEC strain (PIF6A-SctQ) that correlate with the IPTG induction level (0.05 mM IPTG / 0.5 mM IPTG – Figure 17A).

Interestingly, the amount of detectable PCB in a strain harboring the MA plasmid (pBAD::TMH-FLAG-AtPhyB) is less than for the strain lacking the MA under the same IPTG induction conditions (Figure 17A). We have no detectable PCB in the control strain that is not expressed with IPTG, nor in the supernatant of the samples, indicating that the synthesized PCB stays inside the cells and is not exported extracellularly (Figure 17A). Nevertheless, further experiments showed that PCB is potentially toxic to the bacteria, indicated by a reduced growth (Suppl. Figure 5) and a reduced secretion behavior (Figure 17B). A control lacking the PCB synthesis plasmid showed that this effect on secretion behavior is not due to IPTG or L-arabinose levels within the bacteria (Figure 17B), but seems to be PCB dependent. In a next experiment, we screened for a reduction in PCB induction/expression to find an expression level that does not influence the bacteria to a major degree (Figure 17C).

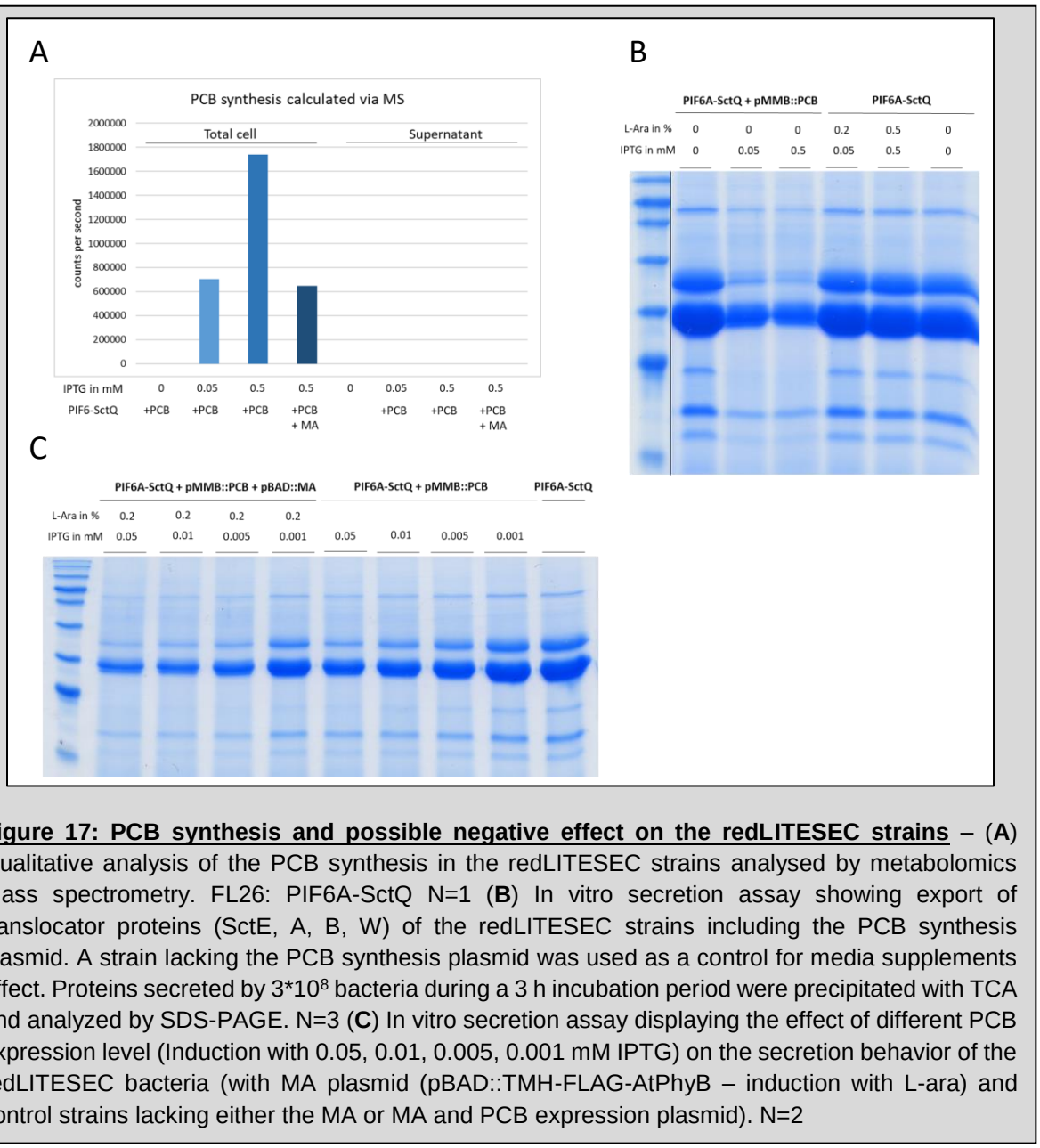

Figure 17: PCB synthesis and possible negative effect on the redLITESEC strains – (**A**) Qualitative analysis of the PCB synthesis in the redLITESEC strains analysed by metabolomics mass spectrometry. FL26: PIF6A-SctQ N=1 (**B**) In vitro secretion assay showing export of translocator proteins (SctE, A, B, W) of the redLITESEC strains including the PCB synthesis plasmid. A strain lacking the PCB synthesis plasmid was used as a control for media supplements effect. Proteins secreted by $3*10^8$ bacteria during a 3 h incubation period were precipitated with TCA and analyzed by SDS-PAGE. N=3 (**C**) In vitro secretion assay displaying the effect of different PCB expression level (Induction with 0.05, 0.01, 0.005, 0.001 mM IPTG) on the secretion behavior of the redLITESEC bacteria (with MA plasmid (pBAD::TMH-FLAG-AtPhyB – induction with L-ara) and control strains lacking either the MA or MA and PCB expression plasmid). N=2

Secretion under PCB synthesis inducing conditions (1 µM IPTG) was nearly comparable to the secretion level without PCB (Figure 17C), which we therefore choose for further experiments for the redLITESEC. With the next experiment, we aimed to test the influence of red light (640 nm) on the T3SS function of the redLITESEC strains (Figure 18), as we could show it for the LITESEC-T3SS (Figure 10). Illumination with red light (640 nm) enables the dimerization of the PhyB-PIF system (Toettcher, Gong, *et al.*, 2011), which should lead to a reduction in secretion activity due to the binding of the essential component SctQ to the MA. Therefore, we performed a secretion assay and incubated the samples either at dark or red light (640 nm) conditions (Figure 18B).

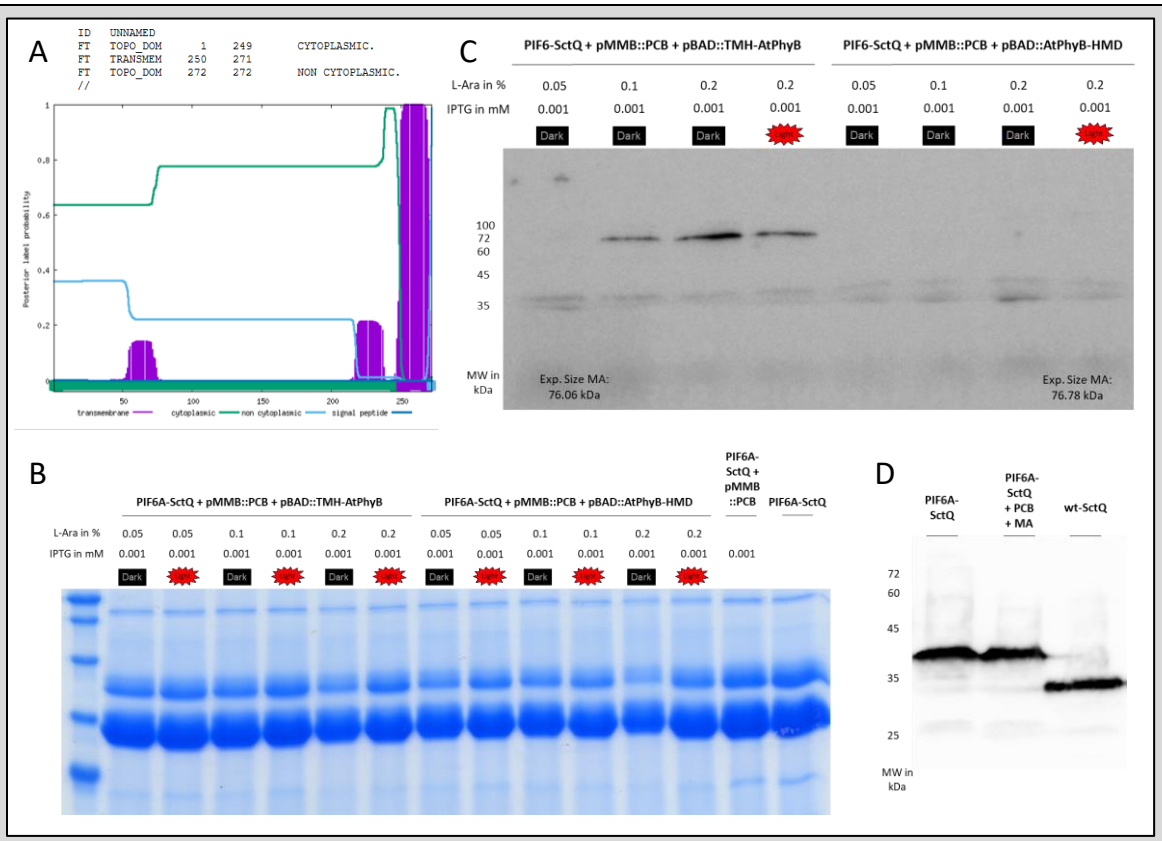

Figure 18: Establishment of the red/far-red light optogenetic system AtPhyB-PIF6A - (**A**) Structural and functional prediction of the C-terminal hypothetical membrane domain (HMD) SCO7096 (Craney et al., 2011) fused to GFP as an example – predicted with Phobius (phobius.sbc.su.se). (**B**) In vitro secretion assay showing export of translocator proteins (SctE, A, B, W) of the redLITESEC strains incubated either at dark or red light (640 nm). Both MA options were tested: i) N-terminal: TMH-FLAG-AtPhyB ii) C-terminal: AtPhyB-FLAG-HMD. A strain lacking the MA and both, the MA (induced with L-ara) and PCB synthesis (induced with IPTG) plasmid were used as controls. Proteins secreted by $3*10^8$ bacteria during a 3 h incubation period were precipitated with TCA and analyzed by SDS-PAGE. N=2 (**C**) Western blot using an anti-FLAG antibody for the culture total cell of $2*10^8$ bacteria per redLITESEC strain to test stability and expression of the both MA: i) TMH-FLAG-AtPhyB (exp. MW: 76.06 kDa) ii) AtPhyB-FLAG-HMD (exp. MW: 76.78 kDa). Left side, molecular weight marker in kDa. N=2 (**D**) Western blot using an anti-SctQ antibody for the culture total cell of $2*10^8$ bacteria per redLITESEC strain to test stability and expression of the fusion protein PIF6A-SctQ (exp. MW: 40.5 kDa). Wt-SctQ was used as a control (exp. MW: 34 kDa). Left side, MW marker in kDa. N=1

To screen for the best expression ratio between bait (PIF6A-SctQ – natively expressed from the genome), cofactor PCB (0.001 mM IPTG – expressed from pMMB67EH) and MA (expressed from pBAD – L-arabinose-inducible), we ranged the induction with L-ara from 0.05% to 0.2% and simultaneously tested both MA versions (Figure 18B). We did not observe a specific reduction in secretion under red light (~ 640 nm) for any conditions (Figure 18B). We therefore tested the protein stability and expression level of both, the bait (PIF6A-SctQ – Figure 18D) and both MA (Figure 18C). The PIF6A-SctQ fusion protein seems stable and expressed comparable to wt SctQ level (Figure 18D). The N-terminal MA (TMH-FLAG-AtPhyB) displayed protein expression dependent on the L-ara induction (Figure 18C), whereas for the C-terminal MA (AtPhyB-FLAG-HMD) no expression could be detected (Figure 18C). Since higher expression of the cofactor PCB showed a strong negative effect on the growth and T3SS function of the bacteria and the C-terminal MA, which literature said to work better for PhyB functionality (Toettcher, Gong, *et al.*, 2011), could not be expressed as a stable fusion protein, we decided to stop research on the redLITESEC at this point.

3.2.2 Protein stability heavily influences the efficiency of protein cargo delivery

I also worked in two cooperation's with the research groups (RG) Stiewe (Institute for Molecular Oncology, Marburg) and RG Hantschel (Institute for Physiological Chemistry, Marburg) to establish the LITESEC application as a delivery platform for certain therapeutic cargos. In cooperation with RG Stiewe, we aimed to deliver the pro-apoptotic proteins PUMA (p53 upregulated modulator of apoptosis) (Yu *et al.*, 2001), p53 (tumor repressor protein) (Vogiatzi *et al.*, 2016) and HSVtk (herpes simplex virus thymidine kinase - converts cancer prodrugs into toxic metabolites) (Hwang, 2006) into cancer cells (cell culture and animal mouse model). We first aimed to establish a proof of principle system for light-controlled cargo delivery into mouse models. For that purpose, we chose a Cre-lox reporter system (Le *et al.*, 1999), which indicates a translocation of a recombinase Cre into loxP-reporter cell lines, leading to a change in fluorescence signal expression from red to green (Sheller-Miller *et al.*, 2019) (Figure 19D). Before we went into cell culture experiments, we did a preliminary experiment to test the secretion efficiency of the cargo: $YopE_{1-138}$-Cre-NLS (including a nuclear localization sequence (Bichsel *et al.*, 2011)) (Figure 19). Although we could detect secreted cargo in the supernatant verified by anti-Cre Western blot and Coomassie staining (Figure 19A, C), it seems that the cargo blocks the injectisome to a certain degree and affects the secretion ability, since most of the cargo remains in the cell (Figure 19B) and the secretion pattern is noticeably reduced, compared to the wt (Figure 19C). Keeping the decreased secretion efficiency of the Cre cargo in mind, we next tested the translocation of the cargo into eukaryotic cell lines (Figure 19E).

We received two cell lines: i) PC-9 (P2) human NSCLC cells, ii) Fibroblasts (P5) BJ-TE, hTERT both including the reporter gene construct: pLV-CMV-LoxP-DsRed-LoxP-eGFP from RG Stiewe (as well as the Cre-template and the Cre-antibody). To test the translocation efficiency of the cargo, we performed an infection assay (Wolters *et al.*, 2015; Lindner *et al.*, 2020) and observed the fluorescence signal of the cell lines over a time period of 48 h (Figure 19E). We detected a change from red to green fluorescence after 48 h in some cells: i) PC-9: pos.: 9.8%, neg.: 3.5%; ii) Fibroblasts: pos.: 1.7%, neg.: 0.7% (142-353 cells from 4-7 field of views from one experiment were analyzed visually). Noticeably, some cells showed both red and green fluorescence after 48 hours, which complicated the analysis (the dominant fluorescence was always counted) (see Discussion for interpretation). Nevertheless, the amount of infected cells during this experiment was not comparable to infection assays that we performed with other cargos like tBID or ß-lactamase (Figure 15), which could be due to a jamming effect (see 1.5 for explanation) of the Cre-cargo at the injectisome.

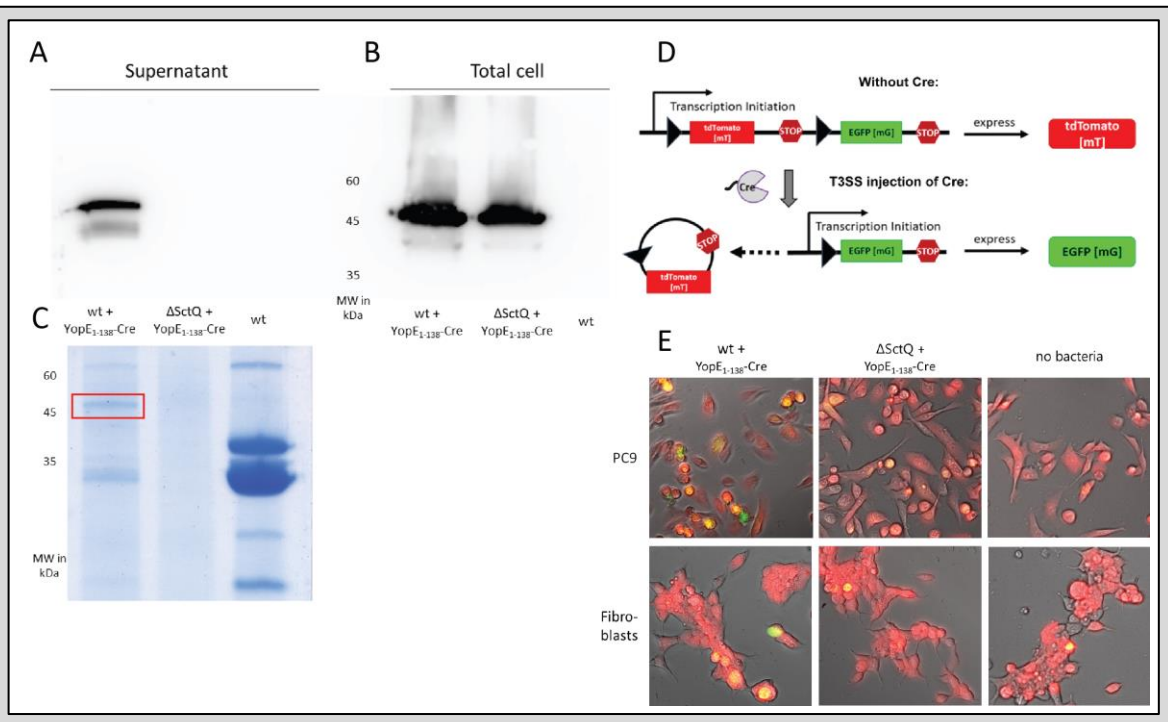

Figure 19: Establishment of a Cre-lox reporter system for the LITESEC-application – (**A**) In vitro secretion assay of the cargo YopE$_{1-138}$-Cre (exp. MW: 54 kDa) verified by anti-Cre Western blot. As controls, a T3SS deficient ΔsctQ strain carrying the Cre-cargo expressing plasmid and a wildtype (wt) strain (ΔHOPEMTasd) were used. Proteins secreted into the supernatant by 3*10^8 bacteria during a 3 h incubation period were precipitated with TCA and analyzed by SDS-PAGE. N=1 (**B**) Total cell samples of the same secretion assay (A). N=1 (**C**) Coomassie SDS-PAGE of the secretion assay in (A). N=1 (**D**) Working principle of Cre-mediated switch from genetic expression of tdTomato (top, red fluorescence) to EGFP (bottom, green fluorescence) (Sheller-Miller et al., 2019). (**E**) Translocation of the cargo: YopE$_{1-138}$-Cre into two cell lines: i) PC-9 (P2) human NSCLC cells, ii) Fibroblasts (P5) BJ-TE, hTERT both including the reporter gene construct: pLV-CMV-LoxP-DsRed-LoxP-eGFP – received from RG Stiewe. Cre translocation leads to a change in fluorescence signal from red to green. Pictures were taken 48 h after infection. N=1

In cooperation with RG Hantschel, we aimed to use the LITESEC-T3SS strains to deliver monobodies (Hantschel, Biancalana and Koide, 2020) into eukaryotic host cells. Monobodies (MB) are small, synthetic antibody-like proteins that can bind different targets and therefore activate or inhibit cellular functions for therapeutic reasons (Oliver, 2017; Carrasco-López *et al.*, 2020). I worked together with a PhD from our collaborator, Chiara Lebon, who is working on the cell delivery of two different monobodies i) AS25 (binds and inhibits the oncoprotein kinase Bcr-AbI (Wojcik *et al.*, 2016)) and ii) MbC (binds and inhibits the tyrosine phosphatase SHP1 – unpublished, O. Hantschel). Our collaborator further introduced two mutations to the monobodies (K7D, A56G) to decrease the protein stability and therefore enhance unfolding properties of the monobody structure, which might also be necessary for T3SS injectisome mediated secretion (Akeda and Galán, 2005).

For this purpose, we designed cargos including a T3SS specific secretion tag, the monobody (MB) or a mutated derivate, a FLAG-tag for Western blot detection, a *tobacco etch virus* (TEV) cleavage side for auto cleavage in the host cells and a split-NanoLuc domain HiBiT for detection of translocation into a specific Hela cell line expressing the larger domain (LgBiT) of a split NanoLuc enzyme, which could be then detected via luminescence (Westerhausen, Nowak, Torres-Vargas, *et al.*, 2020). The resulting different monobody cargos ($YopE_{1\text{-}138}$-TEV-MB-FLAG-HiBiT) were then tested for secretion and translocation properties (Figure 20). Both monobody constructs including their derivatives could be detected in the supernatant in a secretion assay via Coomassie staining and anti-FLAG Western blot, indicating that the constructs were exported efficiently (Figure 20A, B). The reason, why the MB mutant K7D runs slightly higher than the other monobodies could be due to the different isoelectric point (IEP) (e.g. $AS25_{wt} = 6.80$; $AS25_{K7D} = 5.73$). Mentionable, the bacteria that were exporting the monobody cargos showed a reduced overall secretion compared to the wt control (Figure 20A), which could also be due to a jamming effect (see 1.5 for explanation) of the cargo. The overall secretion of the strain secreting the MB $AS25_{wt}$ was more reduced than for the two mutants, indicating that the stability and folding properties of the monobody constructs correlates with the secretion efficiency (Figure 20A). Total cell samples showed comparable concentrations of the monobody cargo than the supernatant samples, suggesting that a fraction of the cargo remains in the cells and is not exported (Figure 20A). With a NanoLuc detection assay, we next tested the translocation efficiency of the monobody constructs. For this purpose, we performed an infection assay with the Hela (LgBiT) cell line and detected the luminescence 1 h after infection (Figure 20C). As a positive control, we used the cargo $YopE_{1\text{-}138}$-HiBiT. Both MB_{wt} cargos had the lowest translocation efficiency, whereas for MbC the K7D mutation (75% efficiency relative to the positive control) and for AS25 the A56G mutation (44% efficiency relative to the positive control) were most efficiently translocated (Figure 20C). As a positive control, the cargo $YopE_{1\text{-}138}$-HiBiT was used.

Those observations together with the data from the Cre-cargo (Figure 19) underline the importance of protein stability for translocation and secretion efficiency for LITESEC-T3SS applications, where more stable folded cargos are exported to a lower degree (Figure 19, 20).

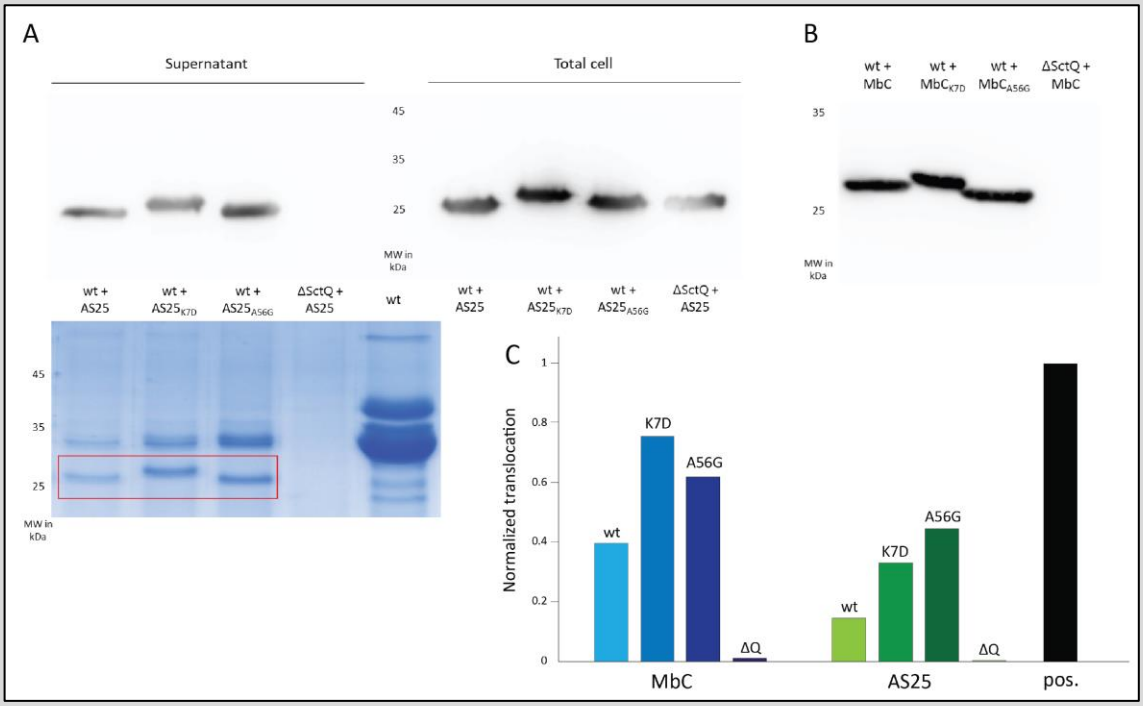

Figure 20: Monobody translocation via T3SS injectisome – (**A**) In vitro secretion assay of the monobody cargo AS25 (exp. MW: 28.78 kDa) and the mutation derivatives K7D and A56G, verified by Coomassie staining and anti-FLAG Western blot from supernatant and total cell samples. As controls, a T3SS deficient ΔsctQ strain carrying the MB-cargo and a wt strain (ΔHOPEMTasd) were used. Proteins secreted by $3*10^8$ bacteria during a 3 h incubation period were precipitated with TCA and analyzed by SDS-PAGE. (**B**) In vitro secretion assay of the monobody cargo MbC (exp. MW: 28.47 kDa) and the mutation derivatives K7D and A56G, verified by anti-FLAG Western blot from supernatant samples. (**C**) Graph depicting the results of a split-NanoLuc translocation assay of the monobody constructs into Hela cells expressing the NanoLuc domain LgBiT (Westerhausen, Nowak, Torres-Vargas, et al., 2020). Relative translocation efficiency related to a positive control secreting the cargo $YopE_{1-138}$-HiBiT. Luminescence detected 1 h after infection via plate reader. N=2

3.2.3 Chaperone co-expression enhances the translocation efficiency

Earlier studies showed that translocation of some *Yersinia* effectors like YopE or YopT is strictly dependent on their cognate chaperone (Trülzsch *et al.*, 2003) and translocation studies with *EHEC* (MacDonald *et al.*, 2017) and *Chlamydia* (Brinkworth *et al.*, 2011) also showed an increasing effect of chaperone co-expression on the amount of delivered proteins. To test whether this observation is applicable for the LITESEC-T3SS, we performed an experiment where we tested the translocation efficiency of pro-apoptotic cargos with and without combined chaperone co-expression (Figure 21). Therefore, we designed expression vectors encoding for a pro-apoptotic protein (tBID or PUMA) fused to the secretion tag $YopE_{1-138}$ with or without additional chaperone co-expression of SycE from the same locus.

The other pro-apoptotic cargos presented in 3.2.2 (p53, HSVtk) either needed a specific cell line or an additional substrate for translocation readout and were therefore not investigated in this experiment. We then tested the translocation efficiency of the pro-apoptotic cargos into HEp-2 cells and compared the amount of infected cells with or without chaperone co-expression (Figure 21). Since PUMA was shown to induce apoptosis after ~ 6 h (Yu *et al.*, 2001), we observed apoptosis at 1 h post infection and 20 h post-infection (Figure 21). Chaperone co-expression led in both cases of $YopE_{1-138}$-tBID and $YopE_{1-138}$-PUMA to an increased translocation efficiency indicated by a higher amount of apoptotic (condensed star-shaped) cells (Figure 21 A, B). Our findings support existing studies (Brinkworth *et al.*, 2011; MacDonald *et al.*, 2017) about a positive effect of chaperone co-expression from the same locus and highlight this effect for translocation applications of LITESEC.

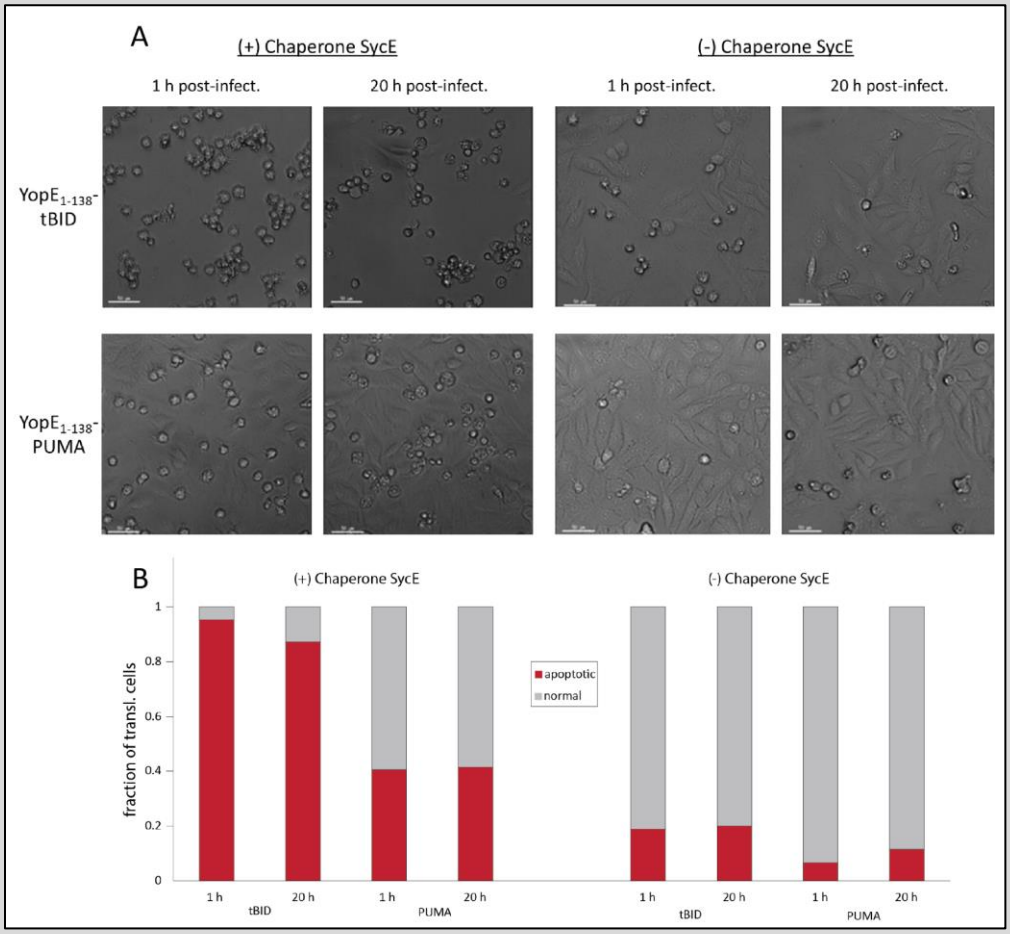

Figure 21: Chaperone co-expression from the same locus enhances translocation efficiency
(**A**) Micrographs depicting cultured HEp-2 cells that have been incubated with Yersinia ΔHOPEMTasd-strains translocating a heterologous T3SS substrate, $YopE_{1-138}$-tBID (Ittig et al., 2015) or $YopE_{1-138}$-PUMA with or without chaperone co-expression from the same locus (pBAD). Cells were observed 1 h and 20 h post-infection. Translocation of tBID/PUMA induces apoptosis, which leads to a condensed star-shaped host cell morphology (and counted as apoptotic). Scale bar, 50 µm. (**B**) Fraction of HEp-2 cells (normal / apoptotic) from (A) after infection. N = 297-508 cells from 4-6 fields of view from two biological replicates were analyzed visually per strain and condition. N=1

3.3 Results – Part III – Investigation of dynamic processes and properties of the cytosolic complex of the T3SS using the established optogenetic interaction switches

Despite being able to govern T3SS function with LITESEC-T3SS by controlling the availability of the essential cytosolic component SctQ (Lindner *et al.*, 2020), the biological explanation for this phenotype is still unclear. Does the sequestration of the cytosolic component lead to a gradual disassembly of the injectisome-bound structure of the cytosolic complex, or is the T3SS function directly controlled by the dynamic exchange of the cytosolic complex at the T3SS interface (Diepold *et al.*, 2015), which is prevented by the sequestration of the cytosolic SctQ? Studies that observe the dynamic behavior of the cytosolic complex remain rare to date (Diepold *et al.*, 2015, 2017; Rocha *et al.*, 2018).

The finding that cytosolic T3SS components interact with effector/chaperone substrates and shuttle them to the injectisome (as it was proposed by (Lara-Tejero *et al.*, 2011)) would further complete the understanding of the dynamic nature of the T3SS. Light-mediated membrane tethering of cytosolic T3SS components, on which the LITESEC application is based, opens a completely new avenue to study such protein interactions and binding dynamics in living bacteria (Lindner *et al.*, 2020) (3.3.2).

I therefore took a closer look at the dynamic properties of the cytosolic complex and its role in protein export using fluorescence microscopy to investigate spot recovery rates during FRAP (**F**luorescence **r**ecovery **a**fter **p**hoto bleaching) experiments and spot persistence (explained later in 3.3.3) at different conditions. If the optogenetic-mediated sequestration of SctQ has an influence on the dynamic exchange of the cytosolic components, we would expect to see a difference between light and dark conditions in our following experiments. Our corresponding hypothesis and expectations are always explained at the introduction of the specific experiment in this section.

With those new investigations, I wanted to support a model, in which the dynamic exchange of the cytosolic components directly influences the function of the T3SS. I further wanted to verify the potential link between dynamics, effector shuttle and secretion through the T3SS by investigation of different cytosolic components (SctQ/L/N) to complete the characterization and associating model about the dynamic nature of the cytosolic components. This would give a first answer to one of the biggest open questions in the field of the T3SS.

Some of the experiments presented in this section were performed only once (always indicated) due to time concerns. Therefore, this section also serves as an outlook in which direction the combination of optogenetics with the T3SS may go in the future.

3.3.1 Does the cytosolic component SctQ have a specific role in effector secretion?

In *Salmonella*, the cytosolic component SctQ was shown to be part of a sorting platform that mediates type III-associated translocator export (Lara-Tejero *et al.*, 2011). A similar role for the *Yersinia* SctQ, which is essential for the T3SS function (Diepold *et al.*, 2015), remains unproven. During the LITESEC studies (which is based on the optogenetic control of SctQ), we recognized that there was a difference in the secretion of native *Yersinia* translocators compared to heterologous cargo proteins. While secreted cargo proteins could not be detected in the supernatant during "off"-conditions (Figure 13), native T3SS substrates were consistently reduced to a basal level (~20%) but still detectable (Figure 10, 11) (Lindner *et al.*, 2020). Based on those observations, we investigated if the export of heterologous cargo is regulated differently compared to the export of native translocators and if SctQ differentiates between different types of translocators. We overexpressed SctQ from a L-arabinose inducible plasmid (pBAD) in a *ΔsctQ* strain and checked for differences in the amount of translocators compared to the wt MRS40 (Figure 22A). Expression level of SctQ from the plasmid at ~0.001% L-ara was comparable to the MRS40 wt level (Figure 22A). Already at 0.005% L-ara, we could observe a nearly complete restoration of secretion function, with most efficient secretion at medium expression levels at ~ 0.01 to 0.02% L-ara (Figure 22A). It is normal that T3SS proteins need higher expression levels, when expressed from a plasmid compared to natural expression levels (A. Diepold – personal communication). However, we could not observe a higher fraction of secreted effectors in the secretion assay, which would have been a hint for a difference in SctQ mediated translocator secretion. We observed that the secretion efficiency decreases again at higher SctQ expression levels (Figure 22A). To test whether this decrease in secretion efficiency was due to a crowding effect of the overexpressed protein SctQ in the bacterial cytosol, we performed a secretion assay in which we overexpressed SctQ in a *ΔsctQ* strain and a MRS40 wt strain naturally expressing SctQ during T3SS inducing conditions (37° C, Ca^{2+}-depletion). As a control, we overexpressed eGFP in a MRS40 wt strain (Figure 22B). Interestingly, while the secretion efficiency was reduced at SctQ overexpression in both the *ΔsctQ* strain and the wt strain, overexpression of eGFP did not lead to a decrease in secretion efficiency (Figure 22B). With a next experiment, we tested the effect of the LITESEC mediated control of SctQ in a ΔHOPEMTasd (S1 wt strain that is lacking the effectors) strain compared to a MRS40 strain (wt strain including all effectors). While the control in secretion ability was the same for both cases, we could observe a difference in the basal secretion pattern under "off" conditions (dark for LITESEC-act) between ΔHOPEMTasd and MRS40 (Figure 22C). Whereas for LITESEC-act (ΔHOPEMTasd) the early translocators SctA/E/W and the effector YopQ were most abundant under "off" conditions, the pattern for LITESEC-act (MRS40) looked different with the most abundance of later translocators YopM/H/E (Figure 22C).

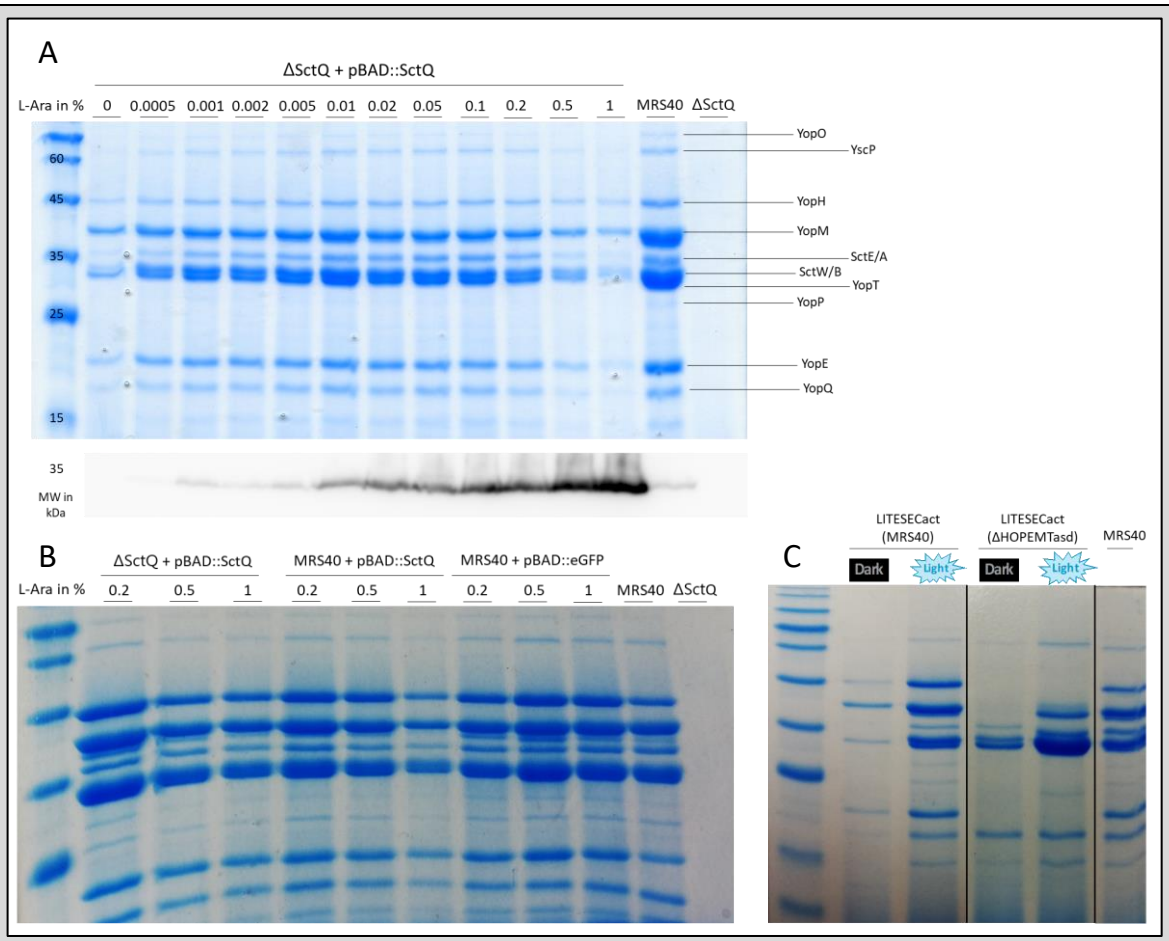

Figure 22: Overexpression of SctQ revealed no specific role in effector secretion – (**A**) In vitro secretion assay of *Yersinia enterocolitica* native translocators (tentative annotation) showing the effect of SctQ overexpression in a ΔsctQ strain verified by Coomassie staining and anti-FLAG Western blot (exp. MW SctQ: 34 kDa). As control, a MRS40 wt strain was used. Proteins secreted by $3*10^8$ bacteria during a 3 h incubation period were precipitated with TCA and analyzed by SDS-PAGE. N=2 (**B**) In vitro secretion assay displaying the effect of protein overexpression SctQ and eGFP on the secretion efficiency. As controls a MRS40 wt strain (pos.) and ΔsctQ (neg.) were used. N=1 (**C**) In vitro secretion assay of the LITESEC-act application in a ΔHOPEMTasd and a MRS40 background under dark and light (~480 nm) conditions. As a control, a MRS40 wt strain was used. Parts of the Coomassie gel were merged (indicated by black lines). N=3

3.3.2 Interaction properties of the cytosolic T3SS components

The assembly of the cytosolic complex requires the presence of all cytosolic components (Diepold *et al.*, 2010, 2017), which makes it difficult to determine the contribution of specific components to effector and structural protein binding by classical knockout experiments. The light-mediated membrane tethering and release of cytosolic T3SS components with optogenetic interaction switches enables a completely new way to investigate protein interactions and binding dynamics in living bacteria (Lindner *et al.*, 2020). This could help to visualize single protein-protein interaction and assembly events under different environmental conditions *in vivo*, even in knockout mutants of other cytosolic components.

Diepold and colleagues could already visualize the localization of the cytosolic components in live bacteria (Figure 23A) (Diepold *et al.*, 2010, 2015, 2017) and further investigated interaction properties of the cytosolic components amongst themselves and under several knockout conditions (Figure 5C), indirectly by immunoblot and native mass spectrometry (Diepold *et al.*, 2017). With the newly established optogenetic interaction switches, we wanted to "shine new light" on those previous findings, by investigating live protein interactions *in vivo* during fluorescence microscopy. By using the membrane binding properties of the established optogenetic interaction switch (Lindner *et al.*, 2020), we visualized the specific interactions between (Bait-) SctQ and SctL and SctK (fused to mCherry) in a *ΔsctN* background, by tethering SctQ to the membrane (Figure 23B), since those interactions were heavily influenced by knockout conditions in earlier studies (Diepold *et al.*, 2017). The membrane-tethering effect of the optogenetic dimerization switch was already presented in Figure 7. Before blue light illumination, the fluorescence signal of mCh-SctL was mainly cytosolic (Figure 23B, C – left side). After illumination, the fluorescence signal localization changed to membrane associated, which indicates a direct interaction between SctQ and SctL (relocalization factor: 3.89) (Figure 23B, C – right side) in the absence of the ATPase SctN. We could observe similar results for the interaction between SctQ and SctK (relocalization factor: 2.48) (Figure 23B).

Based on the successful proof of principle for direct protein interaction studies (Figure 23) we then wanted to search for possible interaction between effector/chaperone and cytosolic T3SS components. Such an interaction was proposed several years ago (Lara-Tejero *et al.*, 2011) and remains the only published study to date. By fluorescently labeling chaperones or just specific N-terminal effector sequences that are shown to be sufficient for T3SS recognition and translocation (Sory *et al.*, 1995), we tested the interaction between SctQ and the chaperone SycH (-mCherry) and between SctQ and a fluorescent protein (mCherry) with two secretion tags (as effector cargo representative): i) $YopE_{1-53}$, which has a T3SS recognition and secretion domain and ii) $YopE_{1-138}$, which also contains a chaperone-binding domain (Figure 24A). It is important to mention that the $YopE_{1-53}/_{1-138}$-mCh cargos were expressed from a plasmid, including the native promotor region SycE, $YopE_{1-53}/_{1-138}$ to get native expression levels, since expression of this promotor region has been shown to be co-regulated with Yop secretion activity (Jonas Pettersson *et al.*, 1996). The protein level of $YopE_{1-53}/_{1-138}$-mCh was very high, indicated by large polar spots inside the cells (Figure 24A). It seems that the cargos jammed the injectisome (Figure 24A), which was supported by a mCherry Western blot, where less secreted cargo was detected in the supernatant (still a LITESEC-supp specific pattern – dark = secretion on / light = secretion off), but most of the cargo remained inside the bacterial cells (Figure 24B). However, we were not able to observe a movement of the investigated cargo to the membrane after blue light irradiation (Figure 24A – dark vs. light), either because the total amount of bait was too high or the interaction between SctQ and cargo/chaperone too weak.

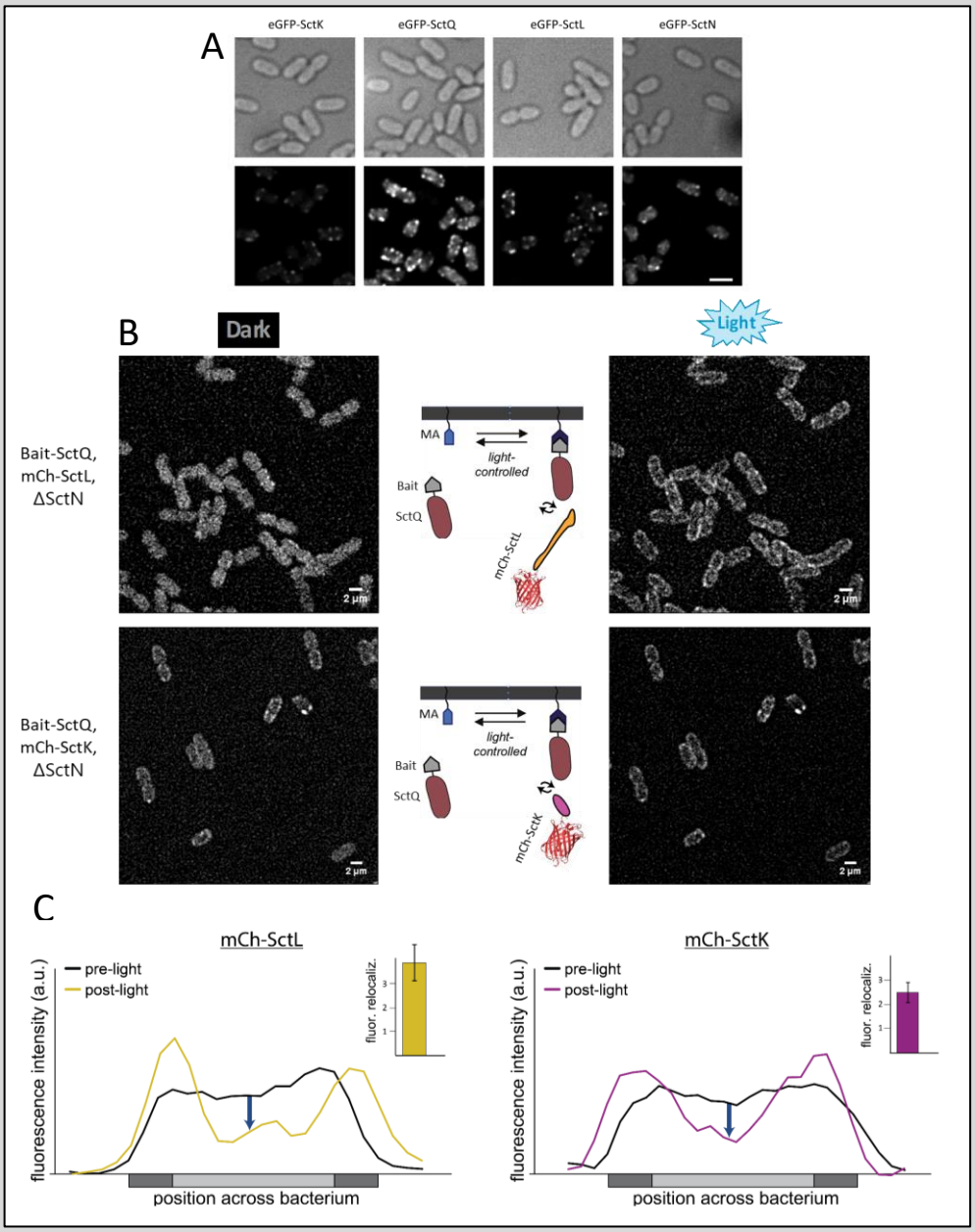

Figure 23: Optogenetics displayed direct T3SS intercytosolic protein interactions[4] – (**A**) Localization of the cytosolic T3SS components in the bacterial cell, adapted from (Diepold et al., 2017). (**B**) Visualization of the cytosolic component SctL or SctK in fusion to mCherry in an SspB_Nano-SctQ + MA, ΔsctN background. Schematic description of the potential interaction between SctQ and different cargos after a blue light mediated membrane tethering (middle). As excitation for the optogenetic interaction, a GFP excitation light of ~ 480 nm wavelength for 1 s was used. Scale bar is 2 µm. N=5 for mCh-SctL, N=2 for mCh-SctK. (**C**) Representative fluorescence signal quantification across bacterial cells for mCh-SctL and mCh-SctK; dark grey: membrane, light grey: cytosol. Insets: Fluorescence relocalization factor (fluor. reloc. = $R_{post\text{-}light}/R_{pre\text{-}light}$, where R represents the ratio of fluorescence intensities at the membrane and in the cytosol, before and after illumination, respectively), based on 64-81 line scans across three cells per strain. Error bars represent the standard deviation.

4

[4] Master student Kirsten Stahl under my supervision obtained parts of the represented data (interaction between SctQ and mCh-SctK).

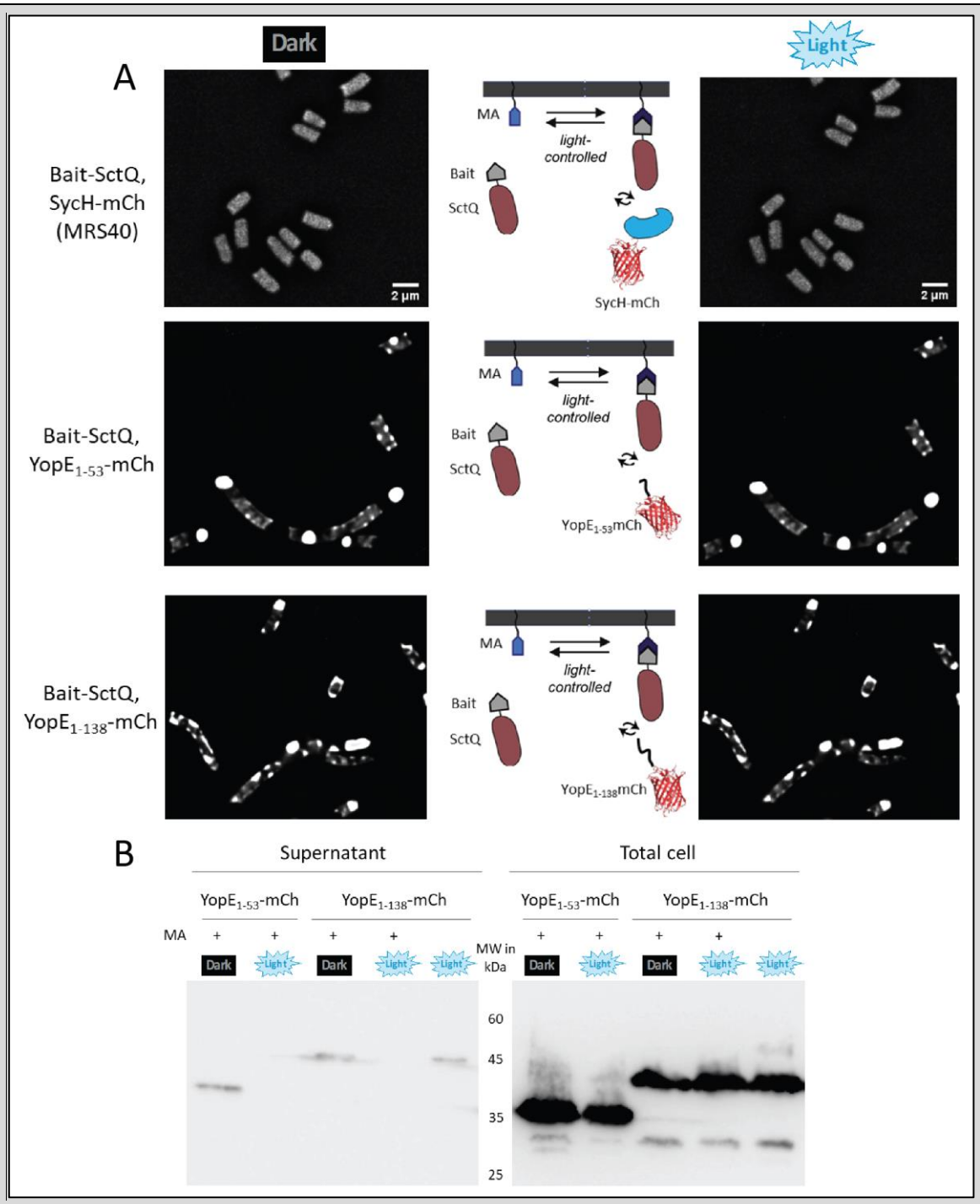

Figure 24: Chaperone/Effector cargo interaction studies using optogenetics – (**A**) Visualization of different cargos i) SycH-mCh, ii) YopE$_{1-53}$-mCh, iii) YopE$_{1-138}$-mCh in an SspB_Nano-SctQ + MA background by fluorescence microscopy. Schematic description of the potential interaction between SctQ and different cargos after a blue light mediated membrane tethering. As excitation for the optogenetic system, a GFP excitation light of ~ 480 nm wavelength for 1 s was used. Scale bar is 2 µm. N=2 (**B**) In vitro secretion assay of different cargos i) YopE$_{1-53}$-mCh (exp. MW: 35,2 kDa), ii) YopE$_{1-138}$-mCh (exp. MW: 44,5 kDa) in an SspB_Nano-SctQ + MA background, verified by anti-mCherry Western blot from supernatant and total cell samples. As a control, SspB_Nano-SctQ without MA was used. Proteins secreted by 3*10^8 bacteria that were cultivated either under dark or blue light conditions during a 3 h incubation period, were analyzed. N=2

3.3.3 Dynamic properties of the cytosolic T3SS components

Although the LITESEC application allowed a control of the T3SS function, by controlling the availability of the essential cytosolic component SctQ, the underlying biological reason for this phenotype is still unclear. By sequestering SctQ with optogenetic switches, do we influence secretion either by controlling the dynamic exchange of the cytosolic component SctQ (Diepold *et al.*, 2017), in line with a direct link between dynamics and secretion (Diepold *et al.*, 2015), or only its presence at the structure at the T3SS?

Based on FRAP (**F**luorescence **r**ecovery **a**fter **p**hoto bleaching) experiments, Diepold and colleagues determined the exchange rate (average recovery half-time t½ of 68.2 ± 7.9 s) of the cytosolic component SctQ (Diepold *et al.*, 2015). We now combined FRAP with the established optogenetic interaction switches to look for dynamic changes of spot recovery after photo bleaching under different light conditions. If the sequestration of SctQ affects the dynamic exchange of other cytosolic components at the injectisome interface, we would expect a difference in fluorescence spot recovery between dark (SctQ cytosolic) and light (SctQ sequestered) conditions. We performed FRAP experiments with the LITESEC-supp2 strain (SspB_Nano-SctQ, mCh-SctL) + MA and screened for spot dynamics of mCh-SctL during an optogenetic control of the bait-SctQ fusion protein (Figure 25). Our theory was that if we affect the dynamic properties of the cytosolic complex by the sequestration of SctQ, we should see an effect on mCh-SctL dynamics as well (since we have investigated a direct binding effect of SctQ to SctL (Figure 23)), keeping in mind that this effect would be indeed just an indirect one.

Bacterial strains were incubated under dark conditions (iLID – “T3SS function on”) so that the injectisome can assemble properly and were handled equally, to have comparable incubation and preparation times for each condition. We then visualized the bacterial cells for each condition during fluorescence microscopy either under dark or constant illumination settings. As controls, we used i) LITESEC-supp strain (bait-SctQ, mCh-SctL) lacking the MA and ii) mCh-SctL. Fluorescence recovery of the mCh-SctL spots after photobleaching was observed over time for each condition (Figure 25). Notably, one control strain (bait-SctQ, mCh-SctL without MA) displayed strongly differing behavior in one of the three experiments. I therefore provided micrographs including every sample and condition from every day (Figure 25C – control (bait-SctQ, mCh-SctL without MA is heavily affected) and one where this control was excluded (from one experiment) (Figure 25D). We recognized a difference between the LITESEC strain observed under dark (off) vs. light (on) conditions with a statistical significance *** $p<0.001$ (indicated for one time point but calculated for all time points) (Figure 25D). Nevertheless, the obtained data from FRAP were very noisy, indicated by the error bars (standard deviation – Figure 25D).

Data curves were then fitted with Sigma blot and the equation $y=a(1-e^{-bx})$ (Huang *et al.*, 2011) (Figure 25D) to determine the half-time recovery rate $t_{1/2}$ (calculated with the equation $t_{1/2}=\ln 0.5/-b$) (Figure 25E). Even when the data have to be interpreted with caution, a trend for a difference in spot recovery of mCh-SctL when we optogenetically control SctQ is visible (Figure 25D). Therefore, it could indeed be that we affect the dynamic exchange of SctL at the injectisome spots by sequestration of another cytosolic component (SctQ). To make clear statements about this phenotype, further experiments have to be performed.

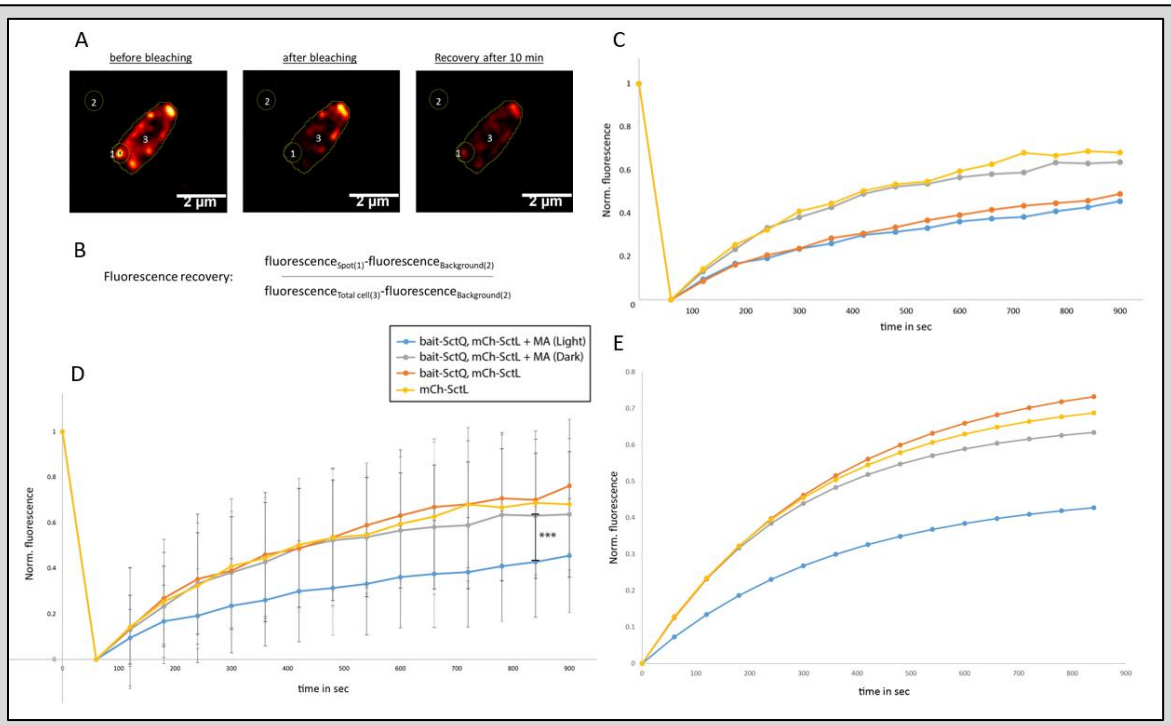

Figure 25: Difference in fluorescence spot recovery of mCh-SctL in LITESEC – (**A**) Schematic representation of the FRAP experiment with mCh-SctL control strain. Cells were observed with fluorescence micrsocopy, pictures were taken before photobleach, directly after bleaching and then fluorescence spot recovery was observed over time either under dark or constant illumination conditions. Photobleaching was performed with a laser 568 nm, 10% intensity, 0.05 s duration. (**B**) Fluorescence revocery calculation: $((\text{fluorescence}_{\text{Spot1}}-\text{fluorescence}_{\text{Background2}})/(\text{fluorescence}_{\text{Total cell3}}-\text{fluorescence}_{\text{Background2}}))$. Microscopy pictures were analyzed with Fiji.com. As excitation for the optogenetic system, a GFP excitation light of ~ 480 nm wavelength for 1 s was used. Scale bar is 2 µm. (**C**) Normalized fluorescence recovery over time (including all conditions and samples from every day) (**D**) Normalized fluorescence recovery over time (control strain bait-SctQ, mCh-SctL) from one experiment day was excluded, since the values were totally off for this strain for this day). For all data points, normalized values that were out of the range of -0.6-+1.6 were excluded from the calculation (usual range from 0-1). Error bars display the standart deviation, calculated (as the micrographs) from 120-247 cells per strain and condition from three independent experiments. Statistical significance between bait-SctQ, mCh-SctL + MA dark vs. light conditions ***, $p<0.001$ in a two-tailed homoscedastic t-test (indicated for one time point, calculated for all time points with the same statistical significance). (**E**) Curves fitted as nonlinear regression, exponential rise to the maximum with the formula: $y=a(1-e^{-bx})$ (Huang et al., 2011) with Sigmablot starting from 0/0. Calculated half time recovery rate $t_{1/2}$: bait-SctQ, mCh-SctL + MA (light) = 247,5 sec; bait-SctQ, mCh-SctL + MA (dark) = 192,5 sec; bait-SctQ, mCh-SctL = 247,5 sec; mCh-SctL = 216,6 sec. N=3

Because the presented FRAP experiment just visualizes an indirect effect of bait-SctQ on mCh-SctL, we next investigated LITESEC-T3SS triple fusions: bait-mCherry-SctQ that allow both a direct visualization in the cell and an optogenetic mediated membrane binding or release (Figure 26) of the fusion protein itself. With a secretion assay, we first tested the functionality of the triple fusions for both secretion and light-dependent secretion control (Figure 26A). While the LITESEC-act triple fusion showed a reduced secretion ability under "off" (dark) conditions (in another experiment, secretion was further reduced under dark conditions at higher L-ara concentrations – Figure 28A), this was not the case for the LITESEC-supp triple fusion (Figure 26A, 28B). We assumed that an internal translational start site of the mCherry fusion protein, which lead to a smaller protein side product missing the C-terminal bait, might explain these findings. We therefore introduced a mCherry$_{(NoIRES)}$ modification, were the internal ribosomal entry site (IRES) is removed (Carroll *et al.*, 2014). In an anti-SctQ Western blot, we could indeed see that the SspB_Nano-mCh$_{(NoIRES)}$-SctQ fusion showed one band less (at around ~ 58 kDa). Interestingly, we could observe an optogenetic membrane tethering effect of both SspB_Nano-mCh-SctQ / SspB_Nano-mCh$_{(NoIRES)}$-SctQ fusions (Figure 26C), indicating that the optogenetic interaction still works for the fluorescent full-length proteins, which is contrary to the observations in secretion assays. This lack in secretion control may be due to a smaller fusion protein product at ~ 50 kDa (Figure 26B) that is missing the optogenetic bait and therefore cannot be sequestered. Even when we overexpressed the MA with a ten times higher L-ara concentration, we still did not observe a reduction in secretion ability under "off" (light) conditions (Figure 27B). Since we want to use the triple fusion to further investigate the dynamic properties of the T3SS and its link to the function, we concentrated on the LITESEC-act triple fusion, which showed light-dependent control in secretion ability.

Next, we designed an experiment to test the dynamic exchange of the LITESEC-act triple fusion Zdk1-mCh-SctQ at the T3SS spots. Previous experiments showed an illumination-dependent control of the secretion function, when the bait-mCh-SctQ fusion protein is sequestered (Figure 26A, Figure 28A). In fluorescence microscopy, we aim to investigate fluorescence spots of the triple fusion under illumination conditions that were shown to affect the function of the T3SS (Figure 28A). There can be two scenarios (Figure 27A): i) Sequestration of SctQ affects the assembly and structure of the cytosolic complex bound to the injectisome, as indicated by disappearance of the bait-mCh-SctQ T3SS spots under long-term sequestration conditions. ii) If the fluorescence spots maintain over time even under "T3SS function off" conditions, sequestration of SctQ is more likely to affect the dynamic exchange of cytosolic components and thus the function itself, as also indicated in the FRAP data (Figure 25). Bacteria were incubated under blue light conditions ("T3SS function on"), so that the T3SS machinery can assemble properly. Strains were then prepared for fluorescence microscopy and observed over a time course of 30 min under either dark or constant blue light

illumination conditions (representative images are displayed in Figure 27C). It seems that for all conditions, T3SS specific spots remain over time, even if there is an overall reduction in fluorescence intensity, likely due to photo bleaching. Noticeably, the control strain without the optogenetic MA displayed a more complete spot maintenance over time (Figure 27C). Those experiments were just performed two times and we recognized during the experimental setup that a correct MA expression that lays within the sweet spot (Figure 28) is crucial for spot observance. Further experiments need to be done to strengthen the data.

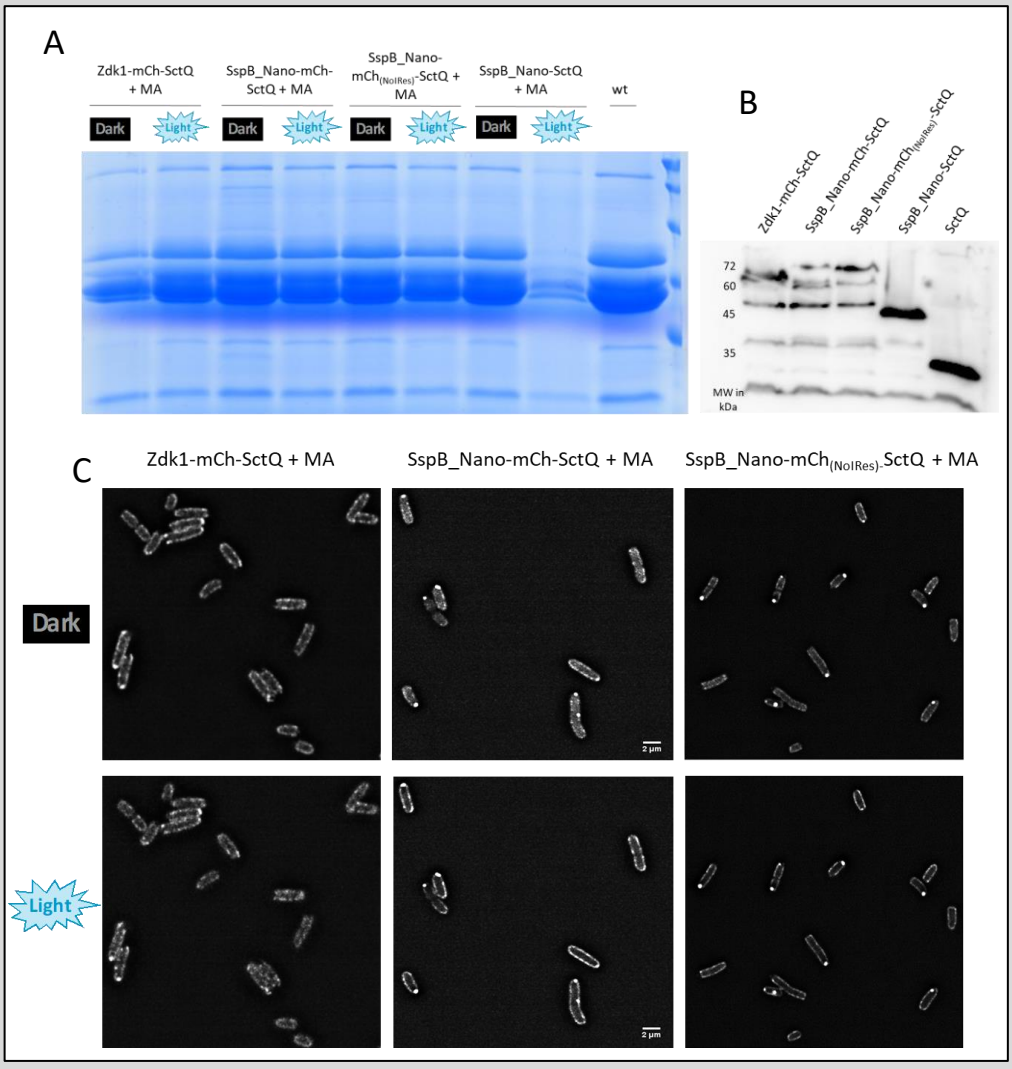

Figure 26: Characterization of LITESEC triple fusions bait-mCh-SctQ – (**A**) In vitro secretion assay showing light-dependent export of translocator proteins (SctE, A, B, W) of the LITESEC triple fusions. As secretion controls, the LITESEC-supp2 strain and a wt (ΔHOPEMTasd) were used. Proteins secreted by $3*10^8$ bacteria during a 3 h incubation period were precipitated with TCA and analyzed by SDS-PAGE. (**B**) Protein stability of the SctQ-fusion proteins: i) Zdk1-mCherry-SctQ (exp. MW: 67,8 kDa), ii) SspB_Nano-mCherry-SctQ (exp. MW: 73,7 kDa), iii) SspB_Nano-mCherry$_{(NoIRES)}$-SctQ (exp. MW: 73,7 kDa), iv) SspB_Nano-SctQ (exp. MW: 46,7 kDa), v) SctQ (exp. MW: 34 kDa) visualized by an anti-SctQ Western blot on total cell samples. (**C**) Visualization of the bait-mCh-SctQ triple fusions + MA under dark and light conditions by fluorescence microscopy. As excitation for the optogenetic system, a GFP excitation light of ~ 480 nm wavelength for 1 s was used. Scale bar is 2 µm.

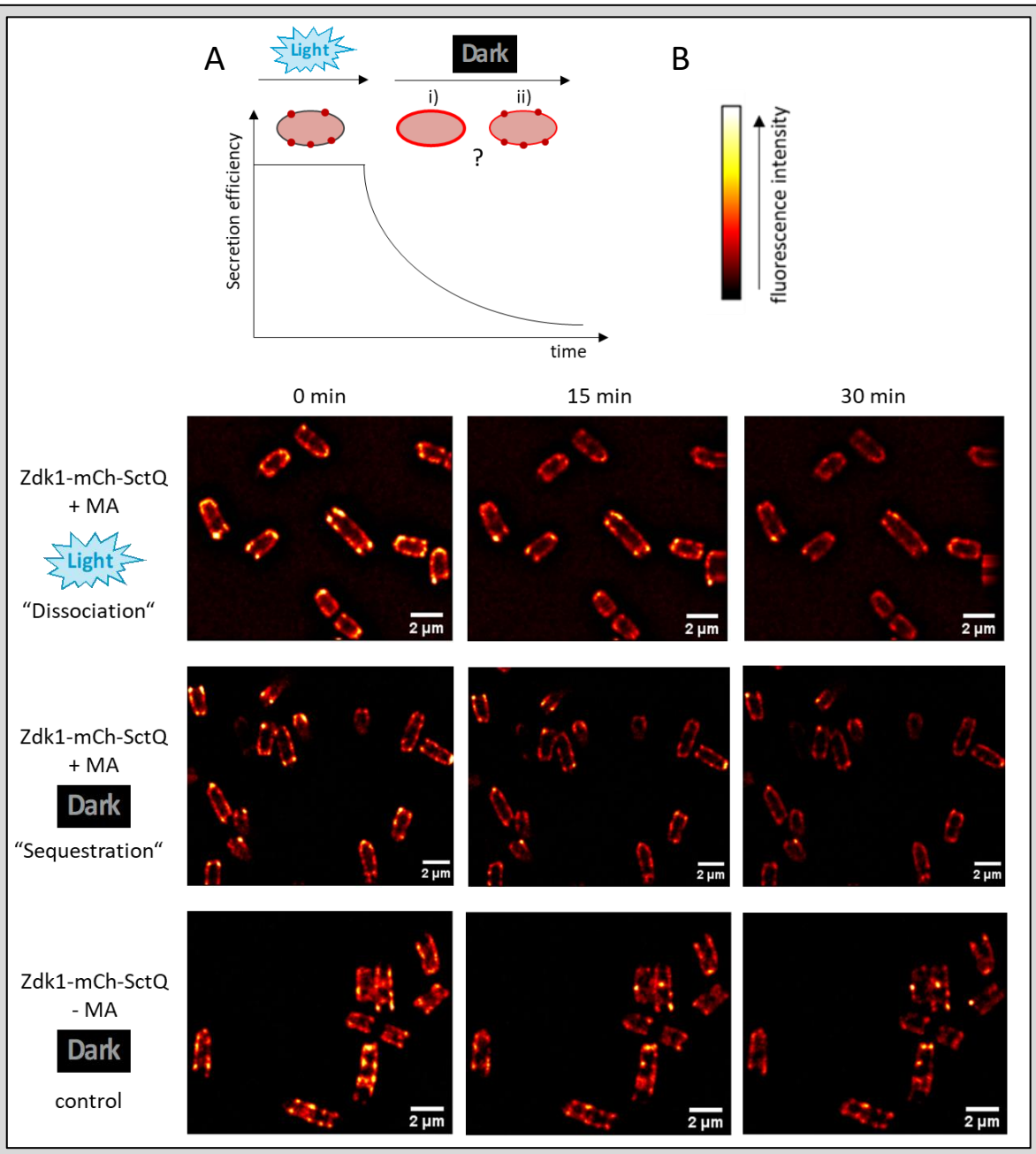

Figure 27: Spot maintenance in the LITESEC-act triple fusion Zdk1-mCh-SctQ – (**A**) Theoretical scheme of the experimental design with two possible scenarios i) and ii) (described in the main text). Bacteria were incubated under "T3SS-on"-conditions (LOVTRAP - light), so that the machinery can assemble properly. Bacteria were then visualized by fluorescence microscopy during a time course either under dark or constant blue light illumination. Preceding experiments have shown a dark dependent control of the secretion function. (**B**) Calibration scale of the red-hot depicted fluorescence intensity in (C). (**C**) Spot maintenance of Zdk1-mCh-SctQ fusion protein + MA (0.5% L-ara induction) over a time course of 30 min. Bacteria were either visualized under constant dark ("T3SS function off") or constant blue light illumination ("T3SS function on") conditions. As a control, a strain without MA was used. As excitation for the optogenetic system, a GFP excitation light of ~ 480 nm wavelength for 0.1 s every 15 s was used. mCherry fluorescence pictures were taken every minute. Scale bar is 2 µm. N=2

3.3.4 Extending optogenetic control to other cytosolic T3SS components

As the flagellar cytosolic components $FliH_2I$ ($SctL_2N$) were proposed to bind chaperones and acts as dynamic shuttle (Bai *et al.*, 2014) and the *Yersinia* ATPase SctN was shown to be involved in effector recognition (Sorg, Blaylock and Schneewind, 2006), we further extended our investigations about the cytosolic components by combining SctL and SctN with an optogenetic dimerization switch for light-controlled membrane tethering and release. Therefore we designed combinations of the iLID system with SctN and SctL and also triple fusions including the $mCh_{(NoIRES)}$-version.

We first tested the function of the new resulting $LITESEC_{SctL}$/$LITESEC_{SctN}$ strains in a secretion assay under dark and blue light conditions (Figure 28C, Figure 30A). Both combinations with SctL and SctN allowed a light-dependent control of the secretion function, indicating a working optogenetic switch. The expression sweet spot of the membrane anchor (MA) of the triple fusions is at ~ 0.2% L-ara for SspB_Nano-$mCh_{(NoIRES)}$-SctL (Figure 28C), which is slightly lower than for Zdk1-mCh-SctQ (~0.2-0.5% L-ara – Figure 28A). Noticeably, the secretion control with SspB_Nano-$mCh_{(NoIRES)}$-SctN was irrespective of the MA expression. It is conceivable that for SctN, the largest of the tested proteins, fewer proteins can bind to the MA, as the number of binding sites (and the overall surface of the membrane) is limited.

As a follow-up experiment on Figure 27, we tested whether fluorescence foci of the SspB_Nano-$mCh_{(NoIRES)}$-SctL + MA triple fusion remain or disappear over time under “secretion off” (light) conditions, as described for Figure 27 (Figure 29A). The bacterial strains were incubated under dark conditions (“T3SS function on” for iLID) so that the T3SS machinery can assemble properly. Strains were then prepared for fluorescence microscopy and observed in a time course over 30 min either under dark or constant blue light illumination conditions (representative images are displayed in Figure 29C). As seen before for Zdk1-mCh-SctQ, it seems that also for SspB_Nano-$mCh_{(NoIRES)}$-SctL + MA, T3SS specific spots remain over time, even if there is an overall reduction in fluorescence intensity, likely due to photo bleaching. Again, the control strain without the optogenetic MA displayed a more complete spot maintenance over time (Figure 29). Since there were large and bright polar inclusion spots, the overall fluorescence detection was noisier (Figure 29). This experiment was just performed once and further experiments therefore needs to be done to strengthen the data.

If the triple fusion fluorescence foci remain over time, as the results indicate, optogenetic-mediated sequestration of SctQ is more likely to reduce exchange at the T3SS spots and thus function (which would be evidence for a direct link between function and dynamic exchange) than the assembly and structure of the cytosolic complex.

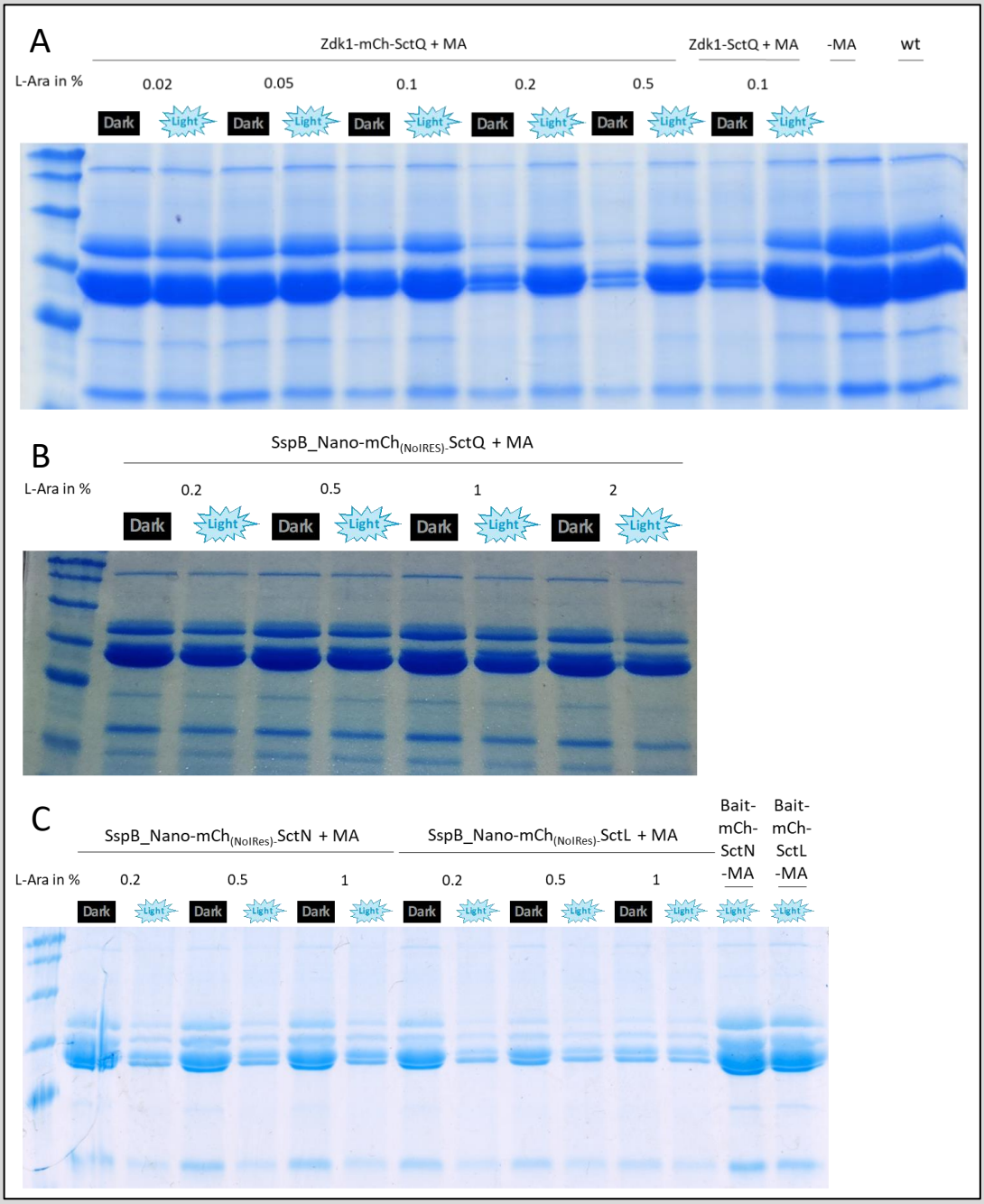

Figure 28: Expression and optogenetic control sweet spots of different triple fusions – (**A**) In vitro secretion assay showing light-dependent export of translocator proteins (SctE, A, B, W) of the LITESEC-act triple fusion (Zdk1-mCh-SctQ) + MA at different L-ara induction levels (ranging from 0.02% to 0.5%). As secretion controls, LITESEC-act2, a strain without MA and a wt (ΔHOPEMTasd) were used. Proteins secreted by $3*10^8$ bacteria that were cultivated under dark or light conditions during a 3 h incubation period were precipitated with TCA and analyzed by SDS-PAGE. N>3 (**B**) In vitro secretion assay of the LITESEC-supp triple fusion (SspB_Nano-mCh$_{(NoIRES)}$-SctQ) + MA at different L-ara induction levels (ranging from 0.2% to 2%). N>3 (**C**) In vitro secretion assay of the triple fusions SspB_Nano-mCh$_{(NoIRES)}$-ScN and SspB_Nano-mCh$_{(NoIRES)}$-ScL at different L-ara induction levels (ranging from 0.2% to 1%). As secretion controls, the strains without MA were used. N=1.

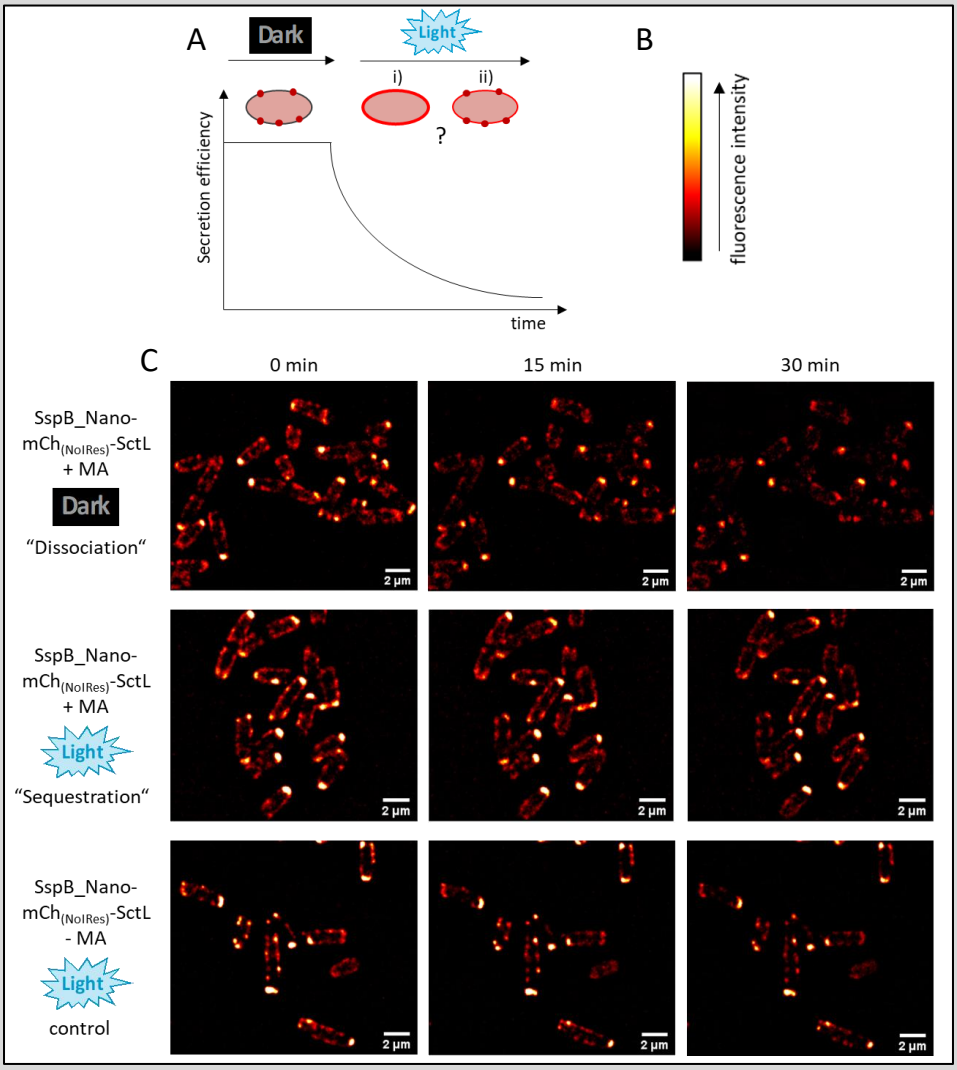

Figure 29: Spot maintenance with the triple fusion SspB_Nano-mCh$_{(NoIRES)}$-SctL – (**A**) Theoretical scheme of the experimental design. Bacteria were incubated under "T3SS-on"-conditions (iLID - dark), so that the machinery can assemble properly. Bacteria were then visualized by fluorescence microscopy during a time course either under dark or constant blue light illumination. Preceding experiments have shown a light dependent control of the secretion function. (**B**) Calibration scale of the red-hot depicted fluorescence intensity in (C). (**C**) Spot maintenance of SspB_Nano-mCh$_{(NoIRES)}$-SctQ fusion protein + MA (0.2% L-ara induction) over a time course of 30 min investigated by fluorescence microscopy. As a control, a strain without MA was used. As excitation for the optogenetic system, a GFP excitation light of ~ 480 nm wavelength for 0.1 s every 15 s was used. mCherry fluorescence pictures were taken every minute. Scale bar is 2 µm. N=1

We next tested the control of the T3SS function with all cytosolic components in combination with optogenetic interaction switches (bait-SctQ, L, N, K) (Figure 30). While showing reduced but still detectable secretion under dark conditions, secretion was nearly abolished under light (off) conditions for bait-SctN/L (Figure 30A) and bait-SctQ (Figure 30B). Since the control strains without the MA plasmid displayed secretion ability comparable to the wt strain, we could assume that the reduced secretion was indeed due to the optogenetic interaction in the bait-SctN/L + MA strains (Figure 30A).

There was a difference between SctL/N triple fusions and single fusions. While the secretion for the single fusions was nearly abolished under light conditions (Figure 30A), there was a basal level in secretion for the triple fusions irrespective of the MA expression level (Figure 28C), maybe also due to a crowding effect of the larger triple fusion proteins that led to an insufficient binding of the bait to the MA. To find an explanation for this phenotype and since the experiments were just performed one-two times, further research has to be done. Interestingly, we could not observe a control in secretion for bait-SctK (Figure 30C), which leads to new open questions about the specific function of the cytosolic components of the T3SS injectisome. It is important to consider that these experiments were just performed once (N=1), so they still have to be verified.

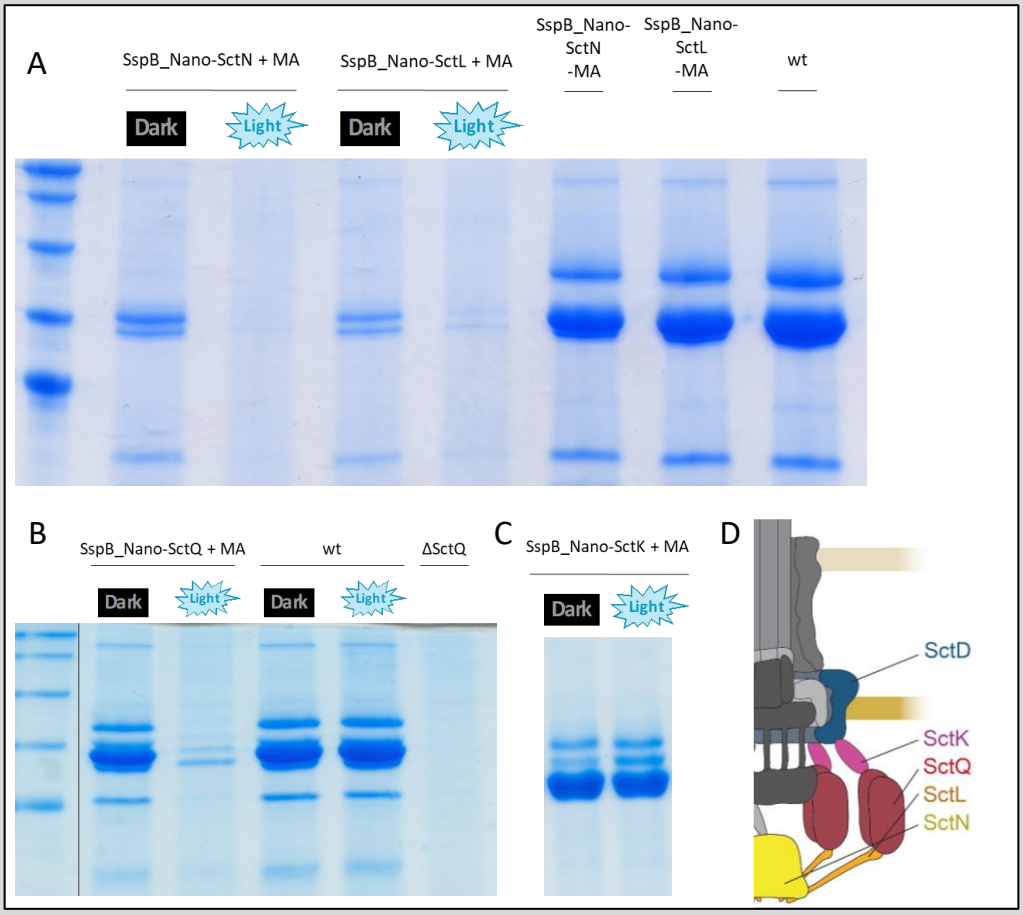

Figure 30: Difference in secretion control between the cytosolic T3SS components – (**A**) In vitro secretion assay showing light-dependent export of translocator proteins (SctE, A, B, W) of the iLID system in combination with the cytosolic components SctL/N. As secretion controls, the strains lacking the MA plasmid and a wt (ΔHOPEMTasd) were used. Proteins secreted by $3*10^8$ bacteria that were incubated under dark or blue light conditions during a 3 h incubation period were precipitated with TCA and analyzed by SDS-PAGE. N=1. (**B**) Light-dependent secretion control in the LITESEC-supp strain. As secretion controls, the wt (ΔHOPEMTasd) strain (pos.) and a ΔsctQ (neg.) were used. N=10. (**C**) In vitro secretion assay showing no light-dependent secretion of the iLID system in combination with the cytosolic component SctK under dark or respective light conditions. N=1. (**D**) Schematic figure of the cytosolic T3SS components – derived and modified from (Diepold et al., 2017).

4.1 Discussion – Part I – LITESEC-T3SS

The LITESEC system presented in this work uses light-controlled sequestration of an essential dynamic T3SS component to precisely regulate the activity of the T3SS. This approach provides a new method for highly time- and space-resolved protein secretion and delivery into eukaryotic cells. The discussion about the LITESEC-T3SS section is mainly adapted from the publication (Lindner *et al.*, 2020), with some points modified and extended.

4.1.1 Control of the T3SS function with LITESEC

The T3SS is a very promising tool for protein delivery into eukaryotic cells, both in cell culture and in healthcare (Ittig *et al.*, 2015; Walker, Stan and Polizzi, 2017; Bai *et al.*, 2018). However, the T3SS indiscriminately injects cargo proteins into contacting host cells. Lack of targetability is therefore a main obstacle in the further development and application of this method (Felgner *et al.*, 2017; Walker, Stan and Polizzi, 2017). Previous methods to control the activity of the T3SS relied on controlled gene expression of one or all components of the injectisome. For example, Song and colleagues expressed all components of the *Salmonella* SPI-1 T3SS from two inducible promoters in a clean expression system (Song *et al.*, 2017), and Schulte *et al*. expressed the T3SS genes from a TetA promoter, which additionally allows the intracellular induction of the T3SS (Schulte *et al.*, 2018). Besides the difficulty to specifically induce secretion in defined places *in situ*, the main drawback of these methods is the slow response (induction of expression and assembly of the T3SS take more than 60 min (Diepold *et al.*, 2010; Song *et al.*, 2017; Schulte *et al.*, 2018)). In addition, in these systems, the T3SS remains active as long as the induced protein(s) are still present, which leads to a higher risk of translocation into non-target cells.

To overcome the lack of specificity of T3SS-dependent protein secretion and translocation into eukaryotic cells, we aimed to control T3SS activity by external light. Our solution exploits the recently uncovered dynamic exchange of various essential T3SS components between an injectisome-bound state and a freely diffusing cytosolic state (Diepold *et al.*, 2015, 2017) to control T3SS-dependent protein secretion by protein sequestration. SctQ, an essential and dynamic cytosolic component of the T3SS (Diepold *et al.*, 2015), was genetically fused to one interaction domain of two optogenetic sequestration systems, the iLID and LOVTRAP systems (Kawano *et al.*, 2015; Wang *et al.*, 2016; Zimmerman *et al.*, 2016), while the membrane-bound interaction domain was co-expressed *in trans*.

The two versions of the resulting LITESEC-T3SS system (**L**ight-**i**nduced **s**ecretion of **e**ffectors through **s**equestration of **e**ndogenous **c**omponents of the **T3SS**) can be applied in opposite directions: in the LITESEC-supp system, protein export is suppressed by blue light illumination; the LITESEC-act system allows to activate secretion by blue light (Lindner *et al.*, 2020).

The LITESEC-supp1 system, which is based on the iLID optogenetic interaction switch (Guntas *et al.*, 2015) (Table 1), showed a significant reaction to light (light/dark secretion ratio of 0.28; 24% vs. 85% of wild-type secretion under light and dark conditions, respectively (Figure 10). Expression of the membrane anchor from a constitutively active promoter on a low expression plasmid, pACYC184 (LITESEC-supp2) retained the light/dark secretion ratio (L/D ratio of 0.26; 24% vs. 93% WT secretion (Figure 11), with the additional advantage that expression of the membrane anchor is constitutive.

For many applications, activation of T3SS protein export upon illumination is preferable. The optogenetic interaction switch employed for this purpose must (i) dissociate upon illumination (allowing activation of the T3SS); (ii) be independent of cofactors that are not present in wild-type bacteria; (iii) be activated by visible or infrared light (compatibility with eukaryotic host cells); (iv) consist of a heterodimer (otherwise, the interaction between individual SctQ molecules, which oligomerize *in vivo*, would be influenced, which would impact protein secretion (Diepold *et al.*, 2015)). Of the available protein optogenetic interaction switches (Mukherjee *et al.*, 2017; Benedetti *et al.*, 2018; Klewer and Wu, 2019), the LOVTRAP system (Wang *et al.*, 2016) fulfils all requirements. However, the first version of the resulting T3SS (LITESEC-act1) only achieved weak activation of T3SS secretion upon illumination (Figure 11). LITESEC-act2, which uses the V416L mutation in the anchor protein LOV2 (Kawano *et al.*, 2013) to decrease the affinity between anchor and bait, could be activated by light more efficiently. Even more strikingly, LITESEC-act3, featuring a reduced expression level of the V416L variant of the membrane anchor, led to a strong activation of T3SS protein secretion upon illumination, while retaining the tight suppression of secretion in the dark (L/D ratio of 4.2; 66% vs. 16% (Figure 11)). In the LITESEC-supp system, the decreased anchor levels in the –supp2 variant did not lead to significant changes in the activation of secretion, suggesting that this system is less sensitive to changes in the anchor/bait ratio, and indicating that the achieved L/D ratio is the optimum for native secretion substrates.

4.1.2 Kinetics of LITESEC activation and deactivation

Both reaction time and recovery dynamics of the sequestration systems are crucial for their applicability to control the function of the T3SS. Fast reaction times to blue light increase the temporal precision of T3SS activation/deactivation, whereas the recovery times influence the duration of the effect on secretion after illumination. Very fast recovery means that the system has to be continuously illuminated for a sustained effect on secretion, while very slow recovery leads to long-term activation/deactivation that is difficult to revert, and renders handling of the cultures difficult due to possible long-term effects of illumination prior to the actual experiment. In time-course experiments we could show that in the iLID-based protein sequestration system, unbinding of the bait in the light state was almost immediate, and that recovery in the dark occurred within few minutes (Figure 7), in line with data from eukaryotic systems (Zimmerman et al., 2016). In the resulting LITESEC-supp system, both activation and deactivation of type III secretion occur relatively quickly, within the first minutes (Figure 14C), which is in the range of the measured turnover of SctQ at the injectisome (half-time of about 70 s under secreting conditions (Diepold et al., 2015)). This suggests that the release and rebinding of the bait protein occurs faster or in a similar time range, consistent with the microscopy results (Figure 7). For the LITESEC-act system, we detected a slower activation and deactivation of protein secretion (Figure 14C). Nevertheless, induction of protein secretion by blue light occurs also within several minutes. Importantly, in the absence of further illumination, protein secretion is stopped within minutes, which greatly limits unwanted unspecific activation for the LITESEC-act system. Long-term activation can be achieved by either constant low-intensity blue light illumination, or short light pulses every few minutes. Ambient laboratory light did not inhibit the LITESEC-supp2 strains, but lead to an intermediary activation of LITESEC-act3 (Suppl. Figure 2).

4.1.3 Experiences from the development of LITESEC

Notably, the export of heterologous cargo was entirely light-dependent (no visible export under inactive conditions (Figure 13)) in both LITESEC variants. The LITESEC-act3 system was less efficient for heterologous cargo expressed from plasmid (around 50% secretion efficiency) and activated more slowly than LITESEC-supp2 (Figure 13, 14). This indicates that despite the V416L point mutation (LITESEC-act2) and the changed anchor/bait expression ratio, parts of SctQ remain tethered to the membrane after illumination and secretion is therefore still affected. For the majority of applications, the tight regulation of secretion in the off state shared by both LITESEC systems will be more important than the maximal translocation rate.

Interestingly, endogenous T3SS translocator proteins were still secreted to a basal level under inactivating light conditions, even in the most tightly controlled strains (LITESEC-act3/-supp2 (Figure 11)). This might indicate that the export of heterologous cargo is regulated differently from the export of the endogenous translocators, which for example also involves protein-specific chaperones. While this hypothesis remains to be rigorously tested, it highlights that beyond their application, LITESEC and similar optogenetic approaches can help to better understand the underlying biological systems.

To explore the influence of the anchor/bait expression ratio on light control of the T3SS in more detail, we measured the light-dependent activation of the LITESEC-act2 system at different expression levels of the anchor protein. The results indicate that intermediate anchor/bait ratios allowed an optimal response to blue light for the LITESEC-act system. Higher ratios retain partial membrane sequestration under light conditions and subsequently impair T3SS activity in the activated stage; conversely, low ratios lead to incomplete sequestration and measurable T3SS activity under non-activating conditions (Figure 12). Taken together, our data strongly suggest a relatively tight sweet spot in the expression ratio of the two interacting proteins, which may be key for the successful optogenetic control of bacterial processes. This is in contrast to the eukaryotic application of the LOVTRAP interaction switches where high anchor/bait concentrations where shown to be optimal (Wang *et al.*, 2016). We therefore propose that optimization of the anchor/bait expression ratio represents an important step in the design of optogenetically controlled processes in prokaryotes.

The successful development and application of the LITESEC system highlights some key features for the control of intracellular processes in prokaryotes by optogenetic interaction switches. The target protein (in our case the essential T3SS component SctQ) (i) has to be functional as a fusion protein to an optogenetic interaction domain, (ii) must be present in the cytosol at least temporarily to allow sequestration to occur, and (iii) must not be functional when tethered to the membrane anchor protein. To fulfil the last criterion, the target protein may feature a) a specific place of action (such as the injectisome for SctQ in the present case), or b) a specific interaction interface that is rendered inaccessible by the interaction with the anchor. In eukaryotic systems, proteins have been sequestered to various structures including the plasma membrane or mitochondria. The simpler cellular organization of bacteria makes the inner membrane an obvious target for protein sequestration, to which interaction domains can be easily targeted to by the addition of N-terminal TMHs. While the nature of the TMH is likely to be secondary for the success of the application, the extended TatA TMH and a short glycine-rich linker worked well for our approach.

Crucially, we found that the expression ratio between anchor and bait proteins is a key determinant for the success of LITESEC and, most, likely, similar approaches to control bacterial processes by light (Figure 12) (Lindner *et al.*, 2020).

The LITESEC system allows to deliver proteins into host cells at a specific time and place. The system gives complete control over the secretion of heterologous T3SS cargo into the supernatant, either by providing illumination (LITESEC-act), or stopping the light exposure (LITESEC-supp). Importantly, secretion by the LITESEC-act system is temporary, and stopped within minutes after the end of illumination with blue light, thereby further reducing unspecific activation.

An important consideration in the application of bacteria for protein translocation into eukaryotic cells is a possible toxic or immunogenic effect of the bacterial vector (Felgner *et al.*, 2017; Walker, Stan and Polizzi, 2017). The *Y. enterocolitica* strain used in this study has been depleted of the main virulence effectors YopH,O,P,E,M,T and is a cell wall synthesis auxotroph, which cannot replicate in the absence of externally added diaminopimelic acid. Accordingly, LITESEC bacteria in which secretion is not activated have little or no visual effect on the host cells, even after long incubation of the cells after infection (Suppl. Figure 4). However, the ongoing development of less immunogenic bacterial vectors through modification or deletion of pathogen-associated molecular patterns and other means (Neeld *et al.*, 2014; Felgner *et al.*, 2016; Walker, Stan and Polizzi, 2017; Bai *et al.*, 2018) remains an essential factor for the successful application of this technique in medicine and biotechnology.

4.1.4 Current and possible future applications of the LITESEC system

A main application of the LITESEC system is the temporally and spatially controlled translocation of proteins into cultured eukaryotic cells (Figure 15). Cell cultures play an important role in research, development and, increasingly, healthcare. Often, specific proteins need to be expressed in all or a subset of the cultured cells at a given time point. At the moment, this is mainly achieved by inducing expression of the target protein in the host cells. This method requires prior transfection of the host cells with the target gene or time-consuming creation of stable transgenic cell lines. Induction of expression itself is relatively slow, and difficult to apply to a certain subset of cells. Our method allows to translocate proteins into unmodified host cells with high specificity. Bacteria that lack their native virulence effectors (such as the *Y. enterocolitica* strain used in this study), but express one or more cargo proteins with a short secretion signal, are brought into contact with host cells.

The chosen subset of host cells are then subjected to dark or blue light conditions (which does not influence bacteria or host cells at the used intensity), which temporarily induces translocation of the cargo into the host cells within short time. An additional advantage of the LITESEC method is that it directly translocates proteins into the host cell, rather than inducing the transcription of mRNA, as is the case in the current inducible transfection systems. The amount of translocated protein can be regulated by the duration of illumination/darkness, and the multiplicity of infection (ratio of bacteria / host cells) (Ittig et al., 2015).

A potential, relatively straightforward extension of our work would allow the specific protein delivery into diseased cells, such as cancer cells, within biological tissues. The T3SS has been used to treat cancer cells in vitro, e.g. by translocating angiogenic inhibitors (Shi et al., 2016), but again, the promiscuity of the T3SS and the resulting unspecific translocation at non-target sites represent a major obstacle in the further development of T3SS-based methods for clinical applications (Walker, Stan and Polizzi, 2017). Most current approaches rely on localized injection of bacteria or the natural tropism of bacteria to tumorous tissue. However, bacteria applied with these methods are not restricted to the target tissue, and unspecific activation presents a problem, especially for potentially powerful applications such as the delivery of pro-apoptotic proteins. By using light to specifically activate the modified T3SS in bacteria at a site of choice, delivery of effector proteins could be temporarily induced at a specific time and place. This method would reduce unspecific activation and side effects, allowing a highly controlled targeting of host cells. Bacteria could be applied to the patient (exploiting the natural tropism of bacteria for tumor tissue to achieve local enrichment in the case of cancer), where injection of the effector protein would be triggered in situ with high spatial and temporal precision using light delivered with the help of endoscopes and minimally-invasive surgery techniques. As the blue light used to control the current LITESEC systems does not penetrate tissue efficiently, activation by red or far-red light would be advantageous. Several such red-light systems have been characterized (Shimizu-Sato et al., 2002; Kaberniuk, Shemetov and Verkhusha, 2016; Reichhart et al., 2016); however, all of these systems require cofactors not usually present in bacteria.

4.2 Discussion – Part II – Applications and Improvement of LITESEC-T3SS

The LITESEC-T3SS combines optogenetics with the bacterial injectisome to create a spatiotemporal controllable protein delivery tool into eukaryotic cells (Lindner *et al.*, 2020) with broad application potential (Bai *et al.*, 2018). My next aim was to improve the application and adapt it to a collection of different cargos. For this purpose, I worked on the incorporation of a far-red light optogenetic switch to the LITESEC application. We also cooperated with RG Stiewe (Molecular Oncology, Marburg) and RG Hantschel (Physiological Chemistry, Marburg) to establish LITESEC as a delivery platform for certain therapeutic cargos. The results presented in this thesis, highlight the importance of protein stability and cognate chaperone co-expression for the efficient cargo translocation into eukaryotic host cells and present essential rules for further application of LITESEC-T3SS.

4.2.1 Establishment attempt of a far-red light optogenetic switch in LITESEC

The establishment of a red/far-red light optogenetic interaction switch such as PhyB-PIF6 (Toettcher, Gong, *et al.*, 2011) would be a step towards possible applications of the LITESEC system within living tissues, since red light can penetrate tissue layers up to a depth of 5 mm, which is five times as much as blue light is able to (1 mm) (Ash *et al.*, 2017). For this purpose, we tested a modified dimerization switch pair AtPhyB-PIF6A that is shortened in protein size and was shown to retain a strong light response (650 nm association / 740 nm dissociation) (Golonka *et al.*, 2019). The cofactor phycocyanobilin (PCB), required by this optogenetic system, is usually not present in bacteria and therefore has to be co-synthesized, as was already shown and applied for optogenetic applications in *E. coli* (Schmidl *et al.*, 2014; Ma *et al.*, 2020). Based on the observation of the importance of a “sweet spot” in expression ratio during the LITESEC studies (Figure 12) (Lindner *et al.*, 2020), we established the PCB synthesis pathway on an IPTG-inducible plasmid (pMMB - Schmidl *et al.*, 2014). The synthesis of PCB in bacteria starts with heme b, which is naturally abundant in most bacteria (Dailey *et al.*, 2017), and is then converted via biliverdin (catalyzed by Ho1) to PCB (catalyzed by PcyA) (Gambetta and Lagarias, 2001). By ranging the expression induction with IPTG, we can adapt the expression ratio to the expression of the anchor AtPhyB and the bait PIF6-SctQ, as the expression ratio between anchor and bait was also shown to be important for function of the red-light dimerization switch (Toettcher, Gong, *et al.*, 2011).

Metabolomics mass spectrometry analysis (performed with help of the MPI internal metabolomics facility – Nicole Paczia) detected synthesized PCB (molecular weight = 586, 69 g/mol) in the bacterial samples and the amount of PCB correlated with the induction level of IPTG (Figure 17A), as expected.

Interestingly, when the strain expressed the MA plasmid including the AtPhyB domain, significantly less PCB was detected, which could be due to an incorporation of PCB into the phytochrome (Figure 17). During growth and secretion experiments, we noticed that PCB has a negative effect on the bacteria, indicated by a decreased growth (Suppl. Figure 5) and secretion function (Figure 17). This was also recognized in studies by (Raghavan, Salim and Yadav, 2020), where PCB lowered the biomass at higher expression levels. Unfortunately, they never further pursued this observation.

By decreasing the IPTG induction to 1 µM, we could minimize the effect of PCB on the bacterial cells and performed further experiments with this expression. However, we could not observe a light-dependent secretion control with the redLITESEC system (Figure 18B), in contrast to what we have previously achieved with the blueLITESEC (Figure 10, 11, 12) (Lindner *et al.*, 2020). Protein expression levels and stability tests of the optogenetic interaction partners showed that, while the bait-SctQ fusion was stable (Figure 18D), the C-terminal MA (AtPhyB-FLAG-HMD) displayed no stable expression in an anti-FLAG Western blot (Figure 18C). Since expression of the cofactor PCB showed a strong negative effect on the growth and T3SS function of *Y. enterocolitica* and the C-terminal MA, which literature said to work better for PhyB functionality (Toettcher, Gong, *et al.*, 2011), was not stably expressed, we decided to stop research on the redLITESEC at this point.

Future work has to consider the potential negative effect of the cofactor PCB on *Yersinia*. Other Enterobacteria, such as *E. coli,* did only show such a negative effect from PCB at high expression levels (Raghavan, Salim and Yadav, 2020), and red light optogenetic applications were established in *E. coli*, for example with the dimerization switch PhyB-PIF3 (Raghavan, Salim and Yadav, 2020). In this study, they established the PhyB-PIF3 dimerization switch to light-dependently control the association of a split T7-RNAP (T7-RNA-Polymerase). Contrary to our studies, they supplied δ-aminolevulinic acid (δ-ALA), a key intermediate in the heme biosynthetic pathway, to the growth medium in order to enhance the production of heme b, which is further bioconverted to PCB (Raghavan, Salim and Yadav, 2020). Since this additional step was just introduced to enhance the synthesis of PCB, which led to a growth and secretion reduction in *Y. enterocolitica* (Figure 17), it seems unlikely that this is the missing element. Another option would be the establishment of a different red-light optogenetic switch that uses another cofactor, biliverdin, which potentially does not harm *Yersinia* as much as PCB. Such systems were up to now just applied in *E. coli* for the purpose of gene expression control (Ong, Olson and Tabor, 2018) and would need further adjustment. If red-light optogenetic systems are not applicable to *Yersinia*, one could consider incorporating blueLITESEC strains into upconverting nanoparticles. These nanoparticles can be excited with red light and then emit blue light luminescence themselves and can also be used in human tissues (Yang *et al.*, 2020).

4.2.2 Protein stability and chaperone co-expression influences the translocation rate of cargos

One potential therapeutic application of the LITESEC-T3SS is the translocation of pro-apoptotic proteins (Vogiatzi *et al.*, 2016) into cancer cells either in cell cultures or living tissue. Controlling this translocation with light would allow for spatially and temporally resolved precision, which would be advantageous over chemotherapy that lacks spatiotemporal specifity. An important point to consider is a possible immunogenic effect of the bacteria to the host. Bacterial antigens inside the human body are recognized by the immune system, which lead to an upregulation of the immune response and the production of pro-inflammatory cytokines (Toussaint *et al.*, 2013). There are studies on addressing these issues, for example by reducing the antigens expressed on the outer surface of the bacterial vector or diminution of replication capacities (Toussaint *et al.*, 2013). The bacterial strain that was applied for LITESEC-T3SS is depleted of all native pathogenic effectors and showed no damaging effect on eukaryotic cell cultures, even when incubated up to 18 h (Lindner et al., 2020) (Suppl. Figure 4). The bacteria are furthermore auxotrophic for the cell wall component diaminopimelic acid and can therefore not grow in its absence (Lindner *et al.*, 2020).

As a proof of principle for the application of LITESEC in living tissues, we worked on an establishment of a Cre-lox reporter system (Zomer *et al.*, 2015) to display light-dependent translocation in cell culture and living tissue (Figure 19). For this purpose, we designed the cargo $YopE_{1-138}$-Cre including the cognate chaperone SycE co-expression from the same locus (constitutive pACYC184 vector (Chakravartty and Cronan, 2015)). Studies have shown that the co-expression of the cognate chaperone from the same locus increases the translocation efficiency of the corresponding native effector (Brinkworth *et al.*, 2011; MacDonald *et al.*, 2017). To test whether this is also applicable for non-native cargos in the LITESEC application, we tested the translocation efficiency of pro-apoptotic cargos into HEp-2 cells with and without chaperone co-expression (Figure 21). Indeed, we could display an enhancing effect of a chaperone co-expression on the translocation efficiency of non-native cargos, indicated by an increased amount of apoptotic cells already at 1 h after infection (Figure 21).

In secretion experiments with the cargo $YopE_{1-138}$-Cre, we could detect the secreted cargo with an anti-Cre Western blot; however, Coomassie SDS-PAGE revealed a reduced secretion of all native translocators for this secretion strain (Figure 19C). Also the translocation efficiency into Lox-P reporter cell lines appeared to be lower than for other cargos (Lindner *et al.*, 2020) (Figure 19D). Studies on other T3SS cargos have shown that stably folded proteins such as GFP slows down the translocation rate of the cargo and jams the injectisome by blocking it to a certain degree (Lee and Schneewind, 2002; Radics, Königsmaier and Marlovits, 2014).

This is coherent with the finding that T3SS cargos have to be unfolded prior to export (Akeda and Galán, 2005). Observations from several experiments presented in this thesis, where stable folded cargos such as mCherry (Figure 24B), Cre (Figure 19A, B) and monobodies (Figure 20) were secreted to a lower amount and the majority of the cargo remained in the cells, support the hypothesis that protein stability correlates with the secretion efficiency of the cargo. During the monobody studies, we could also observe that mutations that were introduced to decrease the protein stability and facilitate the unfolding without influencing the functionality enhanced the secretion and translocation efficiency (Figure 20). For further studies, a design of a modified Cre protein with a decreased protein folding stability, introduced by mutations, could therefore enhance the secretion and translocation efficiency and make it a useful tool to investigate light-dependent protein translocation into living tissues (Sheller-Miller *et al.*, 2019). Nevertheless, there are studies that showed a secretion system dependent delivery of the Cre recombinase into eukaryotic cells, such as for the T3SS of *P. aeruginosa* (Bichsel *et al.*, 2011) or the T4SS (Trokter and Waksman, 2018). Notably, for the T3SS studies with *P. aeruginosa*, a mutant strain was used that displayed a ten times higher translocation ability of the effector ExoS compared to the wt strain PAO1. By performing translocation assays with this mutant strain, in which different N-terminal parts of ExoS were fused as a secretion signal to the Cre cargo, and translocation experiments were performed for 3 h (in our case 1 h), the amount of translocated cells were up to 30 % (Bichsel *et al.*, 2011). We noticed that PC-9 cells had a higher rate of positive translocated cells (9.8%) than fibroblasts (1.7%), perhaps because fibroblasts were very sticky and the bacteria could not reach all the cells within these sticky clumps. In addition, many cells showed both red and green fluorescence, so the time the cells were analyzed after 48 hours may not have been sufficient for recombination. Since other studies also visualized the cells 48 hours after infection and detected a sufficient amount of recombinant cells, this should not be the reason (Bichsel *et al.*, 2011).

4.3 Discussion – Part III – Investigation of dynamic processes and properties of the cytosolic complex of the T3SS using the established optogenetic interaction switches

Beside the control of the T3SS function that was achieved by the introduction of optogenetic dimerization switches (Figure 6) (Lindner *et al.*, 2020), the light-mediated protein tethering and release enables a completely new way to investigate protein interactions and dynamics *in vivo* and real time. By the sequestration of a dynamic cytosolic T3SS component, such as SctQ (Diepold *et al.*, 2015), protein interactions and injectisome assembly or exchange events can be investigated from a new direction. To this end, we extended the application of optogenetic interaction switches and present the obtained results in the next section.

4.3.1 Does the cytosolic component SctQ has a specific role in effector secretion?

During the characterization of the LITESEC system, we recognized that there was a difference in the secretion of native *Yersinia* translocators compared to heterologous cargo proteins, when we light-dependently controlled the availability of SctQ. While heterologous cargo proteins could not be detected in the supernatant at “off”-conditions (Figure 13), native translocators were reduced to a basal level (~20%) but still detectable on a SDS-PAGE Coomassie gel (Figure 11) (Lindner *et al.*, 2020). Because of those observations and the observations from (Lara-Tejero *et al.*, 2011), in which they proposed that SctQ is part of a sorting platform in *Salmonella*, we investigated a potential specific role of SctQ in effector secretion and if SctQ differentiates between different types of cargo.

By expressing SctQ from an inducible plasmid in a SctQ deletion background, we wanted to investigate if some late substrates like the effectors (see 1.3.3 for substrate hierarchy) are more abundant in a secretion assay than compared to the wt, because SctQ specifically is required for secretion of these substrates. However, increasing expression of SctQ did not lead to a specific increase of translocator export (Figure 22A). Notably, already at lower expression levels of SctQ (0.0005% L-ara) compared to SctQ expression levels in the wt (indicated in the Western blot (Figure 22A), exact values were not determined), the secretion function was nearly restored, with a maximum secretion function at 0.01% L-ara induction (Figure 22A). This suggests that even a low copy number of SctQ is sufficient to almost completely restore secretory function. Strikingly, overexpression of SctQ led to an overall decrease in secretion of all substrates, while overexpression of eGFP did not lead to a similar phenotype (Figure 22B), therefore excluding a direct effect of protein overexpression or molecular crowding. A reason for the SctQ-specific phenotype could be that overexpression of this cytosolic component leads to a shift in the expression ratio of the T3SS proteins.

Expression levels of the T3SS proteins are tightly regulated and linked to function (Diepold and Armitage, 2015), and it is possible that overexpression of one component influences the abundance of the cytosolic components stoichiometry and therefore the formation of the cytosolic complex.

Interestingly, by comparing the secretion phenotype of MRS40-based LITESEC (presence of effectors) with ΔHOPEMTasd based LITESEC (absence of effectors) a difference in the basal secretion pattern under “off” conditions was recognized. Results showed that while for LITESEC-act (ΔHOPEMTasd) the early translocators SctA/E/W were most abundant under “off” conditions, the pattern for LITESEC-act (MRS40) looked different with the most abundance of the later translocators YopM/H/E (Figure 22C). Whether the LITESEC-mediated control of SctQ affects the secretion hierarchy and nature of T3SS sorting processes in *Y. enterocolitica,* as such a link between SctQ and the sorting process has been proposed for *Salmonella* (Lara-Tejero *et al.*, 2011), or whether this phenotype merely exhibits reduced representation of the most abundant secretion bands of the specific strain (which would be more likely based on the data) remains to be seen.

4.3.2 Optogenetics reveals new interaction properties of the cytosolic complex

With optogenetics, we want to investigate the open questions about the cytosolic components by using the optogenetic interaction switch for protein interaction and dynamic studies. First, we checked if we can use the optogenetic tethering effect of the bait-SctQ to the membrane to investigate possible direct interactions between SctQ and other cytosolic components under certain conditions. Since the assembly of the cytosolic complex requires the presence of all cytosolic components (Diepold *et al.*, 2010, 2017), it is difficult to determine the binding properties of the cytosolic components amongst themselves by classical knockout experiments. During our experiments, we could show a specific binding of SctQ to the other cytosolic components SctL and SctK in the absence of the ATPase SctN (Figure 23). This observed direct protein interaction between SctQ and SctK is partially new and differs to the observations from (Diepold *et al.*, 2017), where such an interaction could not be detected in the absence of SctN (Figure 5C). Even if there are studies that showed interaction of some cytosolic components prior to injectisome assembly (Johnson and Blocker, 2008; Bernal *et al.*, 2019), optogenetics provides a new way to investigate such protein interactions in a more direct way in real time inside living cells.

In the future, this approach may be used to test further interactions between cytosolic components in living bacteria under different conditions such as knockout backgrounds and secreting vs. non-secreting conditions and therefore investigate the complex interaction network of the cytosolic complex (Diepold *et al.*, 2017; Bernal *et al.*, 2019). Studies have already shown that the binding properties between cytosolic components differ between secreting and non-secreting conditions and are heavily influenced by deletions within the cytosolic complex (Diepold *et al.*, 2017). As the optogenetic membrane tethering principle was shown to be superior to traditional immunoblot studies and could reveal interaction not previously seen under knockout conditions (interaction between SctQ and SctK in a *ΔsctN* background) (Diepold *et al.*, 2017) (Figure 23), one might consider using this principle to investigate unseen or unproven dynamic protein correlations.

Such an unproven correlation in the field of T3SS research is the potential link between cytosolic components and chaperone/effector complexes. In *S. typhimurium*., the cytosolic complex has been proposed to contribute to substrate selection and translocation of effectors and was therefore termed as a “sorting platform” (Lara-Tejero *et al.*, 2011), but this remains the only published study to date. Also in the flagella T3SS, a model was proposed where a $FliH_2I$ ($SctL_2N$) complex binds chaperones and acts as a dynamic carrier (Bai *et al.*, 2014; Wagner *et al.*, 2018). Nevertheless, there are doubts that the cargo shuttle is directly linked to effector secretion, as the measured export rate of up to ~ 60-200 molecules per second (Enninga *et al.*, 2005; Schlumberger *et al.*, 2005; Ittig *et al.*, 2015) is far above the calculated rate of cytosolic turnover for SctQ (Diepold *et al.*, 2015) – reviewed in (Diepold, 2020). A direct contribution of cytosolic components to substrate shuttling and sorting in real time has not yet been demonstrated and is considered the “holy grail” in T3SS research (personal comment from Petra Dersch, University of Münster, Scientific Advisory Board).

To address this open question, we fused mCherry either to the chaperone SycH or to specific effector secretion signals that include either just the secretion domain ($YopE_{1-53}$), or additionally the chaperone-binding domain ($YopE_{1-138}$) (Figure 24A). We could not detect an interaction between SctQ and SycH-mCh, which would be indicated by a movement of the fluorescence signal to the membrane, as it was observed for mCh-SctL/K (Figure 23). We also tested whether co-expression of the chaperone SycE from the same locus would support possible binding to $YopE_{1-138}$-mCh, as this has been shown to be critical for translocation of cargos including this secretion signal (Figure 21). Expression from the native promotor region that has been shown to be co-regulated with the T3SS secretion function (Jonas Pettersson *et al.*, 1996), led to an overexpression of the mCherry cargo, which resulted in large inclusion bodies in the bacterial cells (Figure 24A, B).

We therefore were unable to see a movement of the fluorescence signal to the membrane, which would have indicated an interaction of the cargos with SctQ. Whether a direct link between the cytosolic component SctQ and chaperone/effector cargos, as proposed by (Lara-Tejero *et al.*, 2011), does not exist and therefore could not be observed, or whether the expression ratio between bait and cargo was simply not in the sweet spot, remains open. It is difficult to compare and achieve native expression levels with an artificial inducible plasmid, wherefore we did not express the cargo from an arabinose-inducible vector and decrease the expression level yet. Since specific expression ratios have been shown to be important for the optogenetic membrane tethering principle and functional control (Figure 12), further studies could address this issue by co-expressing cytosolic bait and chaperones (or other proteins for which a potential interaction should be observed) from inducible plasmid vectors. To this end, screens comparing expression ratios from a vector with native protein levels and correlated T3SS function must be performed beforehand.

4.3.3 The cytosolic T3SS components display dynamic properties, investigated with optogenetic interaction switches

Despite being able to control T3SS function by controlling the availability of the essential cytosolic component SctQ (Lindner *et al.*, 2020), the biological explanation for this phenotype is still unclear. Is it because sequestration of SctQ leads to gradual disassembly of the structure of the injectisome, or do we influence the dynamic nature of the cytosolic complex, which was proposed to directly correlate with the T3SS function (Diepold *et al.*, 2015). Studies have already shown that the cytosolic T3SS components SctQ is dynamic and in a constant exchange between the cytosolic state and injectisome-associated sites, as observed by FRAP (Diepold *et al.*, 2015), and that this dynamic behavior is further increased under secreting conditions (Diepold *et al.*, 2015, 2017). Using single molecule tracking, researchers later investigated cytosolic and dynamic co-diffusion of SctQ and SctL (Rocha *et al.*, 2018). For the flagellum it has been shown that several parts of the T3SS display dynamic behaviors such as FliM (SctQ) (Fukuoka *et al.*, 2010), FlhA (SctV) (Li and Sourjik, 2011) or FliI (SctN) (Bai *et al.*, 2014) (reviewed in (Tusk, Delalez and Berry, 2018)), whereas for the injectisome, SctQ and SctL (indirectly) are the only published components that displays a dynamic nature. It is known that the cytosolic complex only fully assembles to the injectisome and that knocking out one component leads to a deficit in the assembly of the other components (Diepold *et al.*, 2017), even when cytosolic sub complexes exist (Bernal *et al.*, 2019), which has also been shown for the flagellum (Notti *et al.*, 2015).

So far, it is not known exactly how the exchange at the T3SS interface works. Are the monomeric proteins at the assembled cytosolic T3SS complex actively replaced by a replacement protein, which could be consistent with a substrate shuttle effect (Lara-Tejero *et al.*, 2011), or do the proteins bound to the T3SS simply unbind over time, and replacement by new proteins therefore occurs only when there is a “free space”.

To address this open question, the presented principle of optogenetically mediated sequestration was used to investigate dynamic exchange of the cytosolic complex, initially in FRAP experiments. Diepold and colleagues could already display the dynamic nature (average recovery half-time t½ of 68.2 ± 7.9 s) of the cytosolic component SctQ (Diepold *et al.*, 2015) using FRAP. Based on the LITESEC studies and the investigation of a direct interaction between StcQ and SctL (Figure 23), we screened for dynamic changes of spot recovery of mCh-SctL, when SctQ is sequestered to the membrane with optogenetics. Our hypothesis was that if we affect the dynamic exchange rate of the cytosolic complex by sequestering SctQ, we should see an effect on mCh-SctL dynamics, as indicated by a difference in the recovery of fluorescence spots between dark (bait-SctQ cytosolic) and light (bait-SctQ membrane bound) conditions. If sequestration of SctQ directly influences the dynamic exchange of SctL at the injectisome interface, we would expect a decrease in fluorescence recovery after photo bleaching under light conditions (sequestration of SctQ) compared with dark conditions (SctQ cytosolic).

Performing FRAP experiments with the LITESEC-supp2 strain (SspB_Nano-SctQ, mCh-SctL) + MA, we screened for spot dynamics of mCh-SctL during an optogenetic mediated control of the bait-SctQ fusion protein (Figure 25). As controls, we used the LITESEC-supp strain (bait-SctQ, mCh-SctL) without the MA and a mCh-SctL strain. We also excluded normalized values, that were out of the range from -0.6 - 1.5 (normalized values are theoretically expected to range between 0 and 1). Data analysis without mCh-SctL control from the described day revealed a significantly reduced spot recovery rate of mCh-SctL in the LITESEC-supp2 strain (SspB_Nano-SctQ, mCh-SctL) + MA under light conditions (Figure 25B-D). The same strain observed under dark conditions displayed comparable spot dynamics to the two controls (Figure 25B-D). We hypothesized that the difference in spot dynamics of mCh-SctL was due to optogenetic control of SctQ and, therefore, LITESEC-T3SS might influence the dynamic exchange of the cytosolic complex, whereas the most prominent explanation for this phenotype would simply be a direct influence of SctQ on SctL through binding and co-sequestration (as it was shown in Figure 23).

It is important to mention that at the moment the data just display a trend, since not all control strains worked as expected for all days and the variation between the days and the data still were noisy (indicated by the error bars of the standard deviation – Figure 25C). Further experiments need to be done to strengthen the data.

Because the reported effect of optogenetically controlled bait-SctQ on mCh-SctL spot dynamics is only a passive effect and we may have only influenced the dynamic exchange of SctL by co-sequestration with SctQ, we further established LITESEC-based bait triple fusions: bait-mCh-SctQ, allowing both light-dependent secretion control and direct visualization of the localization of the fusion protein in the bacterial cell. The created strains were first tested for function and controllability. Our results revealed an incoherent behavior for the LITESEC-supp triple fusion SspB_Nano-mCh-SctQ (Figure 26A, 27B). While the bait could be efficiently tethered to the membrane upon illumination, indicating a functional interaction of the dimerization switch, secretion could not be controlled with light in this strain (Figure 26A, C). By mutating an internal ribosomal entry site (IRES) that has been shown to lead to translation byproducts of mCherry within the fusion protein (Carroll *et al.*, 2014), we hoped to address this deficiency in secretion control. Secretion could still not be controlled with this strain, even when the MA was overexpressed tenfold more than usual (Figure 27B), which should correlate with a more efficient membrane tethering of the fusion protein. Possibly, another side product revealed by the Western blot at ~ 50 kDa (could maybe represent a smaller protein side product missing the C-terminal bait and can therefore not be tethered to the membrane) is responsible for this lack in secretion control. Notably, the same band was detected for the LITESEC-act triple fusion Zdk1-mCh-SctQ, for which we could control the secretion function, even to a tighter degree (Figure 27A). We were not able to find an explanation for this phenotype.

For further studies, we therefore concentrated on the triple fusion (Zdk1-mCh-SctQ). We used this to check whether the T3SS-specific spots remain under light conditions that sequester the bait to the membrane. Our hypothesis for this experimental design was that if we observe stable T3SS spots of the optogenetic bait-mCh-SctQ fusion protein when we sequester SctQ, knowing that the same conditions lead to a decrease in secretory function (model indicated in Figure 27A), LITESEC affects function by controlling the dynamic exchange of the cytosolic component SctQ, rather than just its presence in the structure at the T3SS. This would be in line with a direct link between dynamics and function, as it was proposed before (Diepold *et al.*, 2015). Our data indeed indicated a stable spot maintenance irrespective of light (on) or dark (off) conditions (Figure 27C) comparable to the control strain lacking the MA, even when the overall fluorescence decreased over time, likely due to photo bleaching.

Noticeably, the control without the optogenetic MA maintained fluorescent foci to a higher degree than the other samples (Figure 27C), but experiments were just performed two times and further experiments need to be done to allow a solid interpretation.

As for studies on the other cytosolic components (except SctQ), $FliH_2I$ ($SctL_2N$) has been suggested to bind chaperones in the flagellum and act as dynamic substrate shuttle (Bai *et al.*, 2014) and the *Yersinia* ATPase SctN has been shown to be involved in effector recognition (Sorg, Blaylock and Schneewind, 2006) and later presented to act as a rotary motor and guide substrates to the export gate (Majewski *et al.*, 2019). We extended our studies on the dynamic exchange of the cytosolic components and its link to the secretion function, by combining optogenetic interaction switches with the other cytosolic components SctN/L/K. Sequestration of the bait-mCh-SctK/N triple fusions efficiently controlled secretion function, although this control appears to be different. Whereas we observed a sweet spot in the anchor/bait expression ratio and functional control for the bait-mCh-SctL fusion (secretion control on/off correlates with the expression ratio – Figure 29C), secretion control with SctN appears to be different and could not be further reduced by higher MA expression (Figure 29C), as it was shown for the triple fusion bait-mCh-SctQ/L (Figure 29). This phenotype was possibly due to a steric effect of the large fusion protein (bait-mCh-SctN = 87.5 kDa) at the membrane achor, so that not all bait proteins could be efficiently sequestered. Whether the control of secretion decreases when the MA is expressed at lower levels remains to be investigated. When observing fluorescence spot retention of bait-mCh-SctL in presence or absence of the MA, the spots also appear to remain independent of the illumination, making the hypothesis of a SctQ-sequestration influence on dynamic exchange of the cytosolic complex more likely than on the structure itself (Figure 29)**.** Due to larger polar spots that exhibited bright fluorescence and interfered with the overall fluorescence detection, a more accurate evaluation was not practical up to this point.

Experiments revealed a difference in secretion control between the bait-mCh-SctN/L triple fusions and the corresponding bait-SctN/L double fusions. Whereas secretion was almost abolished in the double fusions under “off” conditions (Figure 30A), the triple fusions showed basal secretion under “off” conditions (Figure 29C), which may also have been due to a steric effect of the larger fusion proteins at the membrane anchor, so that not all bait proteins could be efficiently sequestered. The difference in sweet spot dependence on anchor expression levels of the SctQ fusions compared to the other could be due to the difference in T3SS stoichiometry of the cytosolic complex (SctQ 24 copies, SctL 12 copies, SctN 6 copies per injectisome (Diepold *et al.*, 2017; Wagner *et al.*, 2018).

Noticeably, we observed light-dependent secretion control for SspB_Nano-SctQ/L/N but not for SspB_Nano-SctK (Figure 30). It is important to mention that these experiments were performed only once, and studies about protein stability of the fusion protein or sequestration to the membrane were not performed yet. But if further data could support these results, this opens a new and interesting model, in which the cytosolic components SctQ, SctL and SctN are dynamic and that this dynamic property is associated with effector secretion, whereas SctK does not have this property. The linker protein SctK connects the cytosolic complex to the inner membrane ring protein SctD (Hu *et al.*, 2017) (Figure 3). It is known that the cytosolic complex only assembles to the injectisome in presence of all its components and that knocking out one component leads to a deficit in the assembly of the other components (Diepold *et al.*, 2010, 2017), even when cytosolic sub complexes exist (Diepold *et al.*, 2017; Bernal *et al.*, 2019). Interestingly, SctK has been detected in purified high molecular weight complexes of the cytosolic complex (Johnson and Blocker, 2008), whereas SctK was not found in cytosolic sub complex studies (Bernal *et al.*, 2019). As a linker to SctD, SctK might play a special role among the cytosolic components, being more stable and connected to the injectisome interface than being dynamically exchanged. This needs to be demonstrated in further experiments.

5 Outlook

With the incorporation of optogenetic dimerization switches into the bacterial T3SS injectisome, we established a new way to directly control cellular functions in bacteria with light (Lindner *et al.*, 2020). This can not only be considered a pioneering study for optogenetic applications in bacteria beyond the usual purpose of gene expression control (Liu *et al.*, 2018; Baumschlager and Khammash, 2021), but also represents a new way to study dynamic processes *in vivo*. The developed LITESEC-T3SS provides a tool for spatiotemporal controlled cargo delivery into eukaryotic host cells. This controllability is driving current studies to establish the T3SS as an efficient protein delivery tool for purposes ranging from healthcare to other research areas such as the delivery of nucleases (reviewed in Bai *et al.*, 2018). In view of future applications of LITESEC and in collaboration with our partners, tests are currently being performed to investigate the translocation of the monobody cargo into different cell lines, including adherent (HEp-2 and HEK) and suspension cell lines (JURKAT and K562), as well as subsequent functional tests of the monobody cargo in the cells. The future goal is to establish LITESEC-based control of protein translocation in biological and therapeutic applications, for which we have also presented essential regulations such as cargo protein stability (reducing translocation efficiency) and cognate chaperone co-expression (increasing translocation efficiency).

By the optogenetic mediated sequestration of a dynamic cytosolic T3SS component, such as SctQ, protein interactions and injectisome assembly or exchange events can be investigated from a new direction. Initial experiments presented in this work indicated an influence of SctQ sequestration on dynamic exchange at the injectisome interface. It is therefore more likely that the LITESEC application affects secretion by controlling the dynamic exchange of the cytosolic component SctQ rather than just its presence in the structure at the T3SS, consistent with a direct link between dynamics and secretion. Further research and experiments are needed to support and confirm this hypothesis. Using optogenetically mediated protein association, the finding that cytosolic T3SS components directly interact with effector/chaperone substrates and act as a shuttle, as once proposed (Lara-Tejero *et al.*, 2011), would further complete the understanding of the dynamic nature and function of the T3SS. This work demonstrates the broad application potential of optogenetic dimerization switches to study cellular processes in bacteria.

6 Supplementary information

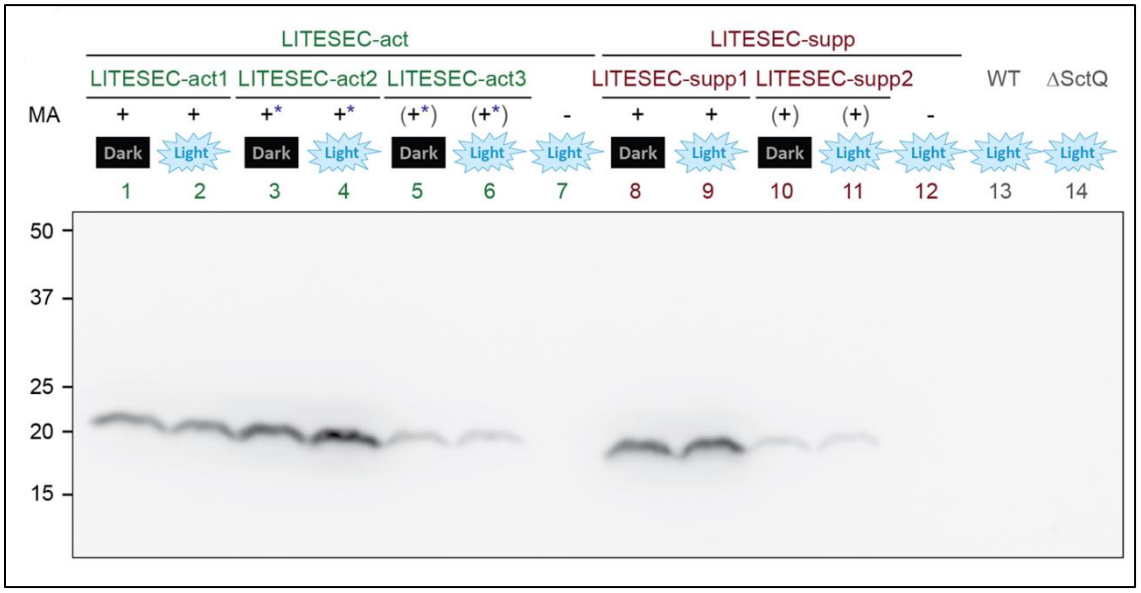

Supplementary Figure 1: Expression levels of membrane anchor proteins in the different LITESEC variant strains – Western blot anti-FLAG of total cellular protein from 2*10^8 bacteria in the indicated strains (corresponding to Figure 11). Left, molecular weight marker in kDa. Expected protein MW: 20.9 kDa for LITESEC-act strains (TMH-FLAG-LOV2 / TMH-FLAG-LOV2V416L), 21.6 kDa for LITESEC-supp strains (TMHFLAG-iLID). MA, expression level of membrane anchor; +, high expression level; (+), low expression level; -, no expression. *, V416L anchor mutant. (Lindner *et al.*, 2020).

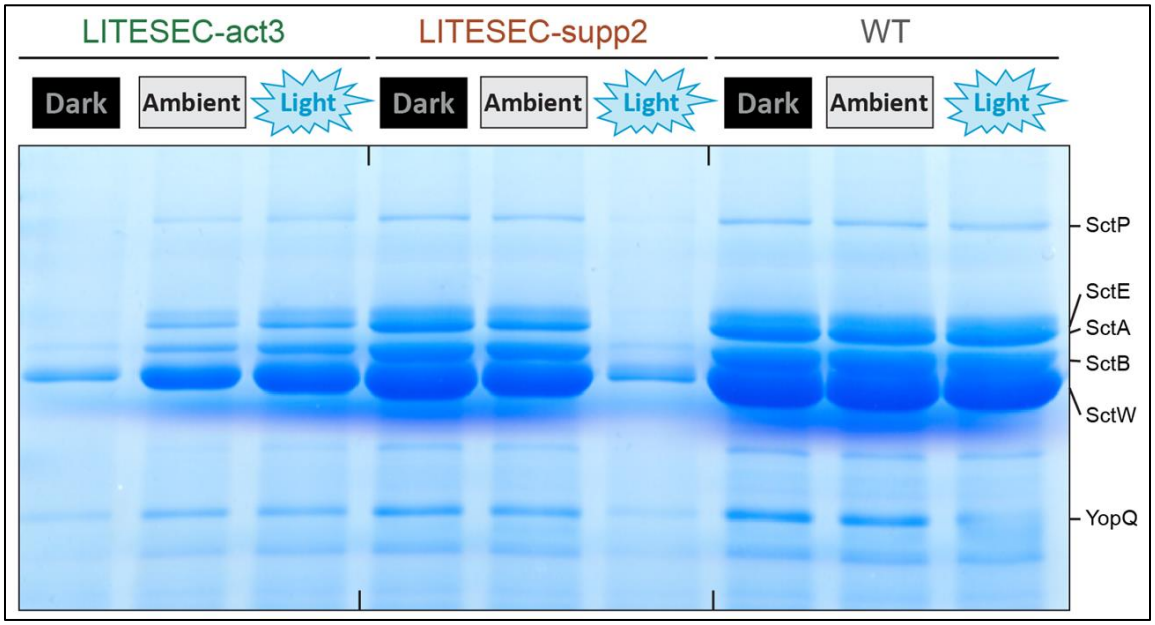

Supplementary Figure 2: Influence of ambient light on LITESEC secretion activity – In vitro secretion assay showing light-dependent export of native T3SS substrates (indicated on the right) in the listed strains, incubated under defined dark or light conditions (see material and methods for details), as well as ambient laboratory light. Proteins secreted by 3*108 bacteria during a 180 min incubation period were precipitated and analyzed by SDS-PAGE. Left side, molecular weight in kDa. (Lindner *et al.*, 2020).

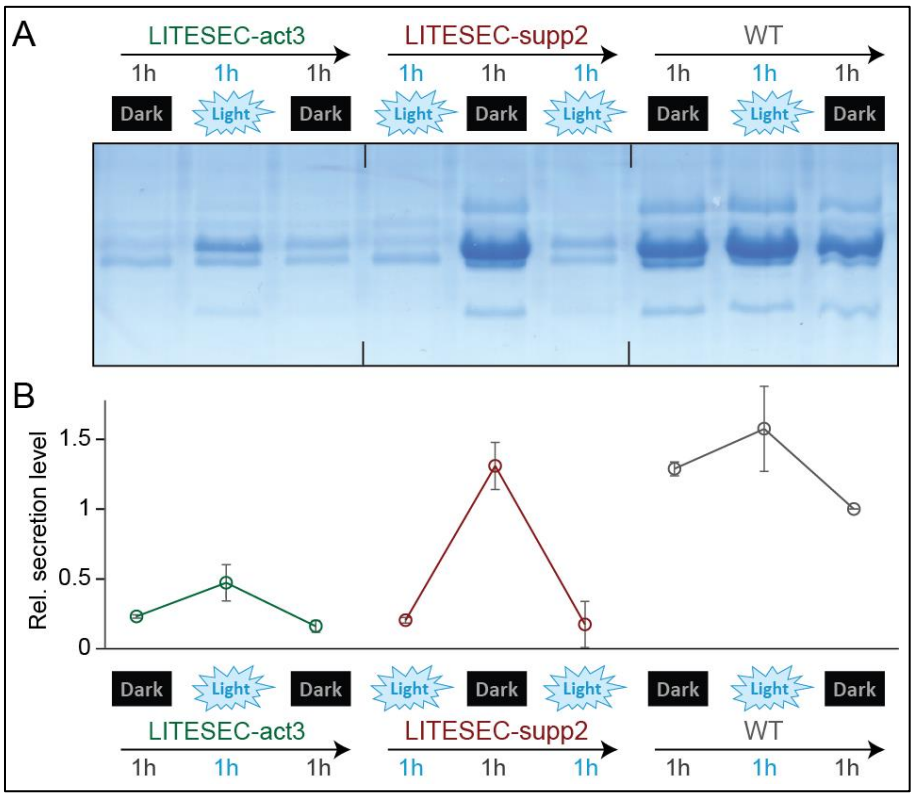

Supplementary Figure 3: Control of secretion of native T3SS substrates over time – (**A**) Export of native T3SS substrates in the indicated strains. Secretion-competent bacteria were subsequently incubated under inactivating, activating and inactivating light conditions for 60 min each, as in Figure 14 and as indicated, and the supernatant of $3*10^8$ bacteria was analyzed. Left side, molecular weight in kDa. (**B**) Quantification of the relative export efficiency (normalized to the wild-type level in the third incubation period) of the strains; N=2. (Lindner *et al.*, 2020).

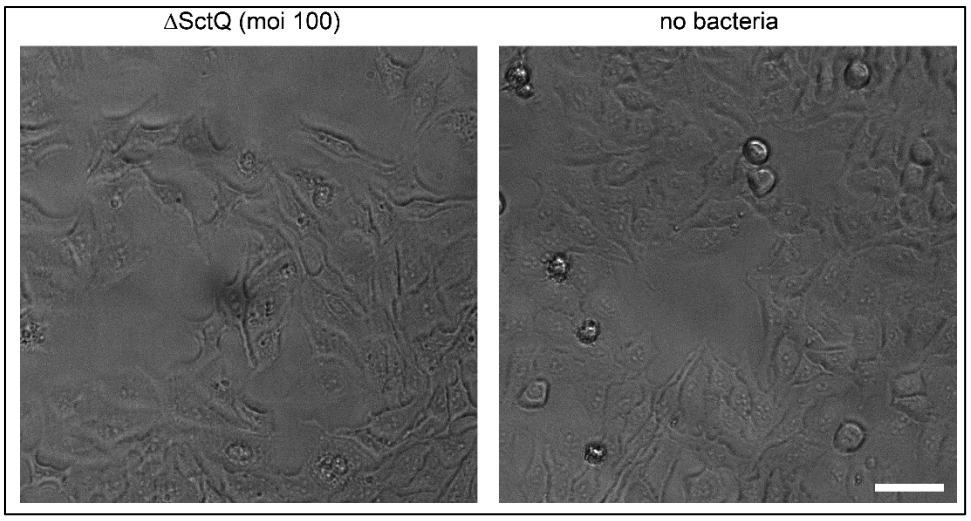

Supplementary Figure 4: Host cells show no visible reaction to T3SS-inactive *Y. enterocolitica* – Left, HEp-2 cells were infected with *ΔsctQ* bacteria for 1 h at a multiplicity of infection (moi) of 100, as in Figure 15. After removal of the bacteria, cells were incubated in medium containing gentamicin for further 17 h to detect possible long-term effects of the presence and contact of bacteria. Right, control incubated under the same conditions without bacteria. Scale bar, 50 µm. (Lindner *et al.*, 2020).

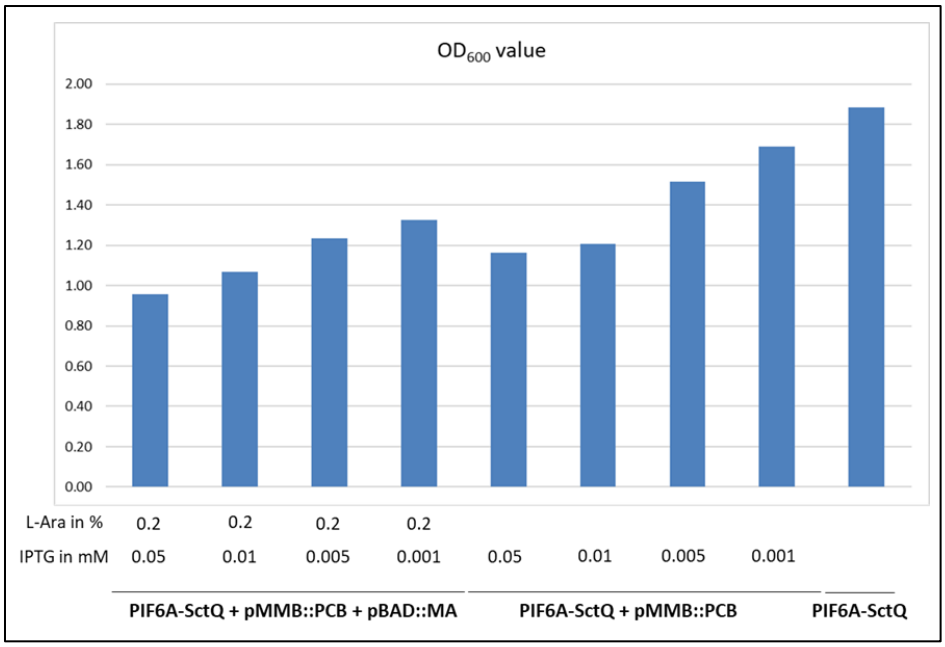

Supplementary Figure 5: Intracellular PCB expression reduce bacterial growth – Bacterial growth determined by the measured optical density at OD_{600}. Strains were inoculated from an overnight culture to a starting OD_{600} of 0.2 and incubated for 3 h under the displayed conditions. pBAD::MA expression was induced with x % L-ara; pMMB::PCB (means pMMB::*RBS-ho1*, *RBS-pcyA*) expression was induced with x mM IPTG. PIF6A-SctQ strain (without MA and PCB synthesis plasmid) was used as a control.

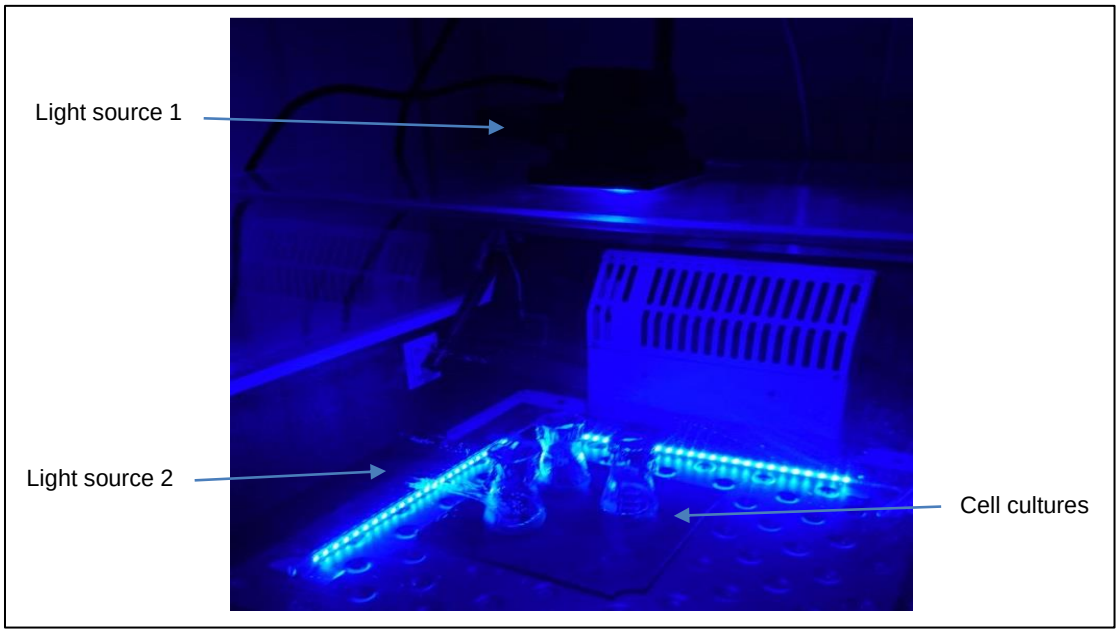

Supplementary Figure 6 Optogenetic experimental setup – The optogenetic experimental setup consists of two blue light sources that were placed around the cell cultures. Light source 1 was a “globo lighting 10 W LED 9 V 34118S” – (Globo Lighting GmbH (St. Peter, A)), Light source 2 was a “Rolux LED-Leiste DF-7024-12 V 1.5 W” – (Rolux Leuchten GmbH (Weyhe, G)). Cell cultures were cultivated at 37° C, to induce the T3SS. Red-light optogenetic experiments were illuminated with two LED’s (640 nm) received from RG Essen.

Supplementary Table 1: Translation table for T3SS components – derived from (Wagner and Diepold, 2020)

Functional name	**Flagellar homolog**		**Ysc**	**Inv-Spa**	**Ssa**
		Sct name	***Yersinia***	***Salmonella* SPI-1**	***Salmonella* SPI-2**
Secretin	–	**SctC**	**YscC**	InvG	SsaC
Outer–inner membrane ring protein	–	**SctD**	**YscD**	PrgH	SsaD
Inner–inner membrane ring protein	FliF	**SctJ**	**YscJ**	PrgK	SsaJ
Core export apparatus protein R	FliP	**SctR**	**YscR**	SpaP	SsaR
Core export apparatus protein S	FliQ	**SctS**	**YscS**	SpaQ	SsaS
Core export apparatus protein T	FliR	**SctT**	**YscT**	SpaR	SsaT
Core export apparatus protein U, switch protein	FlhB	**SctU**	**YscU**	SpaS	SsaU
Major export apparatus protein	FlhA	**SctV**	**YscV**	InvA	SsaV
Base-pod connector	–	**SctK**	**YscK**	OrgA	SsaX
Major pod protein	FliM + FliN	**SctQ**	**YscQ**	SpaO	SsaQ
Stator	FliH	**SctL**	**YscL**	OrgB	SsaK
ATPase	FliI	**SctN**	**YscN**	InvC	SsaN
Stalk	FliJ	**SctO**	**YscO**	InvI	SsaO
Needle filament protein	–	**SctF**	**YscF**	PrgI	SsaG
Inner rod protein/needle adapter	FliE	**SctI**	**YscI**	PrgJ	SsaI
Needle length regulator	FliK	**SctP**	**YscP**	InvJ	SsaP
Hydrophilic translocator, needle tip protein	–	**SctA**	**LcrV**	SipD	SseB
Hydrophobic translocator, pore protein	–	**SctE**	**YopB**	SipB	SseC
Hydrophobic translocator, pore protein	–	**SctB**	**YopD**	SipC	SseD
Pilotin	–	**SctG**	**YscW**	InvH	**–**
Gatekeeper	**–**	**SctW**	**YopN**	InvE	SsaL

7 Material

Chemicals that were used for buffers or cultivation media were purchased from CARL ROTH GmbH & CO KG (Karlsruhe, G), SIGMA-ALDRICH (Steinheim, G), VWR Chemicals (Darmstadt, G) and Becton, Dickinson and Company (New Jersey, USA). All buffers, dNTP's, restriction enzymes and polymerases were purchased from THERMO FISHER SCIENTIFIC (Schwerte, G), CARL ROTH GmbH & CO KG (Karlsruhe, G) and New England Biolabs GmbH (Frankfurt am Main, G). For gel electrophoresis a "Quick-Load® Purple 2-Log DNA Ladder" (New England Bi olabs GmbH) was used. For SDS-PAGE "Mini-PROTEAN® Precast Gels" (Life Science Research – BIO-RAD (California, USA)) and a "BlueClassic Prestained Protein Marker®" (Jena Bioscience (Jena, G)) were used. For staining of a SDS-Gel, an "Instant Blue staining solution" (Expedeon Inc. (San Diego, USA)) was used. For PCR purification and gel extraction a "NucleoSpin® Gel and PCR Clean-up" kit and for plasmid purification of *E. coli* a "NucleoSpin® Plasmid" kit (MACHEREY-NAGEL (Düren, G)) was used. For Western blot method a "Trans-Blot Turbo® Nitrocellulose- or PVDF-transfer pack" and a Trans-Blot Turbo® Transfer System (Life Science Research – BIO-RAD (California, USA)) were used. Pictures of Western blots were taken on a "Luminescent Image Analyzer Las-4000 (Fujifilm (Minato, J) with the corresponding software "ImageReader LAS-4000". Antibodies were purchased from THERMO FISHER SCIENTIFIC (Schwerte, G). Measurements of DNA-concentration or optical density (OD_{600}) of cell cultures were performed on a "DS-11+ Spectrophotometer" (DeNovix Inc. (Wilmington, USA)). Electroporation of *Yersinia* cells were performed with a "MicroPulser™ Electroporator" and "Gene *E. coli* Pulser Cuvettes" 0.2 cm (Life Science Research – BIO-RAD (California, USA)). During fluorescence microscopy the images were taken on a Deltavision Spectris Optical Sectioning Microscope (Applied Precision, Issaquah, WA, USA), equipped with a UPlanSApo x 100/1.40 oil objective (Olympus, Tokyo, Japan) and x 1.6 auxiliary magnification, using an Evolve EMCCD Camera (Photometrics, Tucson, AZ, USA) at a gain level 50. Microscopy pictures were analyzed and processed with ImageJ-Fiji (Schindelin *et al.*, 2012). Platereader experiments were performed with a Tecan® infinite M200 Pro (Tecan group Ltd., Männedorf, Switzerland) combined with the software i-control 1.10. All primers and sequencing were placed in order at EUROFINS GENOMICS (Ebersberg, D). Gene sequences were bioinformatically analyzed and designed with SerialCloner 2.6.1 (Serial Basics) and following online tools (Table 2). Primers that were designed and used during this work are listed in Table 3. Constructs that were made in this work are listed in Table 4. Strains that were created during this work are listed in Table 5.

Table 2: Online Tools – List of online tools that were used for experimental deisgn

Name	URL
Expasy Translate tool	https://web.expasy.org/translate/
WebCutter	http://rna.lundberg.gu.se/cutter2/
Primer 3	http://primer3.ut.ee/
Nucleic Acid Sequence Massager	http://www.attotron.com/cybertory/analysis/seqMassager.htm
NEB cloner	https://nebcloner.neb.com/#!/
Phobius	https://phobius.at/
Blast	https://blast.ncbi.nlm.nih.gov/Blast.cgi

Table 3: Primers – List of primers that were used in this thesis. Restriction sites are shown in red, linkers are shown in blue, start and stop sequences are shown in purple.

Primer	Sequence from 5‘ to 3‘	Reference
AD321_YscQ_1fwd	GACTGGGCCCCTTACCTGAATTGGGGGCTA	Diepold, A.
AD324_YscQ_2rev	GACTTCTAGAAGAGAATGGAGCCCCTAGTAAG	Diepold, A.
AD339_pBAD_seq_fwd	ATGCCATAGCATTTTTATCC	Diepold, A.
AD340_pBAD_seq_rev	GCGTTCTGATTTAATCTGTATCAGG	Diepold, A.
AD341_pKNG_seq_fwd	TATTAATTGATCTGCATCAACTTAACG	Diepold, A.
AD342_pKNG_seq_rev	GACTATACTAGTATACTCCGTCTACTGTACG	Diepold, A.
AD638_ext_TatA_TMH_f	GGTCTCCC**ATG**GGTGGTATCAGTATTTGGCAGTTATTGATTATTGCC GTCATCGTTGTACTGCTTGTCCTATTTGGCACCAAAAAGCTCGGCTC CGACTACAAGGACGACGATGATAAGGGTGGAGCAGGT	Diepold, A.
AD642_MAG_r	GACTGAATTC*TTA*CTCAGTCTCGCACTGAAACC	Diepold, A.
AD698_Zdk1-EGFP_1fw	GACTGGATCC*TTGACTGA*ATGGTGGATAACAAATTCAATAAAGAAAAG A	this work
AD699_Zdk1-EGFP_1rv	ACCACCAGAGCCGCCCGACCCACCAGAACCACCTTTTGGGGCCT	this work
AD700_Zdk1-EGFP_2fw	GGTGGGTCGGGCGGCTCTGGTGGTGGTGCTGGCGTGAGCAAG	this work
AD701_Zdk1-EGFP_2rv	GATCGTCGAC*TTA*CTTGTACAGCTCGTCCATGC	this work
AD704_mCh-LOV2_int_fw	GACGATGATAAGGGTGGAGCAGGTGTGAGCAAGGGCGAGGAG	this work
AD705_mCh-LOV2_rev	GACTGAATTCGCAAGCTT*TTA*AAGTTCTTTTG	this work
AD717_pACYC184_fw	CAGGCACCGTGTATGAAATC	this work
AD718_pACYC184_rev	GAGCCCGATCTTCCCCATC	this work
AD719_pACYC184_rev_SalI	GTCCTCGCCGAAAATGACC	this work
AD720_pFL103_seq	CTTACGGAAAGCTGACCCTG	this work
AD721_mCh_fwd	GGTGGGTCGGGCGGCTCTGGTGGTGTGAGCAAGGGCGAGGAG	this work
AD722_mCh_rev	GATCGTCGAC*TTA*CTTGTACAGCTCGTCCATGC	this work
AD724_mCh_rev_EagI	GATCCGGCCG*TTA*CTTGTACAGCTCGTCCATGC	this work
AD732_ILID_mCh_2fw	GGCGCTGGTGGTGGAGCAGGTGGAGGATCCGGGGAGTTTCTGG	this work
AD733_ILID_mCh_2rev	GACTGAATTCTCAGCTAATTAAGCTTTTAAAAGT	this work
AD734_ILID_fw	GACGATGATAAGGGTGGAGCAGGTGGATCCGGGGAGTTTCTGG	this work
AD735_SspB_Nano_fw	GACTGGATCC*TTGACTGA*ATGAGCTCCCCGAAACGCCC	this work
AD736_SspB Nano_rev	ACCACCAGAGCCGCCCGACCCACCACCAATATTCAGCTCGTCAT	this work
AD737_pACYC184_rev_ EagI	CCGGAAGCGAGAAGAATCATA	this work
AD759_Zdk1_premut_fwd	GACTAGATCTGGCGCAGGTGTGGATAACAAATTCAATAAAGAAAAGA	this work
AD762_SspB_premut_fwd	GACTAGATCTGGCGCAGGTAGCTCCCCGAAACGCCCTAA	this work
AD768_mCh_premut_rev_n ew_EcoRI	GACTGAATTCACCTGCGCCCTTGTACAGCTCGTCCATGC	this work
AD769_SspB_premut_rev_ new_EcoRI	GACTGAATTCACCTGCGCCACCAATATTCAGCTCGTCATAGA	this work
AD771_mCherry_seq_rev	CGCATGAACTCCTTGATGATGG	this work
AD772_mCherry_seq_fw	CGCCTACAACGTCAACATCA	this work
AD902_MA_for_pACYC184 _fw	GACTAGATCTATGGGTGGTATCAGTATTTGGC	this work

AD903_MA_LOV2_for_pACYC184_rev	GACTGTCGACGCAAGCTT*TTA*AAGTTCTTTTG	this work
AD904_MA_iLID_for_pACYC184_rev	GACTGTCGACTCAGCTAATTAAGCTTTTAAAAGT	this work
AD921_MA_on_pACYC_fw_new	GACTAGATCTTTGACTGAATGGGTGGTATCAGTATTTGGC	this work
AD925_bla_rev_new_Flag	GACTGTCGAC*TTA*CTTATCATCGTCGTCCTTGTAGTCCCAATGCTTAATCAGTGAGG	this work
AD1158_tBID_fw	GACTAGATCTCTCGAGTCTAGAGGCAACC	this work
AD1159_tBID_rv	GACTGAAT*TCA*CTTATCATCGTCGTCCTTGTAGTCTCCGCCACCGTCCATCCCATTTCTGGCTAAG	this work
AD1160_AtPhyB_N_fw_int	GACGATGATAAGGGTGGAGCAGGTGTTTCCGGAGTCGGGGGTAG	this work
AD1161_AtPhyB_N_rv	GACTGAAT*TCA*ATGGTGATGGTGATGATGTGC	this work
AD1162_AtPhyB_C_fw	GGTCTCCCATGGTTTCCGGAGTCGGG	this work
AD1163_AtPhyB_C_rev_1 _int	CGGCTCATGCGGCGCAGGCGCGCATAGCGGCGCTTATCATCGTCGTCCTTGTAGTCACCTGCTCCACCATGGTGATGGTGATGATGTGC	this work
AD1164_AtPhyB_C_rev_2_ext	GACTGAAT*TCA*GCCCGCCGCCACCAGCACCAGCGCCACCAGCAGCACCATCACGGTCGCCGCCAGCACCGCCAGCGCCACGCGGCTCATGCGGCGCAGGCG	this work
AD1165_PIF6A_fw	GACTAGATCTGGCGCAGGTGATCAAGAATATATGGAACTGGTGT	this work
AD1166_PIF6A_rev	GACTGAATTCACCTGCGCCGGCTTCATACAGATCCATAATGCTT	this work
AD1167_PIF6A_rev2	ACCACCAGAGCCGCCCGACCCACCGGCTTCATACAGATCCATAATGCTT	this work
AD1168_pMMB67EH_seq_fw	TTTGCGCCGACATCATAACG	this work
AD1169_pMMB67EH_seq_rev	CCGCCAGGCAAATTCTGTT	this work
AD1173_YscQ_fw_NcoI	GACTCC**ATG**G*GG*AGTTTGTTAACCTTGCCACAAG	this work
AD1174_YscQ_rev_EcoRI	GACTGAAT*TCA*TGAAATCGTAACCTCTGTCAG	this work
AD1228_upstr_SycE_fwd	GATCAGATCTT*TGACTGA*GCTGGCACCACAAATTTATAGGT	this work
AD1229_YopE138_ins_rev	GATCGTCGAC*TTA*CAATTGATATGGA*TCC*GCCCGTGGCGAACTGGTCATGATTTT	this work
AD1230_Cre_fw_BglII	GATCAGATCTGGCGCAGGTTCCAATTTACTGACCGTACACC	this work
AD1231_Cre_rev_EcoRI	GATCGAATTCACCTGCGCCATCGCCATCTTCCAGCAGG	this work

Table 4: Plasmids – Plasmids with corresponding properties that were used in this thesis.

Name (Reference)	Genotype	Restriction enzymes	Resist.	Primer used for Insert-PCR	Template for Insert
pFL100 (this work)	*pBAD::TMH-FLAG-(L1)-mCherry-(L2)-LOV2*	NcoI, EcoRI	Amp	AD638/704/705	p81041**
pFL101 (this work)	*pACYC184::Zdk1-(L4)-EGFP*	BamHI, SalI	Cam	AD698/699/ 700/701	P81010**/ pAD301
pFL104 (this work)	*pACYC184::Zdk1-(L4)-mCherry*	BamHI, SalI	Cam	AD638/699/ 721/722	p81010**/ pAD304
pFL107 (this work)	*pBAD::TMH-FLAG-(L1)-mCherry-(L3)-iLID*	NcoI*, EcoRI	Amp	AD638/706/707/ 732/733	p60408**/ pAD304
pFL108 (this work)	*pBAD::TMH-FLAG-(L1)-iLID*	NcoI, EcoRI	Amp	AD638/733/734	p60408**
pFL109 (this work)	*pACYC184::SspB_Nano-(L4)-mCherry*	BamHI, SalI	Cam	AD721/722/ 735/736	p60409**/ pAD304
pFL111 (this work)	*pBAD::Zdk1-(L4)-mCherry*	BglII, EcoRI	Amp	AD759/768	pFL104
pFL113 (this work)	*pBAD::SspB_Nano-(L4)-mCherry*	BglII, EcoRI	Amp	AD762/768	pFL109
pFL114 (this work)	*pBAD::SspB_Nano*	BglII, EcoRI	Amp	AD762/769	pFL109
pFL115 (this work)	*pKNG101::Zdk1-(L4)-mCherry-YscQ*	BglII, MfeI***	Sm	****	pFL111
pFL117 (this work)	*pKNG101::SspB_Nano-(L4)-mCherry-YscQ*	BglII, MfeI***	Sm	****	pFL113
pFL118 (this work)	*pKNG101::SspB_Nano-YscQ*	BglII, MfeI***	Sm	****	pFL114
pAD168 (Diepold et al., 2010)	*pKNG101::ΔYscN*		Sm		
pAD304 (Diepold *et al.*, 2015)	*pUC19-mCherry*		Amp		
pAD608 (this work)	*pBAD::TMH-FLAG-(L1)-LOV2*	NcoI*, EcoRI	Amp	AD638/639/640	p81041**
pAD612 (this work)	*pKNG101::Zdk1-YscQ*	BglII, MfeI***	Sm	****	pAD611
pAD614 (this work)	*pBAD::TMH-FLAG-(L1)-pMAGFast2(2x)*	NcoI*, EcoRI	Amp	AD638/641/642	p67297**
pCH08 (Carlos Helbig Master thesis)	*pKNG::SycH-mCherry*		Sm		
pFL125 (this work)	*pBAD::SspB_Nano-mCherry (noIRes)*	BglII, EcoRI	Amp	AD721/736/762/768	pFL109 / pAD647
pFL126 (this work)	*pACYC184::TMH-FLAG-LOV2 (V416L)*	BamHI, SalI	Cam	AD921/903	pAD610
pFL127 (this work)	*pACYC184::TMH-FLAG-iLID*	BamHI, SalI	Cam	AD921/904	pFL108
pFL128 (this work)	*pAD320::SspB_Nano-mCherry (NoIRes)*	BglII, MfeI***	Sm	AD762/768	pFL125
pFL129 (this work)	*pAD472::Zdk1*	BglII, MfeI***	Sm	****	pAD611
pFL130 (this work)	*pAD472::SspB_Nano*	BglII, MfeI***	Sm	****	pFL114
pFL133 (this work)	*pBAD::YopE1-53-Nanoluc-FLAG*	BglII, EcoRI	Amp		pAD681
pFL134 (this work)	*pBAD::YopE1-138-Nanoluc-FLAG*	BglII, EcoRI	Amp		pAD681
pAD690 (this work)	*pBAD::(NcoI-)Luciferase-Gly2-FLAG-Gly-Ala-Gly-EcoRI-Stop(-HindIII)*	NcoI, HindIII	Amp	AD949/934	pAD681

pAD692 (this work)	*pACYC184::YopE1-53-bla*	BamHI, SalI	Cam	AD965/967	pBMD040
pAD693 (this work)	*pACYC184::YopE1-138-bla*	BamHI, SalI	Cam	AD966/967	pBMD041
pFL137 (this work)	*pBAD::YopE1-53-PUMA-FLAG*	BglII, EcoRI	Amp		pAD662
pFL138 (this work)	*pBAD::YopE1-53-HVSTK-FLAG*	BglII, EcoRI	Amp		pAD664
pFL139 (this work)	*pBAD::YopE1-53-p53-FLAG*	BglII, EcoRI	Amp		pAD666
pFL140 (this work)	*pBAD::YopE1-138-PUMA-FLAG*	BglII, EcoRI	Amp		pAD662
pFL141 (this work)	*pBAD::YopE1-138-HVSTK-FLAG*	BglII, EcoRI	Amp		pAD664
pFL142 (this work)	*pBAD::YopE1-138-p53-FLAG*	BglII, EcoRI	Amp		pAD666
pFL143 (this work)	*pBAD::pYopE-mCherry*	BglII, EcoRI	Amp		pAD304
pFL144 (this work)	*pBAD::TMH-FLAG-AtPhyB-His*	NcoI*, EcoRI	Amp	AD638/1160/1161	AtPhyB(1-651)-pCDF
pFL145 (this work)	*pBAD::AtPhyB-His-FLAG-membrane domain (hypothetical – SCO7096)*	NcoI*, EcoRI	Amp	AD1162/1163/1664	AtPhyB(1-651)-pCDF
pFL146 (this work)	*pBAD::PIF6A*	BglII, EcoRI	Amp	AD1165/1166	PIF6A-eYFP
pFL147 (this work)	*pAD320::PIF6A*	BglII, MfeI***	Sm		pFL146
pFL148 (this work)	*pACYC184::PIF6A-mCherry*	BamHI, SalI	Cam	AD721/722/1165/1167	PIF6A-eYFP/pAD304
pFL149 (this work)	*pMMB67EH::RBS-Ho1, RBS-PcyA*	EcoRI, SalI	Gm		pSR33.4r (63198**)
pFL150 (this work)	*pBAD::YopE$_{1-138}$-tBID-FLAG*	BglII, EcoRI	Amp	AD1158/1159	pt3t
pFL151 (this work)	*pBAD::SycE, YopE$_{1-138}$-PUMA-FLAG*	BglII, BbsI*****	Amp		pFL140
pFL152 (this work)	*pBAD::SycE, YopE$_{1-138}$-HVSTK-FLAG*	BglII, BbsI*****	Amp		pFL141
pFL153 (this work)	*pBAD::SycE, YopE$_{1-138}$-p53-FLAG*	BglII, BbsI*****	Amp		pFL142
pFL154 (this work)	*pBAD::SycE, YopE$_{1-53}$-mCherry*	BglII, BbsI*****	Amp		pAD304
pFL156 (this work)	*pBAD::SycE, YopE$_{1-138}$-mCherry*	BglII, BbsI*****	Amp		pAD304
pFL159 (this work)	*pBAD::YscQ*	NcoI, EcoRI	Amp	AD1173/1174	pYV
pAD727 (this work)	*pBAD::SycE, YopE$_{1-138}$-TEV-Mbc-FLAG-HiBiT*	BglII, BbsI*****	Amp,Carb	AD1193/1194	Mbc
pFL164 (this work)	*pBAD::SycE, YopE$_{1-138}$-TEV-Mbc$_{K7D}$-FLAG-HiBiT*	BglII, BbsI*****	Amp,Carb	AD1193/1194	MbcK7D
pFL165 (this work)	*pBAD::SycE, YopE$_{1-138}$-TEV-Mbc$_{A56G}$-FLAG-HiBiT*	BglII, BbsI*****	Amp,Carb	AD1193/1194	MbcA56G
pFL166 (this work)	*pBAD::SycE, YopE$_{1-138}$-TEV-AS25-FLAG-HiBiT*	BglII, BbsI*****	Amp,Carb	AD1193/1195	AS25
pFL167 (this work)	*pBAD::SycE, YopE$_{1-138}$-TEV-AS25$_{K7D}$-FLAG-HiBiT*	BglII, BbsI*****	Amp,Carb	AD1193/1196	AS25K7D
pFL168 (this work)	*pBAD::SycE, YopE$_{1-138}$-TEV-AS25$_{A56G}$-FLAG-HiBiT*	BglII, BbsI*****	Amp,Carb	AD1193/1197	AS25KA56G
pFL169 (this work)	*pKNG101::SspB_Nano-(SctN)*	BglII, MfeI***	Sm		pFL114

pFL170 (this work)	*pKNG101::SspB_Nano-(SctL)*	BglII, MfeI***	Sm		pFL114
pFL171 (this work)	*pKNG101::SspB_Nano-mCherry(NoIRes)-(SctN)*	BglII, MfeI***	Sm		pFL125
pFL172 (this work)	*pKNG101::SspB_Nano-mCherry(NoIRes)-(SctL)*	BglII, MfeI***	Sm		pFL125
pFL173 (this work)	*pACYC184::SycE, YopE1-138-BamHI-MfeI-SalI pre-mut*	(vector:BamHI)BglII, SalI (inner:BamHI, MfeI)	Cam	AD1128/1129	pYV
pFL175 (this work)	*pACYC184::SycE, YopE1-138-Cre*	BamHI,MfeI (Insert:BglII, EcoRI)	Cam		pFL174
pFL176 (this work)	*pACYC184::SycE, YopE1-138-mCherry*	BamHI,MfeI (Insert:BglII, EcoRI)	Cam		pAD304

* Insert was digested with BsaI instead of NcoI
** Addgene code
*** Insert was digested with EcoRI instead of MfeI
**** Insert was cut out of pre-mutator and ligated to mutator-vector
***** Insert was digested with MfeI instead of BbsI
L1 – GAGG linker
L2 – GSGS linker
L3 – GAGGGAGG linker
L4 – GGSGGSGG linker

Table 5: Strains – *Yersinia enterocolitica* strains that were used in this thesis.

Name	Genotype	Host strain	Comments
dHOPEMTasd	*pYV40 yopO$_{\Delta 2-427}$, yopE$_{21}$ yopH$_{\Delta 1-352}$, yopM$_{23}$ yopP$_{23}$, yopT$_{135}$ Δasd*		Reference: (Kudryashev *et al.*, 2013)
MRS40	Wild-type pYV *Y. enterocolitica* E40 Δ*blaA*		Reference: (Sory *et al.*, 1995)
AD4324	*mCherry-YscQ*	dHOPEMTasd	Reference: (Diepold *et al.*, 2015)
AD4419	*ΔsctQ*	dHOPEMTasd	Reference: (Diepold *et al.*, 2015)
FL4002	*Zdk1-mCherry-YscQ*	dHOPEMTasd	pFL115 x* dHOPEMTasd
FL4003	*Zdk1-YscQ, mCherry-YscL*	dHOPEMTasd	pAD612 x* ADTM4521
FL4004	*SspB_Nano-mCherry-YscQ*	dHOPEMTasd	pFL117 x* dHOPEMTasd
FL4005	*SspB_Nano-YscQ, mCherry-YscL*	dHOPEMTasd	pFL118 x* ADTM4521
FL4009	*Zdk1-mCherry-YscQ ΔYscN*	dHOPEMTasd	pAD168 x* FL02
FL4012	*SspB_Nano-YscQ mCherry-YscL, ΔYscN*	dHOPEMTasd	pAD168 x* FL05
FL4015	*SspB-Nano-mCherry(NoIRes)-YscQ*	dHOPEMTasd	dHOPEMTasd x* pFL128
FL4017	*SspB_Nano-YscK*	dHOPEMTasd	dHOPEMTasd x* pFL130

FL4018	*Zdk1-YscQ*	MRS40	MRS40 x* pAD612
FL4019	*SspB-Nano-YscQ*	MRS40	MRS40 x* pFL118
KS005	*SspB-Nano-YscQ, mCherry-Ysck, ΔYscN*	dHOPEMTasd	Reference: Master thesis Kirsten Stahl (AG Diepold)
FL4021	*dYscQ*	MRS40	MRS40 x* pAD419
FL4022	*Zdk1-YscQ*	dHOPEMTasd	dHOPEMTasd x* pAD612
FL4023	*SspB-Nano-YscQ*	dHOPEMTasd	dHOPEMTasd x* pFL118
FL4024	*SspB_Nano-YscQ, SycH-mCherry*	MRS40	FL19 x* pCH08
FL4025	*SspB_Nano-YscQ, SycH-mCherry*	dHOPEMTasd	FL23 x* pCH08
FL4026	*PIF6A-SctQ*	dHOPEMTasd	dHOPEMTasd x* pFL147
FL4027	*SspB_Nano-SctN*	dHOPEMTasd	dHOPEMTasd x* pFL169
FL4038	*SspB_Nano-mCherry(NoIRes)-SctN*	dHOPEMTasd	dHOPEMTasd x* pFL171
FL4039	*SspB_Nano-mCherry(NoIRes)-SctL*	dHOPEMTasd	dHOPEMTasd x* pFL172
FL4042	*SspB_Nano-SctL*	dHOPEMTasd	dHOPEMTasd x* pFL170

* x = homologous recombination (4.9) between mutator-plasmid and host-strain, recombination leads to an allelic exchange of the native gene and the mutated gene.

8 Methods

8.1 Cultivation of bacteria

All *Y. enterocolitica* strains were cultivated in BHI media (3.7% w/v) (Brain Heart Infusion Broth - VWR Chemicals (Darmstadt, G)). To this media Nalidic acid (Nal) (35 µg/ml) and 2, 6-Diaminopimelic acid (DAP) (60 µg/ml) were always added, because the used *Yersinia* strains are auxotrophic for DAP and have a genome encoded resistance against NAL. All *E. coli* strains were cultivated in LB media (tryptone (10% w/v), yeast extract (5% w/v), NaCl (10% w/v) - CARL ROTH GmbH & CO KG (Karlsruhe, G)). If necessary, further antibiotics Ampicillin (Amp) (200 µg/ml) (for plates, the more stable form Carbenicillin (Carb) was used), Canamycin (Cam) (25 µg/ml), Streptomycin (Sm) (50 µg/ml) depending on the integrated plasmids were added to the cultivation media. For an overnight culture, 2-5 ml of cultivation media with corresponding antibiotics were inoculated with a specific strain from the glycerol stock strain collection and were cultivated overnight at 28° C (*Y. enterocolitica*) or 37° C (*E. coli*) in a shaking incubator. For cultivation plates, 15 % w/v Agar (Becton, Dickinson and Company (New Jersey, USA)) was added to the media.

8.2 Strain construction

8.2.1 Plasmid construction - PCR

All plasmids that were designed and made in this work are listed in Table 3. Primer that were designed and used for PCR of the plasmid-specific inserts are listed in Table 2. The PCR reaction mix (total volume 50 µl) contains H_2O (79.5% w/v), 10x Phusion buffer HM (10 % w/v) (New England Biolabs GmbH (Frankfurt am Main, G)), dNTP-mix (2 % w/v) (ROTI MIX PCR3 10 mM - CARL ROTH GmbH & CO KG (Karlsruhe, G)), fwd-primer / rev-primer (4 % w/v - 10 mM stock), Phusion polymerase (0.3% w/v - New England Biolabs GmbH) and template DNA (0.4 – 1 % w/v). The PCR reaction was performed in an “Eppendorf® Mastercycler® Nexus” - SIGMA-ALDRICH (Steinheim, G) and default PCR settings that are shown in Table 6.

Table 6. PCR settings – Settings that were used for PCR reaction

	Step	C°	m:s	go to	loops
	1	98,0	00:30	/	/
→	2	98,0	00:10	/	/
34x	3	55,0	00:20	/	/

4	72,0	t_E*	2	34
5	72,0	05:00	/	/
6	4,0	∞	/	/

* t_E depends on length of PCR product – usually 30 s for ~1 kB

PCR products were then purified by using a purification kit (3 – using manual of the kit) or by gel electrophoresis (1:6 6x loading dye (Bromphenol blue (0.25 % w/v), Xylene cyanol FF (0.25 % w/v), Glycerol (30 % w/v) in PCR reaction mix, load on an agarose gel (1 % w/v Agarose, 1x TAE buffer (TRIS-acetate (40 mM), EDTA (1 mM), pH = 8.3), EtBr (0,05 % w/v)) – settings: 135 V, 500 mA, 30 min) and following gel extraction (3 – using manual of the kit) of the band of correct size that was cut out.

8.2.2 Plasmid construction - digestion

Purified PCR products and corresponding vector were digested with corresponding restriction enzymes (Table 3) and settings (shown on NEB cloner – Table 1) depending on the used enzymes (usually 1 h at 37° C and specific restriction buffer). The digested vector was treated with Antarctic Phosphatase (2% w/v) (plus 10x phosphatase buffer - 10% w/v) (New England Biolabs GmbH (Frankfurt am Main, G)) that dephosphorylates the 5' and 3' ends and impede self-religation of the vector (Rina *et al.*, 2000). The digestion then was purified by gel electrophoresis (4.2.1) and gel extraction (3).

8.2.3 Plasmid construction – ligation

The digested PCR insert and vector were then ligated in a ligation mix (total volume 15 µl) that contains H_2O (15 µl – x), digested vector (100 ng), digested insert (3:1 molar ratio to vector), "10x T4 DNA Ligase buffer"(10 % w/v) and "T4 DNA Ligase"(5 % w/v) (New England Biolabs GmbH (Frankfurt am Main, D). The ligation mix was incubated for 1 h at room temperature (RT).

8.2.4 Transformation of *Escherichia coli*

Transformation of *E. coli* was either performed with *Top10* (strain for plasmid propagation) or with *Sm10 λpir*$^{+}$ (strain that contains *pir* gene for pKNG101 propagation - pKNG101 can only replicate if π is provided in trans (as in the *E. coli Sm10λpir*$^{+}$ strain) or if it integrates into the host chromosome (or *pYV* plasmid in *Yersinia*) (Koné Kaniga, Delor and Cornelis, 1991) - used for 2-Step homologous recombination (4.7)). For transformation of chemical competent *E. coli* (were made competent with TSS buffer (tryptone (1 % w/v), yeast extract (0.5 % w/v), NaCl (1 % w/v), PEG 3350 (10 % w/v), DMSO (5 % w/v), $MgCl_2$ (50 mM), pH = 6.5 – protocol adapted from (Chung and Miller, 1993)), 15 µl of ligation mix was added to the defrosted *E. coli* cells and incubated on ice for at least 30 min. The cells were then heat shocked for 1 min at 42° C water bath, incubated for 1 min on ice and were resuspended in 800 µl LB and incubated for 1 h at 37° C shaker (800 rpm). After incubation, the cells were spun down for 2 min and 8.000 rcf and resuspended in 50 µl remaining supernatant- the rest was discarded. 20 µl were plated on LB-plates with corresponding antibiotics and incubated at 37° C o/n.

8.2.5 Transformation of *Yersinia enterocolitica*

Transformation of *Y. enterocolitica* was performed with *dHOPEMTasd* (S1-strain in which effector genes *H, O, P, E, M, T* and *asd* genes were deleted (Kudryashev *et al.*, 2013)). For transformation of electro competent *Y. enterocolitica* (Protocol “electro competent cells” – adapted from protocol by C. Pfaff 2005), 1-2 µl of miniprep plasmid DNA was added to the defrosted *Y. enterocolitica* cells and incubated on ice for at least 15 min. The cells were then transferred into pre-cooled electroporation cuvettes (3) and electroporated with a micropulser (3) and the setting Ec2 (2.5 kV). Directly afterwards, cells were resuspended in 800 µl BHI + DAP (60 µg/ml) and transferred into new tubes. After incubating for 2 h at 28° C shaker (700 rpm) the cells were spun down for 2 min and 8.000 rcf and resuspended in 50 µl of remaining supernatant – the rest was discarded. 50 µl were plated on BHI + NAL + DAP + corresponding antibiotics (4.1) and incubated at 28° C for 2-3 days.

8.2.6 Colony PCR

Colonies that were grown on the transformation plates were verified with a colony PCR. 20 µl of the PCR reaction mix (4.2.1) was used for each reaction tube. Usually 12 to 24 colonies were picked with a sterile pipette tip, transferred first to a well labelled master plate and afterwards to the reaction tube.

PCR was performed as described in 4.2.1 but with 10 min in the first 98° C step (to lyse the cells). 5 µl of PCR product then was loaded on an agarose gel and verified by gel electrophoresis (4.2.1).

8.3 Yersinia cultures for T3SS induction

From an overnight culture (4.1) of strains that were planned to be examined, 100 µl (for non-secreting conditions) or 120 µl (for secreting conditions) were inoculated in corresponding media (1:50 dilution for non-secreting conditions, 1:41.67 for secreting conditions). The cultivation media contains BHI (3.7 % w/v), NaI (35 µg/ml), DAP (50 µg/ml), $MgCl_2$ (20 mM), glycerol (0.4 % w/v) and corresponding antibiotics (4.1). For non-secreting conditions $CaCl_2$ (5 mM) and for secreting conditions EGTA (5 mM) was added. The cultures were cultivated for 90 min at 28° C and then shifted to a 37° C water bath and inoculated for 2-3 h (if the strain contained an inducible plasmid, the plasmid was induced with 0.2 % w/v L-arabinose before shifting to 37° C).

8.4 Analysis of protein expression and secretion activity

After induction of T3SS (4.3) 2 ml of bacteria culture was spun down for 10 min at 4° C and 12.000 rcf while measuring the OD_{600} of the cell cultures to use for later calculations. For visualization of secreted proteins, 1.8 ml of the supernatant was mixed with 200 µl TCA (TCA is used for protein precipitation (Link and LaBaer, 2011)). After centrifugation for 15 min at 4° C and 20.000 rcf, the protein pellet was washed twice with 900 µl ice-cold acetone and spin down for 5 min at 4° C and max. speed in between and then could be used for further analysis. If the expressed T3SS proteins were quantified, the total cell pellet without supernatant was used for further analysis. For normalization of cell density, the pellet then was resuspended in calculated amount of 1x sample buffer (SDS (2 % w/v), Tris * HCl (0.1 M), glycerol (10 % w/v), DTT (0.05 M, pH = 6.8). The calculation of sample buffer is shown in Table 7.

Table 7. Sample buffer calculation – Calculation of used 1x sample buffer depends on kind of sample

Sample	Calculation
TC from 2 ml to get 0.3 ODu* in 15 µl	measured OD_{600} * 2 * 15 / 0.3
SN from 1.8 ml to get 0.6 ODu* in 15 µl	measured OD_{600} * 1.8 * 15 / 0.6

* 1 ODu = 1 ml of a culture at OD 1 = about $5*10^8$ bacteria (for Yersinia)

After heating the sample for 5 min at 99° C, 15 µl were loaded on a SDS-gel (3) and run for 45-90 min at 130 V and 40 mA. The SDS-gel was then stained with staining solution (3) for an optional time length (depends on how strong the colorizing effect should be) or used for Western blot (4.6).

8.5 Western blot

The SDS-gel (4.4) was blotted on a nitrocellulose membrane using a Blot Transfer-system (3) with the settings: 1.3 A, 25 V, 7 min. After blotting, the membrane was put in 15 ml milk solution (5 % w/v nonfat dried milk powder (PanReac AppliChem ITW Reagents (Darmstadt, G)) in 1x PBS (NaCl (137 mM), KCl (2.7 mM), Na_2HPO_4 (10 mM), KH_2PO_4 (2 mM), pH = 7.4)) and incubated o/n at 4° C on a shaker. The blot was washed once with 1x PBS and then incubated with the first antibody (diluted in milk solution (5 % w/v)) for 1 h at RT on a shaker.
Then the blot was washed 1x with 1x PBS, 1x with 1x PBS-T (1x PBS + Tween 20 (0.2 % w/v)), 1x with 1x PBS (washing steps always were performed for 1 min). After washing, the blot was incubated with the second antibody (diluted in milk solution (5 % w/v)) for 1 h at RT on a shaker. Then the blot was washed again 1x with 1x PBS, 4x with 1x PBS-T, 1x with 1x PBS. After removing the 1x PBS buffer, 800 µl of detection reagent ("Luminata™ Forte Western HRP Substrate" – MERCK (Darmstadt, G)) was added to the blot and spreaded evenly with a drigalski spatula. Pictures of the blot were taken with a Luminescent Image Analyzer (3).

8.6 Fluorescence microscopy

For fluorescence microscopy, strains were cultivated as described above under non-secreting conditions. 2 ml of culture then was harvested for 4 min at 2,400 *g* and the cell pellet was resuspended in 400 µl of minimal medium (HEPES (100 mM), $(NH_4)_2SO_4$ (5 mM), NaCl (100 mM), sodium glutamate (20 mM), $MgCl_2$ (10 mM), K_2SO_4 (5 mM), casamino acids (0.5% w/v)) including DAP (60 µg/ml). 2 µl of the resuspension were spotted onto agar slides (1.5% w/v agarose in minimal medium) and topped with a circular cover slip (25 mm ⌀). Samples were analyzed on an inverse fluorescence microscope (Deltavision Elite). For pulse activation of the optogenetic interaction switches, 0.1 s of GFP excitation light (~ 480 nm, light intensity ~ 2.5 mW cm^{-2}) was applied. Unless stated differently, exposure times were 500 ms for mCherry fluorescence, using a mCherry filter set (575/25 excitation and 625/45 nm emission filter sets), and 200 ms for GFP fluorescence, using a GFP filter set (475/28 and 525/48 nm, respectively). Per image, a z stack containing 7 to 15 frames per wavelength with a spacing of 150 nm was acquired. Micrographs were processed using softWoRx 7.0.0, and the ImageJ 1.52i-based Fiji software package(Schindelin *et al.*, 2012; Schneider, Rasband and Eliceiri, 2012) was used for image analysis and display.

8.7 Optogenetic cell cultivation

For optogenetic experiments, the strains for secretion assays or Western blots (to determine the amount of secreted proteins) were cultivated under secreting conditions. At the indicated time points after induction of the system by a temperature shift to 37°, the cultures were cultivated at 37°C for 1 - 3 h in an optogenetic experimental setup in a shaking incubator, consisting of two blue light sources that were placed around the bacterial cultures (light source 1, “Globo lighting 10 W LED 9 V 34118S”, Globo Lighting GmbH; light source 2, “Rolux LED-Leiste DF-7024-12 V 1.5 W” , Rolux Leuchten GmbH. Bacteria were cultivated at 37°C under blue light or dark conditions (light intensity at culture location at a wavelength of 488 nm was ~ 1 mW cm^{-2}), and further processed as described.

8.8 Two-step homologous recombination

For two-step homologous recombination an o/n culture (2.5 ml of media + corresponding ingredients (4.1)) of the acceptor strain (*Yersinia*) and the mutator strain (*E.coli – SM10λpir*$^{+}$) were grown. 1 ml of o/n culture was spun down for 2 min at 10.000 rcf, the pellet was resuspended in 1 ml LB + DAP and spun down again. The pellet then was resuspended in 100 µl LB + DAP and 20 µl of the acceptor strain and the mutator strain were mixed in a sterile Eppendorf tube. 20 µl of the mix was spotted on a LB + DAP plate and incubated at 28° C for 4 h. After incubation, the grown spot was scratched and resuspended in 1 ml LB + DAP. 20 µl of the resuspended bacteria were plated on a LB + DAP + Nal + Sm (Sm selects for the first recombination step – integration of the mutator plasmid “PKNG101+Mutation” with a Sm-resistance into the pYV plasmid of *Yersinia* (Koné Kaniga, Delor and Cornelis, 1991)). Then they were incubated for 2-3 days at 28° C. From single grown colonies, 6-8 were inoculated in 2.5 ml of BHI + Nal + DAP + Sm and cultivated o/n at 28° C on a shaker (“RRK0 cultures”). 1.5 µl of the o/n culture were transferred into fresh tubes containing 2.5 ml of BHI + Nal + DAP and cultures were grown for at least 8 h at 28° C on a shaker (“RRK1 cultures”) (media is without Sm to initiate the second recombination step – the removal of the mutator plasmid (Koné Kaniga, Delor and Cornelis, 1991)). After 8 h of incubation, 1.5 µl of culture were transferred into new tubes containing fresh 2.5 ml BHI+ Nal + DAP and incubated o/n at 28° C on a shaker. 20 µl of a 1:10 dilution of the o/n culture were plated on BHI + Nal + DAP + sucrose (8 % w/v) (sucrose selects for the absence of the mutator plasmid (Koné Kaniga, Delor and Cornelis, 1991)) and incubated o/n at 28° C. The next day, a colony PCR (4.2.5) was performed on single colonies to check for site directed mutagenesis.

8.9 Infection assays

HEp-2 cells were maintained in Roswell Park Memorial Institute (RPMI) 1640 medium (Gibco) supplemented with 7.5% newborn calf serum (NCS, Sigma-Aldrich) in 5% CO_2 at 37°C. For the ß-lactamase translocation assay, the infection assay was adapted from ref. (Wolters *et al.*, 2015). HEp-2 cells were seeded into Nuncion Delta Surface 96 flat well plates (Thermo Scientific) at a cell density of $2.0x10^4$ cells/well. Prior to infection, 5 mM DAP was added to medium of the seeded HEp-2 cells. 200 µl of bacterial overnight culture was inoculated in BHI supplemented with DAP (60 µg ml^{-1}), $MgCl_2$ (20 mM), and glycerol (0.4% w/v). Expression of the cargo protein from the pBAD plasmid was induced with 0.2% arabinose (w/v), unless stated differently. The cultures were incubated for 90 min at 37°C under activating conditions (dark for LITESEC-supp / light for LITESEC-act) to induce T3SS formation. After incubation, cultures were centrifuged for 4 min at 4,500 *g* and 4°C. The bacteria were resuspended in ice-cold PBS containing DAP (60 µg ml^{-1}) to a density of approximately $2.5x10^8$ cfu ml^{-1}, incubated on ice in "off" conditions (light for LITESEC-supp / dark for LITESEC-act) for 15 min, then added to a semi-confluent layer of HEp2-cells at a multiplicity of infection (MOI) of approximately 140, and incubated under blue light or dark conditions for 60 min at 37°C in 5% CO_2. Following incubation, the cell culture medium was removed and 100 µl of working solution were added (1:3 dilution RPMI 1640 medium without phenol red (Gibco) in PBS (Gibco) with 25 mM probenecid acid (Alfa Aesar) dissolved in cell culture grade DMSO (Santa Cruz)). For ß-lactamase translocation assays, 20 µl of CCF2-AM were added (0.12 µl solution A, 1.2 µl solution B and 18.68 µl solution C (solutions A, B and C provided from Invitrogen CCF2-AM loading kit)). After 5 min of incubation, the working solution and CCF2-AM were removed and 100 µl of fresh working solution was added. Plates were then incubated at 37°C in 5% CO_2 for 10 min. Next, cells were fixed by addition of 100 µl of ice-cold 1% para-formaldehyde (PFA) (w/v) and incubation on ice for 10 min. As a last step, the PFA solution was replaced by PBS. Fields of view were chosen in the DIC channel, preventing any bias, and all fields of view were analyzed. Translocation of $YopE_{1-53}$-ß-lactamase was detected by comparing the fluorescence emission at 525/48 nm (FRET-based emission of uncleaved CCF2) vs. 435/48 nm (emission of cleaved CCF2, equivalent to substrate translocation), both at an excitation at 390/18 nm. Both channels were background-corrected. For the apoptosis assay, the protocol outlined in ref. (Ittig *et al.*, 2015) was adapted as follows. HEp-2 cells were seeded to a density of $1.18x10^5$ cells/well into Nuncion Delta Surface 24-well plate (Thermo Scientific). Prior to infection, DAP (60 µg ml^{-1}) and 0.2% arabinose (w/v) were added to each well of HEp-2 cells. Bacteria were first grown at 28°C for 90 min and then shifted to 37°C for 120 minutes, collected by centrifugation, and resuspended in PBS (pre-warmed to 37°C) containing 5 mM DAP at a density of approximately $2.5x10^8$ cfu/ml.

The bacteria were added to a semi-confluent layer of HEp2-cells at an MOI of approximately 140, and incubated under blue light or dark conditions for 60 min at 37°C in 5% CO_2. Following incubation, the cell culture medium was removed and 300 µl of RPMI medium (GIBCO 1640) containing gentamycin (100 µg ml^{-1}) was added. Cells were incubated for further 60 min at 37°C in 5% CO_2 under the specified light conditions and were then imaged with a binocular microscope (5x objective) or on an inverse fluorescence microscope (Deltavision Elite) (20x objective). Fluorescence and cell shape of HEp-2 cells were manually classified by blinded observers.

8.10 Luciferase assay

20 ml day cultures were inoculated from stationary overnight cultures (1:50 dilution) in non-secreting cultivation medium, as described above, and incubated for 90 min at 28°. Subsequently, expression of the Nanoluc cargo proteins from the pBAD plasmid was induced with 0.2% arabinose (w/v). The cultures were incubated for 120 min at 37°C under activating conditions (dark for LITESEC-supp / light for LITESEC-act) to induce T3SS formation. After that, strains were incubated for 10 min under dark conditions, and 5 mM EGTA was added to start secretion. Bacteria were then incubated for 60 min each (20 min each for the determination of switching kinetics) at the indicated conditions. Samples were taken immediately before EGTA addition and at the indicated times afterwards. In the samples, 10 mM $CaCl_2$ was added to stop secretion. Bacteria were harvested and the supernatant was used for the enzymatic assay. The enzymatic NanoLuc detection assay was performed according to manufacturer instructions, similar to ref. (Westerhausen, Nowak, Torres-Vargas, *et al.*, 2020). 5 µl supernatant was mixed with 25 µl H_2O and 30 µl of NanoLuc detection reagent (Nano-Glo Luciferase Assay Substrate in Luciferase Assay Buffer, PROMEGA Corporation, Madison). Bioluminescence was detected in an Elisa Plate Reader Infinite M20 Pro (BioTek Instruments, Vermont), smallest field of view, large binning and an aquisition time of 1,000 ms. For split-Nanoluc detection assays, Hela (LgBiT) (Westerhausen, Nowak, Torres-Vargas, *et al.*, 2020) were used.

List of abbreviations	
°C	Degree Celsius
µl	Microliter
µM	Micro molar
Amp	Ampicillin
ATP	Adenosin-triphosphat
Cam	Chloramphenicol
DAP	2,6- Diaminopimelic acid
DMSO	Dimethyl sulfoxide
DNA	Deoxy-ribonucleic acid
dNTP	Deoxy-nucleotidtriphosphate
DTT	1,4-Dithiothreitol
EDTA	Ethylendiamintetra acidic acid
EGFP	Enhanced Green Fluorescent Protein
EGTA	Ethylene glycol-bis(2-aminoethylether)-N,N,N′,N′-tetra acetic acid
EtBr	Ethidium bromide
EtOH	Ethanol
h	Hours
HCl	Hydrochloric acid
HEPES	4-(2-hydroxyethyl)-1-piperazineethanesulfonic acid
HMD	hypothetical membrane domain
IM	Inner membrane
IPTG	Isopropyl-β-D-thiogalactopyranosid
kb	Kilobase
kDA	Kilodalton
kV	Kilovolt
L-ara	L-arabinose
LOV	LOVTRAP
M	Molar
mA	Milliampere
MA	Membrane anchor
MB	monobody
mg	Milligram
min	Minutes
ml	Milliliter
mM	Millimolar
Nal	Nalidic acid
ng	Nanogram
nm	Nanometre
o/n	Over night
OD600	Optical density at a wavelength of 600 nm
ODu	OD per volume
PAGE	Polyacrylamide gel electrophoresis
PCR	Polymerase chain reaction
PEG	Poly(ethylene glycol)
POI	„Protein of interest“
rcf	Relative centrifugal force (x g)
rpm	Revolutions per minute
RT	Room temperature
s	Second
SDS	Sodiumdodecylsulfate
Sm	Streptomycin
SN	Supernatant
T	Temperature
T3SS	Type III secretion system
TC	Total cell
TCA	Trichloroacetic acid
TMH	Transmembrane helix domain
TRIS	Tris(hydroxymethyl)aminomethane
V	Volt
wt	Wild type
% w/v	Weight/volume

9.References

Akeda, Y. and Galán, J. E. (2005) 'Chaperone release and unfolding of substrates in type III secretion', *Nature*, 437(7060), pp. 911–915. doi: 10.1038/nature03992.

Ash, C. *et al.* (2017) 'Effect of wavelength and beam width on penetration in light-tissue interaction using computational methods', *Lasers in Medical Science*, 32(8), pp. 1909–1918. doi: 10.1007/s10103-017-2317-4.

Autenrieth, S. E. *et al.* (2010) 'Immune Evasion by Yersinia enterocolitica: Differential Targeting of Dendritic Cell Subpopulations In Vivo', *PLoS Pathogens*. Edited by B. T. Cookson, 6(11), p. e1001212. doi: 10.1371/journal.ppat.1001212.

Bai, F. *et al.* (2014) 'Assembly dynamics and the roles of FliI ATPase of the bacterial flagellar export apparatus', *Scientific Reports*, 4(1), pp. 1–7. doi: 10.1038/srep06528.

Bai, F. *et al.* (2018) 'Bacterial type III secretion system as a protein delivery tool for a broad range of biomedical applications', *Biotechnology Advances*, 36(2), pp. 482–493. doi: 10.1016/J.BIOTECHADV.2018.01.016.

Baumschlager, A. and Khammash, M. (2021) 'Synthetic Biological Approaches for Optogenetics and Tools for Transcriptional Light-Control in Bacteria', *Advanced Biology*. John Wiley and Sons Inc. doi: 10.1002/adbi.202000256.

Benedetti, L. *et al.* (2018) 'Light-activated protein interaction with high spatial subcellular confinement', *Proceedings of the National Academy of Sciences of the United States of America*, 115(10), pp. E2238–E2245. doi: 10.1073/pnas.1713845115.

Berger, C. *et al.* (2021) 'Structure of the Yersinia injectisome in intracellular host cell phagosomes revealed by cryo FIB electron tomography', *Journal of Structural Biology*, 213(1), p. 107701. doi: 10.1016/j.jsb.2021.107701.

Bernal, I. *et al.* (2019) 'Molecular organization of soluble type III secretion system sorting platform complexes', *bioRxiv*, p. 648071. doi: 10.1101/648071.

Berry, B. J. and Wojtovich, A. P. (2020) 'Mitochondrial light switches: optogenetic approaches to control metabolism', *FEBS Journal*. Blackwell Publishing Ltd, pp. 4544–4556. doi: 10.1111/febs.15424.

Bichsel, C. *et al.* (2011) 'Bacterial Delivery of Nuclear Proteins into Pluripotent and Differentiated Cells', *PLoS ONE*. Edited by W.-C. Chin, 6(1), p. e16465. doi: 10.1371/journal.pone.0016465.

Blaylock, B. *et al.* (2006) 'Characterization of the Yersinia enterocolitica type III secretion ATPase YscN and its regulator, YscL.', *Journal of bacteriology*, 188(10), pp. 3525–34. doi: 10.1128/JB.188.10.3525-3534.2006.

Bliska, J. B. *et al.* (2013) 'Modulation of innate immune responses by Yersinia type III secretion system translocators and effectors.', *Cellular microbiology*, 15(10), pp. 1622–31. doi: 10.1111/cmi.12164.

Bölin, I. and Wolf-Watz, H. (1988) 'The plasmid-encoded Yop2b protein of Yersinia pseudotuberculosis is a virulence determinant regulated by calcium and temperature at the level of transcription', *Molecular Microbiology*, 2(2), pp. 237–245. doi: 10.1111/j.1365-2958.1988.tb00025.x.

Bottone, E. J. (1999) 'Yersinia enterocolitica: overview and epidemiologic correlates', *Microbes and Infection*, 1(4), pp. 323–333. doi: 10.1016/S1286-4579(99)80028-8.

Bottone, E. J. and Mollaret, H.-H. (1977) '*Yersinia Enterocolitica* : A Panoramic View of a Charismatic Microorganism', *CRC Critical Reviews in Microbiology*, 5(2), pp. 211–241. doi: 10.3109/10408417709102312.

Brinkworth, A. J. *et al.* (2011) 'Chlamydia trachomatis Slc1 is a type III secretion chaperone that enhances the translocation of its invasion effector substrate TARP', *Molecular Microbiology*, 82(1), pp. 131–144. doi: 10.1111/j.1365-2958.2011.07802.x.

Broz, P. *et al.* (2007) 'Function and molecular architecture of the Yersinia injectisome tip complex', *Molecular Microbiology*, 65(5), pp. 1311–1320. doi: 10.1111/j.1365-2958.2007.05871.x.

Burghout, P. *et al.* (2004) 'Role of the pilot protein YscW in the biogenesis of the YscC secretin in Yersinia enterocolitica', *Journal of Bacteriology*, 186(16), pp. 5366–5375. doi: 10.1128/JB.186.16.5366-5375.2004.

Buttner, D. (2012) 'Protein Export According to Schedule: Architecture, Assembly, and Regulation of Type III Secretion Systems from Plant- and Animal-Pathogenic Bacteria', *Microbiology and Molecular Biology Reviews*, 76(2), pp. 262–310. doi: 10.1128/MMBR.05017-11.

Bzymek, K. P., Hamaoka, B. Y. and Ghosh, P. (2012) 'Two translation products of Yersinia yscQ assemble to form a complex essential to type III secretion', *Biochemistry*, 51(8), pp. 1669–1677. doi: 10.1021/bi201792p.

Carrasco-López, C. *et al.* (2020) 'Development of light-responsive protein binding in the monobody non-immunoglobulin scaffold', *Nature Communications*, 11(1), pp. 1–13. doi: 10.1038/s41467-020-17837-7.

Carroll, P. *et al.* (2014) 'Identification of the translational start site of codon-optimized mCherry in Mycobacterium tuberculosis.', *BMC research notes*, 7, p. 366. doi: 10.1186/1756-0500-7-366.

Chait, R. *et al.* (2017) 'Shaping bacterial population behavior through computer-interfaced control of individual cells', *Nature Communications*, 8(1), pp. 1–11. doi: 10.1038/s41467-017-01683-1.

Chakravartty, V. and Cronan, J. E. (2015) 'A series of medium and high copy number arabinose-inducible Escherichia coli expression vectors compatible with pBR322 and pACYC184.', *Plasmid*, 81, pp. 21–6. doi: 10.1016/j.plasmid.2015.03.001.

Charpentier, X. and Oswald, E. (2004) 'Identification of the secretion and translocation domain of the enteropathogenic and enterohemorrhagic Escherichia coli effector Cif, using TEM-1 beta-lactamase as a new fluorescence-based reporter.', *Journal of bacteriology*, 186(16), pp. 5486–95. doi: 10.1128/JB.186.16.5486-5495.2004.

Chen, F. and Wegner, S. V. (2017) 'Blue Light Switchable Bacterial Adhesion as a Key Step toward the Design of Biofilms', *ACS Synthetic Biology*, 6(12), pp. 2170–2174. doi: 10.1021/acssynbio.7b00197.

Christen, M. *et al.* (2010) 'Asymmetrical distribution of the second messenger c-di-GMP upon bacterial cell division', *Science*, 328(5983), pp. 1295–1297. doi: 10.1126/science.1188658.

Chung, C. T. and Miller, R. H. (1993) 'Preparation and storage of competent Escherichia coli cells.', *Methods in enzymology*, 218, pp. 621–7. Available at: http://www.ncbi.nlm.nih.gov/pubmed/8510550 (Accessed: 6 May 2018).

Cornelis, G. *et al.* (1987) 'Yersinia enterocolitica, a Primary Model for Bacterial Invasiveness', *Clinical*

Infectious Diseases, 9(1), pp. 64–87. doi: 10.1093/clinids/9.1.64.

Cornelis, G. R. *et al.* (1998) 'The virulence plasmid of Yersinia, an antihost genome.', *Microbiology and molecular biology reviews : MMBR*, 62(4), pp. 1315–52. Available at: http://www.ncbi.nlm.nih.gov/pubmed/9841674 (Accessed: 6 April 2018).

Cornelis, G. R. (2006) 'The type III secretion injectisome', *Nature Reviews Microbiology*, 4(11), pp. 811–825. doi: 10.1038/nrmicro1526.

Craney, A. *et al.* (2011) 'Bacterial transmembrane proteins that lack N-terminal signal sequences', *PLoS ONE*, 6(5), pp. e19421–e19421. doi: 10.1371/journal.pone.0019421.

Dailey, H. A. *et al.* (2017) 'Prokaryotic Heme Biosynthesis: Multiple Pathways to a Common Essential Product', *Microbiology and Molecular Biology Reviews*, 81(1). doi: 10.1128/mmbr.00048-16.

Deisseroth, K. (2011) 'Optogenetics', *Nature Methods*, 8(1), pp. 26–29. doi: 10.1038/nmeth.f.324.

Deng, W. *et al.* (2017) 'Assembly, structure, function and regulation of type III secretion systems', *Nature Reviews Microbiology*, 15(6), pp. 323–337. doi: 10.1038/nrmicro.2017.20.

Dewoody, R. S., Merritt, P. M. and Marketon, M. M. (2013) 'Regulation of the Yersinia type III secretion system: Traffic control', *Frontiers in Cellular and Infection Microbiology*. Frontiers, p. 4. doi: 10.3389/fcimb.2013.00004.

Diepold, A. *et al.* (2010) 'Deciphering the assembly of the Yersinia type III secretion injectisome.', *The EMBO journal*, 29(11), pp. 1928–40. doi: 10.1038/emboj.2010.84.

Diepold, A. *et al.* (2015) 'Composition, Formation, and Regulation of the Cytosolic C-ring, a Dynamic Component of the Type III Secretion Injectisome', *PLOS Biology*. Edited by A. M. Stock, 13(1), p. e1002039. doi: 10.1371/journal.pbio.1002039.

Diepold, A. *et al.* (2017) 'A dynamic and adaptive network of cytosolic interactions governs protein export by the T3SS injectisome', *Nature Communications*, 8(May), pp. 1–12. doi: 10.1038/ncomms15940.

Diepold, A. (2020) 'Assembly and post-assembly turnover and dynamics in the type III secretion system', in *Current Topics in Microbiology and Immunology*. Springer Science and Business Media Deutschland GmbH, pp. 35–66. doi: 10.1007/82_2019_164.

Diepold, A. and Armitage, J. P. (2015) 'Type III secretion systems: the bacterial flagellum and the injectisome', *Philosophical Transactions of the Royal Society B: Biological Sciences*, 370(1679), p. 20150020. doi: 10.1098/rstb.2015.0020.

Diepold, A., Wiesand, U. and Cornelis, G. R. (2011) 'The assembly of the export apparatus (YscR,S,T,U,V) of the Yersinia type III secretion apparatus occurs independently of other structural components and involves the formation of an YscV oligomer', *Molecular Microbiology*, 82(2), pp. 502–514. doi: 10.1111/j.1365-2958.2011.07830.x.

Ekestubbe, S. *et al.* (2016) 'The Amino-Terminal Part of the Needle-Tip Translocator LcrV ofYersinia pseudotuberculosisIs Required for Early Targeting of YopH andIn vivoVirulence.', *Frontiers in cellular and infection microbiology*, 6, p. 175. doi: 10.3389/fcimb.2016.00175.

Endo, M. and Ozawa, T. (2017) 'Strategies for development of optogenetic systems and their applications', *Journal of Photochemistry and Photobiology C: Photochemistry Reviews*. Elsevier B.V., pp. 10–23. doi: 10.1016/j.jphotochemrev.2016.10.003.

Enninga, J. *et al.* (2005) 'Secretion of type III effectors into host cells in real time.', *Nature methods*, 2(12), pp. 959–65. doi: 10.1038/nmeth804.

Fàbrega, A. and Vila, J. (2012) 'Yersinia enterocolitica: Pathogenesis, virulence and antimicrobial resistance', *Enfermedades Infecciosas y Microbiologia Clinica*. Elsevier Doyma, pp. 24–32. doi: 10.1016/j.eimc.2011.07.017.

Felgner, S. *et al.* (2016) 'Optimizing Salmonella enterica serovar Typhimurium for bacteria-mediated tumor therapy.', *Gut microbes*, 7(2), pp. 171–7. doi: 10.1080/19490976.2016.1155021.

Felgner, S. *et al.* (2017) 'Tumour-targeting bacteria-based cancer therapies for increased specificity and improved outcome', *Microbial Biotechnology*, 10(5), pp. 1074–1078. doi: 10.1111/1751-7915.12787.

Figueira, R. and Holden, D. W. (2012) 'Functions of the Salmonella pathogenicity island 2 (SPI-2) type III secretion system effectors', *Microbiology*. Microbiology Society, pp. 1147–1161. doi: 10.1099/mic.0.058115-0.

Foultier, B. *et al.* (2001) 'Characterization of the ysa Pathogenicity Locus in the Chromosome of Yersinia enterocolitica and Phylogeny Analysis of Type III Secretion Systems'. doi: 10.1007/s00239-001-0089-7.

Fukuoka, H. *et al.* (2010) 'Exchange of rotor components in functioning bacterial flagellar motor', *Biochemical and Biophysical Research Communications*, 394(1), pp. 130–135. doi: 10.1016/j.bbrc.2010.02.129.

Galán, J. E. *et al.* (2014) 'Bacterial type III secretion systems: specialized nanomachines for protein delivery into target cells.', *Annual review of microbiology*, 68, pp. 415–38. doi: 10.1146/annurev-micro-092412-155725.

Gambetta, G. A. and Lagarias, J. C. (2001) 'Genetic engineering of phytochrome biosynthesis in bacteria.', *Proceedings of the National Academy of Sciences of the United States of America*, 98(19), pp. 10566–71. doi: 10.1073/pnas.191375198.

Gauthier, A. and Finlay, B. B. (2003) 'Translocated Intimin Receptor and Its Chaperone Interact with ATPase of the Type III Secretion Apparatus of Enteropathogenic Escherichia coli', *Journal of Bacteriology*, 185(23), pp. 6747–6755. doi: 10.1128/JB.185.23.6747-6755.2003.

Giraldo, R. (2019) 'Optogenetic Navigation of Routes Leading to Protein Amyloidogenesis in Bacteria', *Journal of Molecular Biology*, 431(6), pp. 1186–1202. doi: 10.1016/j.jmb.2019.01.037.

Gohlke, U. *et al.* (2005) 'The TatA component of the twin-arginine protein transport system forms channel complexes of variable diameter.', *Proceedings of the National Academy of Sciences of the United States of America*, 102(30), pp. 10482–6. doi: 10.1073/pnas.0503558102.

Golonka, D. *et al.* (2019) 'Deconstructing and repurposing the light-regulated interplay between Arabidopsis phytochromes and interacting factors', *Communications Biology*, 2(1), p. 448. doi: 10.1038/s42003-019-0687-9.

Green, E. R. and Mecsas, J. (2016) 'Bacterial Secretion Systems: An Overview', *Microbiology Spectrum*, 4(1). doi: 10.1128/microbiolspec.vmbf-0012-2015.

Guglielmi, G., Falk, H. J. and De Renzis, S. (2016) 'Optogenetic Control of Protein Function: From Intracellular Processes to Tissue Morphogenesis', *Trends in Cell Biology*. Elsevier Ltd, pp. 864–874. doi: 10.1016/j.tcb.2016.09.006.

Guntas, G. *et al.* (2015) 'Engineering an improved light-induced dimer (iLID) for controlling the localization and activity of signaling proteins', *Proceedings of the National Academy of Sciences*, 112(1), pp. 112–117. doi: 10.1073/pnas.1417910112.

Hajra, D., Nair, A. V. and Chakravortty, D. (2021) 'An elegant nano-injection machinery for sabotaging the host: Role of Type III secretion system in virulence of different human and animal pathogenic bacteria', *Physics of Life Reviews*. doi: 10.1016/j.plrev.2021.05.007.

Hantschel, O., Biancalana, M. and Koide, S. (2020) 'Monobodies as enabling tools for structural and mechanistic biology', *Current Opinion in Structural Biology*. Elsevier Ltd, pp. 167–174. doi: 10.1016/j.sbi.2020.01.015.

He, L. *et al.* (2021) 'Optogenetic Control of Non-Apoptotic Cell Death', *Advanced Science*, 8(13), p. 2100424. doi: 10.1002/advs.202100424.

Heroven, A. K. and Dersch, P. (2014) 'Coregulation of host-adapted metabolism and virulence by pathogenic yersiniae', *Frontiers in cellular and infection microbiology*, 4, p. 146.

Hu, B. *et al.* (2017) 'In Situ Molecular Architecture of the Salmonella Type III Secretion Machine', *Cell*, 168(6), pp. 1065-1074.e10. doi: 10.1016/j.cell.2017.02.022.

Huang, J. *et al.* (2011) 'Differential regulation of adherens junction dynamics during apical–basal polarization', *Journal of Cell Science*, 124(23), pp. 4001–4013. doi: 10.1242/jcs.086694.

Huang, Z. *et al.* (2020) 'Regulating enzymatic reactions in Escherichia coli utilizing light-responsive cellular compartments based on liquid-liquid phase separation', *bioRxiv*. bioRxiv, p. 2020.11.26.395616. doi: 10.1101/2020.11.26.395616.

Hueck, C. J. (1998) 'Type III protein secretion systems in bacterial pathogens of animals and plants.', *Microbiology and molecular biology reviews : MMBR*, 62(2), pp. 379–433.

Hwang, L. H. (2006) 'Gene therapy strategies for hepatocellular carcinoma', *Journal of Biomedical Science*, 13(4), pp. 453–468. doi: 10.1007/s11373-006-9085-7.

Ittig, S. J. *et al.* (2015) 'A bacterial type III secretion-based protein delivery tool for broad applications in cell biology.', *The Journal of cell biology*, 211(4), pp. 913–31. doi: 10.1083/jcb.201502074.

Izoré, T., Job, V. and Dessen, A. (2011) 'Biogenesis, regulation, and targeting of the type III secretion system', *Structure*, 19(5), pp. 603–612. doi: 10.1016/j.str.2011.03.015.

Jacobi, C. A. *et al.* (1998) '*In vitro* and *in vivo* expression studies of *yopE* from *Yersinia enterocolitica* using the *gfp* reporter gene', *Molecular Microbiology*, 30(4), pp. 865–882. doi: 10.1046/j.1365-2958.1998.01128.x.

Johnson, S. and Blocker, A. (2008) 'Characterization of soluble complexes of the *Shigella flexneri* type III secretion system ATPase', *FEMS Microbiology Letters*, 286(2), pp. 274–278. doi: 10.1111/j.1574-6968.2008.01284.x.

Kaberniuk, A. A., Shemetov, A. A. and Verkhusha, V. V (2016) 'A bacterial phytochrome-based optogenetic system controllable with near-infrared light.', *Nature methods*, 13(7), pp. 591–7. doi: 10.1038/nmeth.3864.

Kaniga, K, Delor, I. and Cornelis, G. R. (1991) 'A wide-host-range suicide vector for improving reverse genetics in gram-negative bacteria: inactivation of the blaA gene of Yersinia enterocolitica.', *Gene*, 109(1), pp. 137–41.

Kaniga, Koné, Delor, I. and Cornelis, G. R. (1991) 'A wide-host-range suicide vector for improving reverse genetics in Gram-negative bacteria: inactivation of the blaA gene of Yersinia enterocolitica', *Gene*, 109(1), pp. 137–141. doi: 10.1016/0378-1119(91)90599-7.

Kawano, F. *et al.* (2013) 'Fluorescence Imaging-Based High-Throughput Screening of Fast- and Slow-Cycling LOV Proteins', *PLoS ONE*. Edited by A. J. Roe, 8(12), p. e82693. doi: 10.1371/journal.pone.0082693.

Kawano, F. *et al.* (2015) 'Engineered pairs of distinct photoswitches for optogenetic control of cellular proteins', *Nature Communications*, 6, pp. 1–8. doi: 10.1038/ncomms7256.

Klewer, L. and Wu, Y. (2019) 'Light-Induced Dimerization Approaches to Control Cellular Processes', *Chemistry – A European Journal*, 25(54), pp. 12452–12463. doi: 10.1002/chem.201900562.

Köberle, M. *et al.* (2009) 'Yersinia enterocolitica Targets Cells of the Innate and Adaptive Immune System by Injection of Yops in a Mouse Infection Model', *PLoS Pathogens*. Edited by R. R. Isberg, 5(8), p. e1000551. doi: 10.1371/journal.ppat.1000551.

De Koning-Ward, T. F. and Robins-Browne, R. M. (1995) *Contribution of Urease to Acid Tolerance in Yersinia enterocolitica*, *INFECTION AND IMMUNITY*. Available at: https://journals.asm.org/journal/iai (Accessed: 24 September 2021).

Kudryashev, M. *et al.* (2013) 'In situ structural analysis of the Yersinia enterocolitica injectisome.', *eLife*, 2, p. e00792. doi: 10.7554/eLife.00792.

Lara-Tejero, M. *et al.* (2011) 'A sorting platform determines the order of protein secretion in bacterial type III systems.', *Science (New York, N.Y.)*, 331(6021), pp. 1188–91. doi: 10.1126/science.1201476.

Le, Y. *et al.* (1999) 'Nuclear targeting determinants of the phage P1 Cre DNA recombinase', *Nucleic Acids Research*, 27(24), pp. 4703–4709. doi: 10.1093/nar/27.24.4703.

Lee, J. *et al.* (2008) 'Surface sites for engineering allosteric control in proteins', *Science*, 322(5900), pp. 438–442. doi: 10.1126/science.1159052.

Lee, V. T. and Schneewind, O. (2002) 'Yop fusions to tightly folded protein domains and their effects on Yersinia enterocolitica type III secretion', *Journal of Bacteriology*, 184(13), pp. 3740–3745. doi: 10.1128/JB.184.13.3740-3745.2002.

Li, H. and Sourjik, V. (2011) 'Assembly and stability of flagellar motor in Escherichia coli', *Molecular Microbiology*, 80(4), pp. 886–899. doi: 10.1111/j.1365-2958.2011.07557.x.

Lindner, F. *et al.* (2020) 'LITESEC-T3SS - Light-controlled protein delivery into eukaryotic cells with high spatial and temporal resolution', *Nature Communications*, 11(1). doi: 10.1038/s41467-020-16169-w.

Link, A. J. and LaBaer, J. (2011) 'Trichloroacetic acid (TCA) precipitation of proteins.', *Cold Spring Harbor protocols*, 2011(8), pp. 993–4. doi: 10.1101/pdb.prot5651.

Liu, Z. *et al.* (2018) 'Programming bacteria with light-sensors and applications in synthetic biology', *Frontiers in Microbiology*, 9(NOV), p. 2692. doi: 10.3389/fmicb.2018.02692.

Loquet, A. *et al.* (2012) 'Atomic model of the type III secretion system needle', *Nature*, 486(7402), pp. 276–279. doi: 10.1038/nature11079.

Ma, C. *et al.* (2020) 'Biosynthesis of phycocyanobilin in recombinant Escherichia coli', *Journal of Oceanology and Limnology*, 38(2), pp. 529–538. doi: 10.1007/s00343-019-9060-6.

MacDonald, J. *et al.* (2017) 'Co-expression with the type 3 secretion chaperone CesT from enterohemorrhagic E. coli increases accumulation of recombinant Tir in plant chloroplasts', *Frontiers in Plant Science*, 8. doi: 10.3389/fpls.2017.00283.

Majewski, D. D. *et al.* (2019) 'Cryo-EM structure of the homohexameric T3SS ATPase-central stalk complex reveals rotary ATPase-like asymmetry', *Nature Communications*, 10(1), pp. 1–12. doi: 10.1038/s41467-019-08477-7.

Marketon, M. M. *et al.* (2005) 'Plague bacteria target immune cells during infection.', *Science*, 309(5741), pp. 1739–41. doi: 10.1126/science.1114580.

McNally, A. *et al.* (2016) '"Add, stir and reduce": Yersinia spp. as model bacteria for pathogen evolution', *Nature Reviews Microbiology*. Nature Publishing Group, pp. 177–190. doi: 10.1038/nrmicro.2015.29.

de Mena, L., Rizk, P. and Rincon-Limas, D. E. (2018) 'Bringing Light to Transcription: The Optogenetics Repertoire', *Frontiers in Genetics*, 9, p. 518. doi: 10.3389/fgene.2018.00518.

Milne-Davies, B. *et al.* (2019) 'Life After Secretion—Yersinia enterocolitica Rapidly Toggles Effector Secretion and Can Resume Cell Division in Response to Changing External Conditions', *Frontiers in Microbiology*, 10, p. 2128. doi: 10.3389/fmicb.2019.02128.

Mukherjee, A. *et al.* (2017) 'Optogenetic tools for cell biological applications.', *Journal of thoracic disease*, 9(12), pp. 4867–4870. doi: 10.21037/jtd.2017.11.73.

Mukherjee, M. *et al.* (2018) 'Engineering a light-responsive, quorum quenching biofilm to mitigate biofouling on water purification membranes', *Science Advances*, 4(12), p. eaau1459. doi: 10.1126/sciadv.aau1459.

Natale, P., Brüser, T. and Driessen, A. J. M. (2008) 'Sec- and Tat-mediated protein secretion across the bacterial cytoplasmic membrane-Distinct translocases and mechanisms', *Biochimica et Biophysica Acta - Biomembranes*. Elsevier, pp. 1735–1756. doi: 10.1016/j.bbamem.2007.07.015.

Navarro, L., Alto, N. M. and Dixon, J. E. (2005) 'Functions of the Yersinia effector proteins in inhibiting host immune responses', *Current Opinion in Microbiology*. Elsevier Ltd, pp. 21–27. doi: 10.1016/j.mib.2004.12.014.

Neeld, D. *et al.* (2014) 'Pseudomonas aeruginosa injects NDK into host cells through a type III secretion system.', *Microbiology (Reading, England)*, 160(Pt 7), pp. 1417–1426. doi: 10.1099/mic.0.078139-0.

Notti, R. Q. *et al.* (2015) 'A common assembly module in injectisome and flagellar type III secretion sorting platforms', *Nature Communications*, 6(1), pp. 1–11. doi: 10.1038/ncomms8125.

O'Neal, L. *et al.* (2017) 'Optogenetic manipulation of cyclic di-GMP (c-di-GMP) levels reveals the role of c-di-GMP in regulating aerotaxis receptor activity in Azospirillum brasilense', *Journal of Bacteriology*, 199(18). doi: 10.1128/JB.00020-17.

Oliver, H. (2017) 'Monobodies as possible next-generation protein therapeutics – a perspective', *Swiss Medical Weekly*. EMH Swiss Medical Publishers Ltd., p. w14545. doi: 10.4414/smw.2017.14545.

Ong, N. T., Olson, E. J. and Tabor, J. J. (2018) 'Engineering an E. coli Near-Infrared Light Sensor', *ACS Synthetic Biology*, 7(1), pp. 240–248. doi: 10.1021/acssynbio.7b00289.

Park, D. *et al.* (2018) 'Visualization of the type III secretion mediated salmonella–host cell interface using cryo-electron tomography', *eLife*, 7. doi: 10.7554/eLife.39514.

Pathak, G. P. *et al.* (2014) 'Benchmarking of optical dimerizer systems.', *ACS synthetic biology*, 3(11), pp. 832–8. doi: 10.1021/sb500291r.

Pettersson, J *et al.* (1996) 'Modulation of virulence factor expression by pathogen target cell contact.', *Science*, 273(5279), pp. 1231–3.

Pettersson, Jonas *et al.* (1996) 'Modulation of virulence factor expression by pathogen target cell contact', *Science*, 273(5279), pp. 1231–1233. doi: 10.1126/science.273.5279.1231.

Portaliou, A. G. *et al.* (2017) ' Hierarchical protein targeting and secretion is controlled by an affinity switch in the type III secretion system of enteropathogenic Escherichia coli ', *The EMBO Journal*, 36(23), pp. 3517–3531. doi: 10.15252/embj.201797515.

Pozidis, C. *et al.* (2003) 'Type III Protein Translocase', *Journal of Biological Chemistry*, 278(28), pp. 25816–25824. doi: 10.1074/jbc.M301903200.

Radics, J., Königsmaier, L. and Marlovits, T. C. (2014) 'Structure of a pathogenic type 3 secretion system in action', *Nature Structural and Molecular Biology*, 21(1), pp. 82–87. doi: 10.1038/nsmb.2722.

Raghavan, A. R., Salim, K. and Yadav, V. G. (2020) 'Optogenetic Control of Heterologous Metabolism in E. coli', *ACS Synthetic Biology*, 9(9), pp. 2291–2300. doi: 10.1021/acssynbio.9b00454.

Reichhart, E. *et al.* (2016) 'A Phytochrome Sensory Domain Permits Receptor Activation by Red Light', *Angewandte Chemie International Edition*, 55(21), pp. 6339–6342. doi: 10.1002/anie.201601736.

Rina, M. *et al.* (2000) 'Alkaline phosphatase from the Antarctic strain TAB5', *European Journal of Biochemistry*, 267(4), pp. 1230–1238. doi: 10.1046/j.1432-1327.2000.01127.x.

Rocha, J. M. *et al.* (2018) 'Single-molecule tracking in live: Yersinia enterocolitica reveals distinct cytosolic complexes of injectisome subunits', *Integrative Biology (United Kingdom)*, 10(9), pp. 502–515. doi: 10.1039/c8ib00075a.

Rosqvist, R., Magnusson, K. E. and Wolf-Watz, H. (1994) 'Target cell contact triggers expression and polarized transfer of Yersinia YopE cytotoxin into mammalian cells', *EMBO Journal*, 13(4), pp. 964–972. doi: 10.1002/j.1460-2075.1994.tb06341.x.

de Rouvroit, C. L., Sluiters, C. and Cornelis, G. R. (1992) 'Role of the transcriptional activator, VirF, and temperature in the expression of the pYV plasmid genes of *Yersinia enterocolitica*', *Molecular Microbiology*, 6(3), pp. 395–409. doi: 10.1111/j.1365-2958.1992.tb01483.x.

Ryu, M. H. *et al.* (2010) 'Natural and engineered photoactivated nucleotidyl cyclases for optogenetic applications', *Journal of Biological Chemistry*, 285(53), pp. 41501–41508. doi: 10.1074/jbc.M110.177600.

Schindelin, J. *et al.* (2012) 'Fiji: an open-source platform for biological-image analysis', *Nature Methods*, 9(7), pp. 676–682. doi: 10.1038/nmeth.2019.

Schlumberger, M. C. *et al.* (2005) 'Real-time imaging of type III secretion: Salmonella SipA injection into host cells', 102(35), pp. 12548–12553. doi: 10.1073/pnas.0503407102.

Schmidl, S. R. *et al.* (2014) 'Refactoring and optimization of light-switchable Escherichia coli two-component systems', *ACS Synthetic Biology*, 3(11), pp. 820–831. doi: 10.1021/sb500273n.

Schneider, C. A., Rasband, W. S. and Eliceiri, K. W. (2012) 'NIH Image to ImageJ: 25 years of image analysis', *Nature Methods*, 9(7), pp. 671–675. doi: 10.1038/nmeth.2089.

Schulte, M. *et al.* (2018) 'A versatile remote control system for functional expression of bacterial virulence genes based on the tetA promoter', *International Journal of Medical Microbiology*. doi: 10.1016/j.ijmm.2018.11.001.

Sentürk, O. I. *et al.* (2020) 'Red/Far-Red Light Switchable Cargo Attachment and Release in Bacteria-Driven Microswimmers', *Advanced Healthcare Materials*, 9(1). doi: 10.1002/adhm.201900956.

Sheller-Miller, S. *et al.* (2019) 'Cyclic-recombinase-reporter mouse model to determine exosome communication and function during pregnancy', *American Journal of Obstetrics and Gynecology*, 221(5), pp. 502.e1-502.e12. doi: 10.1016/j.ajog.2019.06.010.

Shimizu-Sato, S. *et al.* (2002) 'A light-switchable gene promoter system', *Nature Biotechnology*, 20(10), pp. 1041–1044. doi: 10.1038/nbt734.

Song, M. *et al.* (2017) 'Control of type III protein secretion using a minimal genetic system', *Nature Communications*, 8, p. 14737. doi: 10.1038/ncomms14737.

Sorg, J. A., Blaylock, B. and Schneewind, O. (2006) 'Secretion signal recognition by YscN, the Yersinia type III secretion ATPase', *Proceedings of the National Academy of Sciences of the United States of America*, 103(44), pp. 16490–16495. doi: 10.1073/pnas.0605974103.

Sory, M.-P. *et al.* (1995) 'Identification of the YopE and YopH domains required for secretion and internalization into the cytosol of macrophages, using the cyaA gene fusion approach', *Proceedings of the National Academy of Sciences of the United States of America*, 92(26), pp. 11998–12002.

Spreter, T. *et al.* (2009) 'A conserved structural motif mediates formation of the periplasmic rings in the type III secretion system', *Nature Structural & Molecular Biology*, 16(5), pp. 468–476. doi: 10.1038/nsmb.1603.

Stanley, S. A. *et al.* (2003) 'Acute infection and macrophage subversion by Mycobacterium tuberculosis require a specialized secretion system', *Proceedings of the National Academy of Sciences of the United States of America*, 100(22), pp. 13001–13006. doi: 10.1073/pnas.2235593100.

Sun, P. *et al.* (2008) 'Structural characterization of the Yersinia pestis type III secretion system needle protein YscF in complex with its heterodimeric chaperone YscE/YscG.', *Journal of molecular biology*, 377(3), pp. 819–30. doi: 10.1016/j.jmb.2007.12.067.

Tang, R. *et al.* (2021) 'mem-iLID, a fast and economic protein purification method', *Bioscience Reports*, 41(7), p. 20210800. doi: 10.1042/bsr20210800.

Toettcher, J. E., Gong, D., *et al.* (2011) 'Light control of plasma membrane recruitment using the Phy-PIF system.', *Methods in enzymology*, 497, pp. 409–23. doi: 10.1016/B978-0-12-385075-1.00017-2.

Toettcher, J. E., Voigt, C. A., *et al.* (2011) 'The promise of optogenetics in cell biology: interrogating molecular circuits in space and time.', *Nature methods*, 8(1), pp. 35–8. doi: 10.1038/nmeth.f.326.

Toussaint, B. *et al.* (2013) 'Live-attenuated bacteria as a cancer vaccine vector', *Expert Review of Vaccines*, 12(10), pp. 1139–1154. doi: 10.1586/14760584.2013.836914.

Trokter, M. and Waksman, G. (2018) 'Translocation through the conjugative type IV secretion system requires unfolding of its protein substrate', *Journal of Bacteriology*, 200(6). doi: 10.1128/JB.00615-17.

Trülzsch, K. *et al.* (2003) 'Analysis of chaperone-dependent Yop secretion/translocation and effector function using a mini-virulence plasmid of Yersinia enterocolitica', *International Journal of Medical Microbiology*, 293(2–3), pp. 167–177. doi: 10.1078/1438-4221-00251.

Tsirigotaki, A. *et al.* (2017) 'Protein export through the bacterial Sec pathway', *Nature Reviews Microbiology*, 15(1), pp. 21–36. doi: 10.1038/nrmicro.2016.161.

Tusk, S. E., Delalez, N. J. and Berry, R. M. (2018) 'Subunit Exchange in Protein Complexes', *Journal of Molecular Biology*. Academic Press, pp. 4557–4579. doi: 10.1016/j.jmb.2018.06.039.

Uliczka, F. *et al.* (2011) 'Unique Cell Adhesion and Invasion Properties of Yersinia enterocolitica O:3, the Most Frequent Cause of Human Yersiniosis', *PLoS Pathogens*. Edited by J. E. Galán, 7(7), p. e1002117. doi: 10.1371/journal.ppat.1002117.

Vogiatzi, F. *et al.* (2016) 'Mutant p53 promotes tumor progression and metastasis by the endoplasmic reticulum UDPase ENTPD5', *Proceedings of the National Academy of Sciences*, 113(52), pp. E8433–E8442. doi: 10.1073/pnas.1612711114.

Wagner, S. *et al.* (2010) 'Organization and coordinated assembly of the type III secretion export apparatus', *Proceedings of the National Academy of Sciences of the United States of America*, 107(41), pp. 17745–17750. doi: 10.1073/pnas.1008053107.

Wagner, S. *et al.* (2018) 'Bacterial type III secretion systems: A complex device for delivery of bacterial effector proteins into eukaryotic host cells', *FEMS Microbiology Letters*. doi: 10.1093/femsle/fny201.

Wagner, S. and Diepold, A. (2020) 'A unified nomenclature for injectisome-type type III secretion systems', in *Current Topics in Microbiology and Immunology*. Springer Science and Business Media Deutschland GmbH, pp. 1–10. doi: 10.1007/82_2020_210.

Walker, B. J., Stan, G.-B. V and Polizzi, K. M. (2017) 'Intracellular delivery of biologic therapeutics by bacterial secretion systems.', *Expert reviews in molecular medicine*, 19, p. e6. doi: 10.1017/erm.2017.7.

Wang, H. *et al.* (2016) 'LOVTRAP: An optogenetic system for photoinduced protein dissociation', *Nature Methods*, 13(9), pp. 755–758. doi: 10.1038/nmeth.3926.

Westerhausen, S., Nowak, M., Torres-Vargas, C. E., *et al.* (2020) 'A NanoLuc luciferase-based assay enabling the real-time analysis of protein secretion and injection by bacterial type III secretion systems.', *Molecular microbiology*, p. 745471. doi: 10.1111/mmi.14490.

Westerhausen, S., Nowak, M., Torres-Vargas, C. E., *et al.* (2020) 'A NanoLuc luciferase-based assay enabling the real-time analysis of protein secretion and injection by bacterial type III secretion systems', *Molecular Microbiology*, 113(6), pp. 1240–1254. doi: 10.1111/mmi.14490.

Wilharm, G. *et al.* (2004) 'Yersinia enterocolitica type III secretion: Evidence for the ability to transport proteins that are folded prior to secretion', *BMC Microbiology*, 4(1), pp. 1–9. doi: 10.1186/1471-2180-4-27.

Wojcik, J. *et al.* (2016) 'Allosteric inhibition of Bcr-Abl kinase by high affinity monobody inhibitors directed to the Src homology 2 (SH2)-kinase interface', *Journal of Biological Chemistry*, 291(16), pp. 8836–8847. doi: 10.1074/jbc.M115.707901.

Wolters, M. *et al.* (2015) 'Analysis of Yersinia enterocolitica Effector Translocation into Host Cells Using Beta-lactamase Effector Fusions.', *Journal of visualized experiments : JoVE*, (104). doi: 10.3791/53115.

Worrall, L. J. *et al.* (2016) 'Near-atomic-resolution cryo-EM analysis of the Salmonella T3S injectisome basal body', *Nature*, 540(7634), pp. 597–601. doi: 10.1038/nature20576.

Wren, B. W. (2003) 'The Yersiniae — a model genus to study the rapid evolution of bacterial pathogens', *Nature Reviews Microbiology*, 1(1), pp. 55–64. doi: 10.1038/nrmicro730.

Xia, A. *et al.* (2021) 'Optogenetic Modification of Pseudomonas aeruginosa Enables Controllable Twitching Motility and Host Infection', *ACS Synthetic Biology*, 10(3), pp. 531–541. doi: 10.1021/acssynbio.0c00559.

Yang, C. *et al.* (2020) 'Upconversion optogenetic micro-nanosystem optically controls the secretion of light-responsive bacteria for systemic immunity regulation', *Communications Biology*, 3(1), pp. 1–14. doi: 10.1038/s42003-020-01287-4.

Yother, J. and Goguen, J. D. (1985) 'Isolation and characterization of Ca2+-blind mutants of Yersinia pestis', *Journal of Bacteriology*, 164(2), pp. 704–711. doi: 10.1128/jb.164.2.704-711.1985.

Yu, J. *et al.* (2001) 'PUMA induces the rapid apoptosis of colorectal cancer cells', *Molecular Cell*, 7(3), pp. 673–682. doi: 10.1016/S1097-2765(01)00213-1.

Zimmerman, S. P. *et al.* (2016) 'Tuning the Binding Affinities and Reversion Kinetics of a Light Inducible Dimer Allows Control of Transmembrane Protein Localization', *Biochemistry*, 55(37), pp. 5264–5271. doi: 10.1021/acs.biochem.6b00529.

Zomer, A. *et al.* (2015) 'In vivo imaging reveals extracellular vesicle-mediated phenocopying of metastatic behavior', *Cell*, 161(5), pp. 1046–1057. doi: 10.1016/j.cell.2015.04.042.

Acknowledgements

The first and biggest word of thanks goes to my mentor and supervisor Andreas Diepold. Thank you for all the kindness and patience during the last four years, your encouraging words, your warmth and sympathy when I needed it most. Thank you also for creating an atmosphere of friendly pressure whenever it was appropriate and supportive – especially for me. Thank you for all the nice discussions and advice that helped me not only on my path as a scientist, but also as a person. I will take away a lot of what I have learned during this time.

Another thank goes to my TAC committee members Dr. Martin Thanbichler and Dr. Lars-Oliver Essen – I always enjoyed those constructive meetings. Thank you for accompanying me during the PhD.

A big thank goes to the current and former members of RG Diepold, Katja, Stephan, Dimi, Bailey, Lisa, Carlos, Kirsten, Moritz, Hend, Anna-Lena, Saskia, Vera, Coco, Keith, Haozhe, Francesca, Dorothy and Emma. I really enjoyed spending time with you – in the lab and beside the lab. Thank you Katja for your encouraging words when I was sad, your care and reliability. Thank you Stephan for all the nice discussions, the boat trips and drinks during our time. I have always looked up to you as a scientist.

A big thank you to my family and friends who supported and believed in me from the beginning. Thank you mom and dad for everything - I did my best so that you can be proud of me. Big thank to Dimi, who has been a friend and brother and accompanied me on the science and the personal path.

A big thank you to Timo Glatter for the nice conversations, the many laughs and the friendly nicknames. The Patentator made it, yeah.

A thank you to Horst Henseling for always building fancy tools for my optogenetics work.

Thank you to Prof. Andreas Gahlmann, University of Virginia, for important contributions and discussions during the inception of this study; Prof. Klaus Hahn, University of North Carolina, for the LOVTRAP system templates (Addgene 81010, 81036, 81041); Prof. Brian Kuhlman, University of North Carolina, for the iLID system templates (Addgene 60408, 60409); Dr. Felicity Alcock, University of Oxford, for suggestions for the design of the transmembrane anchor; Dr. Seraphine Wegner, Max Planck Institute for Polymer Research, Mainz, for helpful discussions about optogenetic interaction switches; Prof. Petra Dersch, University of Münster, for the gift of HEp-2 cells; Dr. Simon Ittig, T3 Pharmaceuticals AG, Basel, for the kind provision of the plasmid encoding $YopE_{1-138}$-tBID.

I would like to thank Prof. Dr. Lotte Søgaard-Andersen for giving me the opportunity to do research in the Department of Ecophysiology at the Max Planck Institute for Terrestrial Microbiology in Marburg.

Last but not least, I would like to thank my thesis committee and everyone who will read this thesis - I hope you enjoy reading it as much as I enjoyed working on it.

Flo

Erklärung

Ich versichere, dass ich meine Dissertation mit dem Titel:

Control and investigation of effector export by the bacterial type III secretion system using optogenetics

selbstständig verfasst und keine anderen als die in der Arbeit angegebenen Hilfsmittel verwendet und an sämtliche Stellen, die im Wortlaut oder dem Sinn nach anderen Werken entnommen sind, mit Quellenangaben oder Vermerken kenntlich gemacht habe.

Diese Dissertation wurde in der jetzigen oder einer ähnlichen Form noch bei keiner anderen Hochschule eingereicht und hat noch keinen sonstigen Prüfungszwecken gedient.

Marburg, den 24.11.2021

F. Lindner

Florian Lindner

Einverständniserklärung

Ich erkläre mich damit einverstanden, dass die vorliegende Dissertation:

„Control and investigation of effector export by the bacterial type III secretion system using optogenetics“

in Bibliotheken allgemein zugänglich gemacht wird. Dazu gehört, dass sie

- von der Bibliothek der Einrichtung, in der ich meine Arbeit anfertig habe, zur Benutzung in ihren Räumen bereitgehalten wird;

- in konventionellen und maschinenlesbaren Katalogen, Verzeichnissen und Datenbanken verzeichnet wird;

- im Rahmen der urheberrechtichen Bestimmungen für Kopierzwecke genutzt werden kann.

Marburg, den 24.11.2021

F. Lindner

Florian Lindner

Dr. Andreas Diepold